Reduction of Biomechanical Models and Subject Specific Properties for

Real-Time Simulation of Surgical Trocar Insertion

By

RAVI KUMAR   CHANNA NAIK

September 1, 2010

A thesis submitted to the Faculty of the Graduate School of

The State University of New York at Buffalo in partial

completion of the requirements for the degree of

MASTER OF SCIENCE

Department of Mechanical Engineering

ACKNOWLEDGEMENTS

ABSTRACT

Trocar insertion is the first step in Laparoscopy, Thoracoscopy and most other micro surgery procedures. It is a difficult procedure to learn and practice because procedure is carried out almost entirely without any visual feedback of the organs underlying the tissues being punctured. A majority of injuries is attributed to excessive use of force by surgeons. Practicing on cadavers and synthetic tissues may not accurately simulate the process. So there is a need for haptic based computer simulator to train and enhance the trocar insertion skills.

For realistic force and torque haptic feedbacks, there is need for realistic modeling of tissue layers and real-time finite element computation. Geometrical complexities of anatomical structures, non-linear complex material properties and their variations with sex, age, person body built, makes patient specific accounting of material properties very difficult. These complexities also make the real time computation of biomechanical models to be prohibitively expensive.

In the first half of this thesis a novel method of obtaining patient specific initial conditions, boundary conditions, tissue layers dimensions and their mechanical properties are proposed. A typical patient sample is worked out and cross verified with the available data. In the second half of the thesis, to reduce simulation computation load, a novel method of accounting different tissue mechanical properties by defining tissue specific mapping functions to a single linear function and parallel interpolation of the computation results to the real tissue properties for real-time simulation is proposed.

TABLE OF CONTENTS

Chapter 5:   Material Properties Treatment

Chapter 6: Real-Time Computation

LIST OF FIGURES

LIST OF TABLES

CHAPTER 1

INTRODUCTION

Introduction and Motivation

Trocar insertion is the first step in Laparoscopy, Thoracoscopy and most other micro surgery procedures. It is a difficult procedure to learn and practice because procedure is carried out almost entirely without any visual feedback of the organs underlying the tissues being punctured. A majority of injuries is attributed to excessive use of force by surgeons. Approximately 1 in every 1000 patients undergoing laparoscopic abdominal surgery will experience bowel or vessel perforation injury by trocars during initial access, *Ref [01].* So there is need for a haptic based trocar insertion simulator using which insertions could be practiced and skills enhanced.
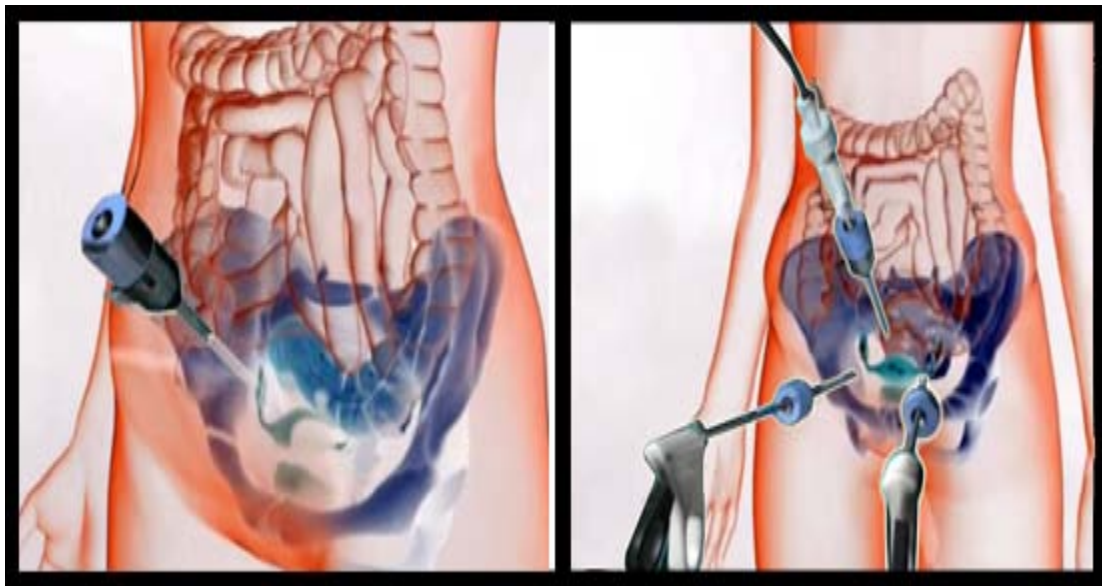
Fig 01.01: *Trocar insertions at navel and other regions in lower abdomen in typical laparoscopic procedures. Adapted from Ref [02].*

1.2 Background

Geometric complexity of anatomical structures, realistic real time deformation of graphical reconstructions is prohibitively computationally intensive.

Real time deformation of virtual anatomy is roughly approximated through simpler methodologies using simple or complex spring models and simple graphical interpolations using Non-Uniform Rational B-Splines(NURBS), Bezier patches or other polynomial interpolations which are not based upon biomechanical tissue properties and physical relationships such as mass, inertia and applied force hence they do not accurately represent the complex deformations and force-feedback interactions that take place during surgery.

Finite element analysis is widely regarded as the most appropriate alternative to above mentioned quick and dirty methods. The highly computational nature of FE method makes its direct application to real time force feedback and visualization of tissue deformation not practical for most simulations. Limitation is primarily due to overabundance of information provided by standard FE approaches. Mathematics is to be optimized to yield only the information essential for the surgical task then computational time will be drastically reduced.

Finite element modeling of soft tissues has its application to both real-time and non real-time surgical needs. In the *Ref [09 to 11]*, it finds applications in non real-time needs, such as, facial surgical visualization and animation, breast deformation during biopsy and real-time applications such as suturing and tissue cutting. In the *Ref [12 to 22]*, it is applied to real-time need of needle insertion procedures.

1.3   Research Question

Trocar insertion problem and the motivation to build a haptic based simulator leaves with the following set of questions to be addressed in the course of research.

How to account for various subjects specific boundary and initial conditions?

How to account for the variations in tissue thicknesses of abdominal wall with subjects?

How to account for the variations in the complex non-linear material properties of abdominal wall tissue with sex, age, person body built and insertion region of interest?

How to simplify the mathematics of the problem, so that the finite element simulation with haptic interface can be done in real-time?

In this thesis work an attempt has been made to address all the above questions by referencing, *Ref [03 to 08]* and proposing new ideas.
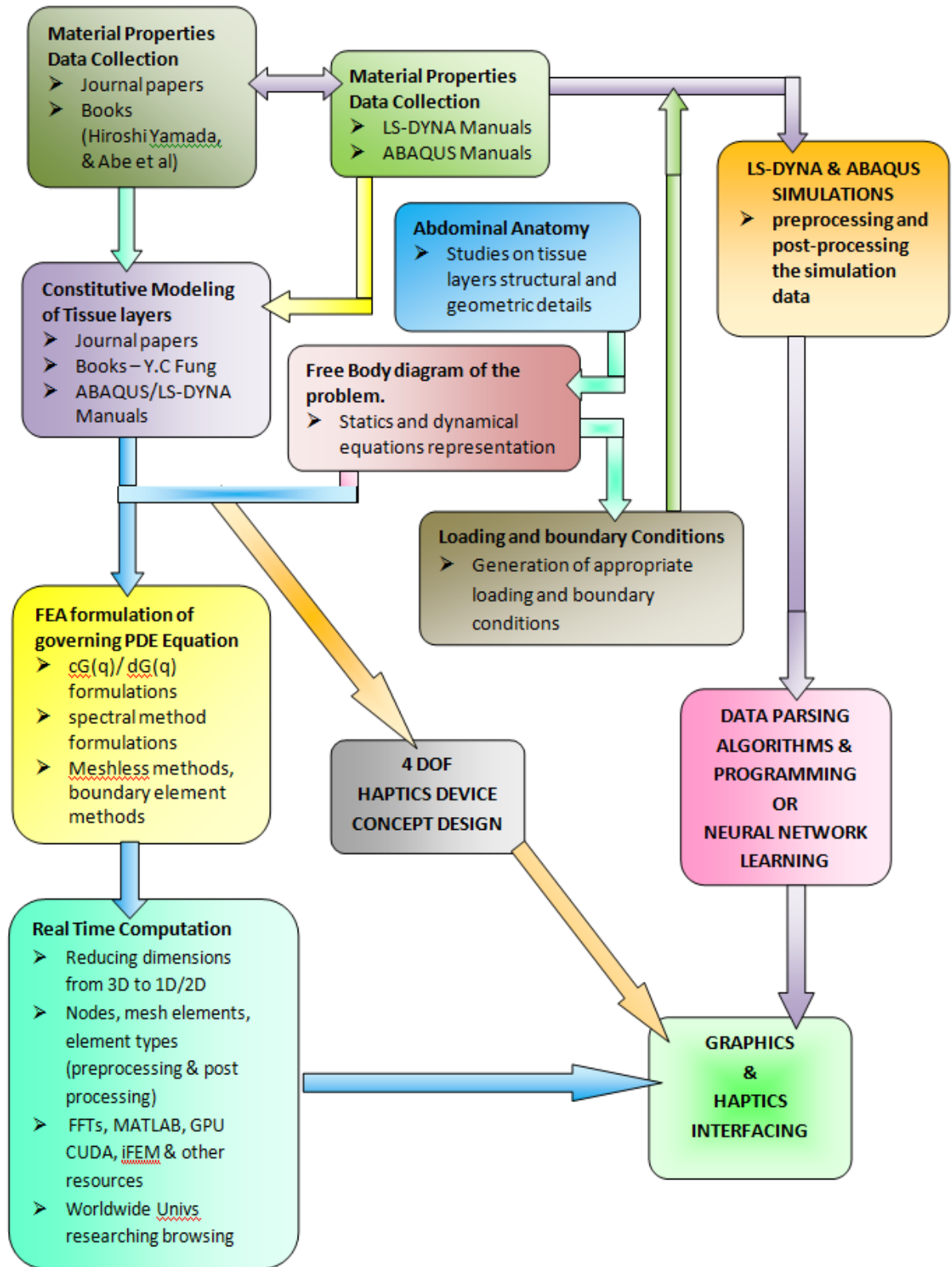
Fig 01.02: *Scope of trocar insertion haptic simulator problem research.*

CHAPTER 2

TROCAR INSERTION ANALYSIS

Introduction

Minimal invasive surgery procedures involve insufflation of peritoneal cavity with carbon dioxide gas to a pressure of 12 to 14 mm Hg. Insufflation basically expands the abdominal wall which provides enough space for operating on visceral organs with surgical tools of which trocars are the first ones to be used to create ports for tools entry. The procedure of insufflation puts abdominal wall in a state of stress which may act as a preconditioning of soft tissues which would enable abdominal tissues to show a constant and repeatable mechanical properties.

2.2   Initial Condition Analysis

During insufflation abdominal wall changes from a cylindrical shape to a dome shape, with more expansion in sagittal plane than in transverse plane, with increase in 15% surface area and 1.27×10^{-3} m^3 volume increase. Abdominal wall shows a maximum displacement of 40 mm at mid-sagittal and mid-transverse planes and a minimum of 5 mm displacements at lateral sides where it is constrained by ribs and pelvis, *Ref [24]*. Though there are regional variations in the displacements of abdominal wall which creates corresponding initial strain levels, the wall is put to a constant stress throughout. The dome shape of the wall is described with two principal radii one in mid sagittal plane and other in mid transverse plane. *Table 02.01* shows the maximum stress and strain levels in the subjects of 30-70 years of age, different BMIs and both sex.

Fig 02.01: *Flat abdomen before inflation and dome shape abdomen after inflation. Adapted from Ref [23].*

Plane	Maximum initial stress (kPa)	Maximum initial strain (%)
Transverse	2.57±0.43kPa	4.98±0.25 %
Sagittal	2.59±0.39kPa	10.54±0.25%

Table 02.01: *Maximum initial stress and strains in transverse and sagittal planes Ref [23].*

Plane	Average initial radius (m)	Average final radius (m)
Transverse	0.216 ± 0.012	0.165 ± 0.004
Sagittal	0.633 ± 0.067	0.332 ± 0.027

Table 02.02: *Maximum initial stress and strains in transverse and sagittal planes Ref [23].*

There are no significant variations in the initial and final transverse and sagittal radii with sex, BMI within the age group of 30-70 years. From the above *Table 02.01*, it can be estimated that trocar insertion procedure occurs at the double the initial strain, below 30% and the process is essentially tissue shearing at low strains compared to possible ultimate elongations and failure due to shear stresses. Using the equation (C2:02) and with the known abdominal wall thickness, initial stress can be calculated.

Assuming no abdominal wall bending rigidity

$$(P_i - P_o) = \left(\frac{T_1}{r_1} + \frac{T_2}{r_2} \right) \qquad\qquad -----(C2:01)$$

P_i, P_o :*internal and external pressures*
r_1, r_2 : *principal radii of curvatures*
T_1, T_2 :*tensions in principal axes* $\qquad\qquad -----Ref$ [25]

Above equation $(C2:01)$ *can be reduced to*

$$\sigma = \frac{p r_1 r_2}{2t(r_1 + r_2)} \qquad\qquad -----(C2:02)$$

σ : *tensile stress in the abdominal wall*
p :*relative internal pressure*
r_1, r_2 :*transverse and sagittal radii of curvatures* $\qquad -----Ref$ [25]

2.3 Trocar Sizes and Shapes

Trocar comes in standard sizes of diameter of 5 mm to 15mm. They can be grouped into several categories. The two major but overlapping categories are reusable and disposable. A few manufacturers make resposable trocars, which have a reusable cannula and a

disposable trocar and valve component. Reusable, disposable, and resposable trocars can be further grouped according to whether they have cutting or noncutting blades. In addition, trocars with or without cutting blades may have optical devices that permit visualization of the blade and abdominal wall tissue. Generally, disposable trocars with cutting blades have retractable shields that cover the cutting tip after entering the abdominal cavity, while reusable cutting trocars do not.

2.3.1 Cutting Trocars

Trocars with cutting blades have two basic designs. Pyramidal-tipped trocars have sharp edges that cut tissues in three planes as they pass through the abdominal wall. Reusable versions of these do not have retractable shields. Flat-blade trocars have two sharp edges and cut tissue in a single plane. Disposable pyramidal-tipped and flat-blade trocars generally have retractable shields.

2.3.2 Noncutting Trocar

Trocars without cutting blades have three basic designs. Pointed conical trocars penetrate the abdominal wall by separating tissue fibers along paths of least resistance. Blunt conical trocars, one version uses a blunt obturator to dilate an expandable sheath that is inserted through the abdominal wall over a Veress needle. Other blunt trocars are intended to be placed through an incised wound, such as would occur with the open technique. Optical trocars are a subset of trocars. Three devices are commercially available, one has a cutting blade and two are bladeless. Each uses a laparoscope that is inserted down the trocar's shaft to visualize tissue planes and landmarks. The bladeless optical trocars have a clear conical tip with flanges that separate fascial and muscle fibers

as the trocar is pushed through the abdominal wall. The bladed trocar has a clear half-sphere dome that allows tissue visualization. Its blade is activated by a trigger mechanism and cuts the tissue in view, then automatically retracts. *Ref [01]*.

Fig 02.02: *Pyramidal-blade reusable and disposable trocars. Adapted from Ref [01].*

Fig 02.03: *Flat-blade trocars. Adapted from Ref [01].*
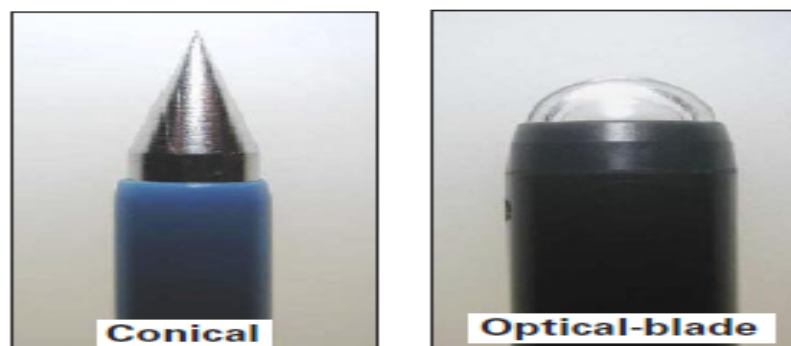
Fig 02.04: *Conical and optical-blade trocars. Adapted from Ref [01].*

Fig 02.05: Non-blade trocars. Adapted from Ref [01].
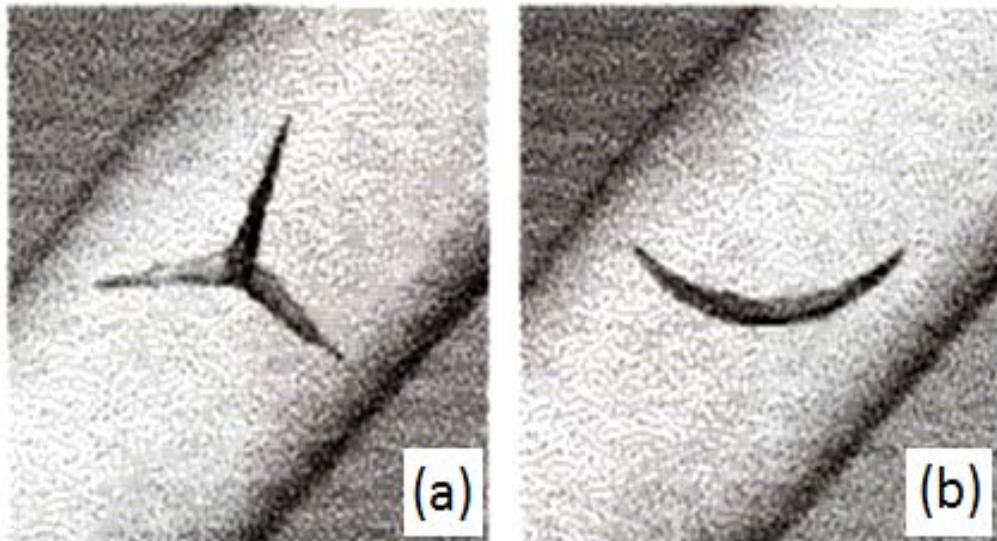
Fig 02.06: Vascular lacerations caused by (a) a pyramidal trocar tip; (b) a tip shield. Adapted from Ref [28].

2.4   Trocar Insertion Time Motion Analysis

Start time (min)	Steep displacement time (min)	Rupture time (min)	Release time (min)
1.34	1.35	1.44	1.46
3.125	3.14	3.19	3.21
3.395	3.41	3.44	3.46
2.49	2.51	2.53	2.55
4.02	4.035	4.065	4.085

Table 02.03: *Time analysis of trocar insertion. Ref [24].*

Time gap	Seconds
Average total time	7.9
Average start to Steep displacement time	1.5
Average steep displacement to rupture time	4.4
Average rupture to release time	2

Table 02.04: *Time gap analysis from the Table 02.03.*
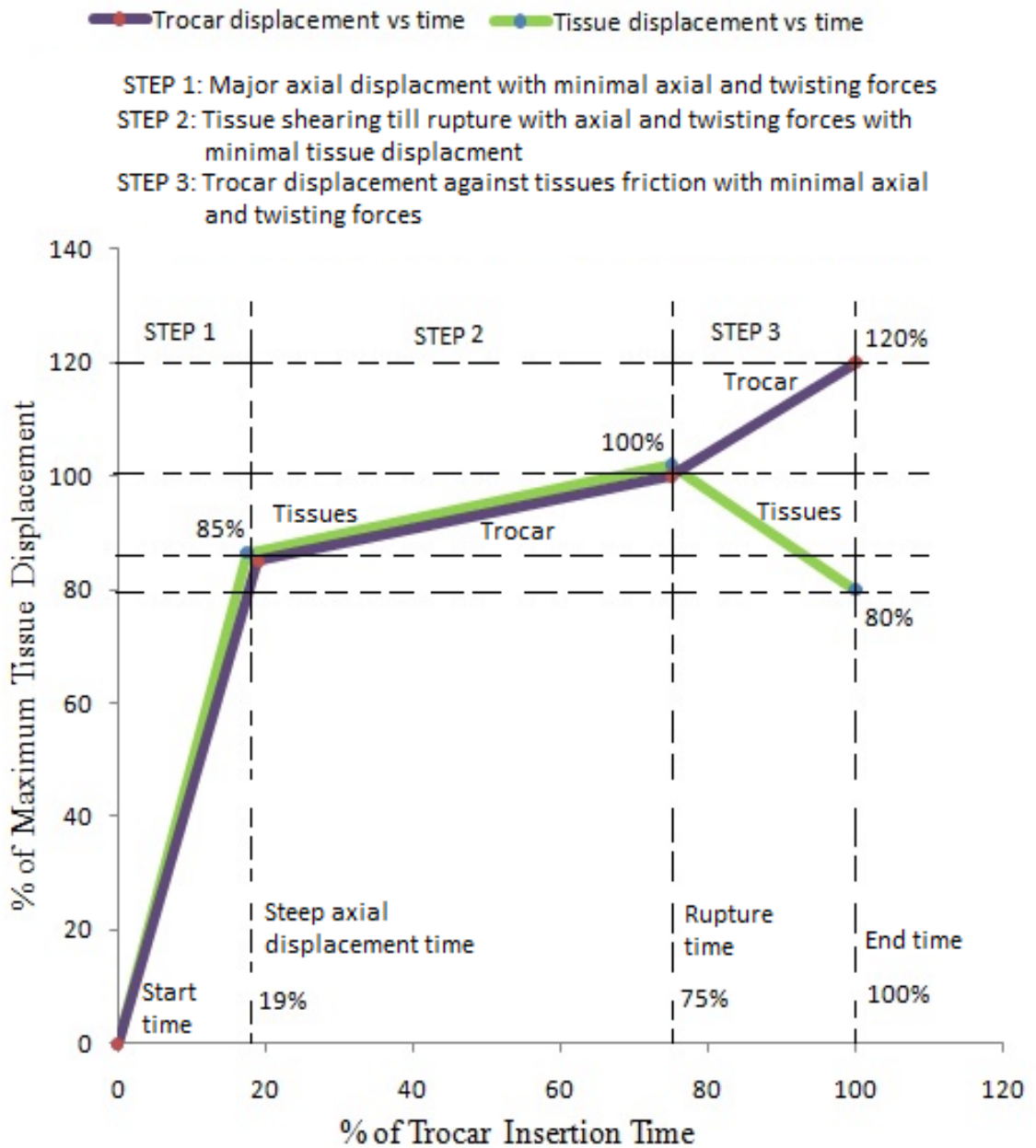
Fig 02.07: *Schematic diagram of the trocar insertion procedure with time and displacements considerations. Ref [24].*

2.4.1 Twisting Motion Analysis

An average of 0^0 - 90^0 - 0^0 twist angle at a rate of 2 cycles per second is normally observed in the trocar insertion procedure. A maximum shear rate of 180^0 sec^{-1} can be expected. This shear rate is not exactly the same shear rate the tissues undergo as it depends on the type of trocar tip and also the slip between trocar tip and the tissues.

2.4.2 Estimated Axial Loading Strain Rates

Trocar insertion step	Strain rate value	Strain rate value in % of initial length	Comment
Step 1	1.875 cm s^{-1}	37.5 % of Length/s	Very high strain rate, one order greater than the normal testing strain rate
Step 2 & 3	0.032 cm s^{-1}	0.41 % of Length/s	Very near to the normal testing strain rate

Table 02.05: *Typical axial strain rates during trocar insertion procedure.*

2.5 Boundary Conditions

A single boundary condition is sufficient to describe all the trocar insertions. In a cylindrical coordinate system, displacements r,θ, Z are fixed and rotations R_r , R_θ , R_z are free to rotate. Trocar insertion shows large deformations.70 mm axial deformations can be expected. A maximum of 100 mm radius of influence can be expected at upper abdominal wall and a minimum of 25 mm at lateral abdominal wall where it is constrained by ribs and pelvis.
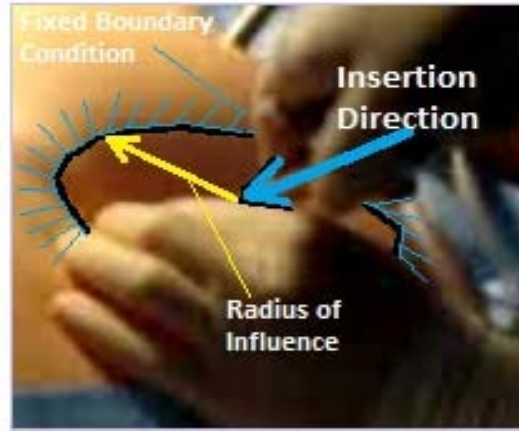
Fig 02.08: *Boundary condition for trocar insertion procedure. Ref [24].*

2.6   Failure Analysis

Tissue failure in during trocar insertion can be ductile fracture rupture in terms of macroscopic material failure analysis. As it mainly involves shearing of tissues, the simple yield Von Mises yield criterion would represent it adequately. As tissues show non-linear hyperelastic behavior and ruptures without yield, there is a necessity to define an artificial yielding to avoid numerical computation instability.

The Von Mises yield criterion expressed as a functional form, principal stresses and stress tensor components are as follows

(a) $f(J_2) = 0$.

(b) $\sqrt{3J_2} = \sigma_y$ or, $(\sigma_1 - \sigma_2)^2 + (\sigma_2 - \sigma_3)^2 + (\sigma_3 - \sigma_1)^2 = 2{\sigma_y}^2$

(c) $(\sigma_{11} - \sigma_{22})^2 + (\sigma_{22} - \sigma_{33})^2 + (\sigma_{11} - \sigma_{33})^2 + 6(\sigma_{23}^2 + \sigma_{31}^2 + \sigma_{12}^2) = 6k^2 = 2\sigma_y^2$

---------- (C2 : 03)

14

Where,

σ_y is the yield stress in uniaxial tension

J_2 second principal invariants of the deviatoric part of the Cauchy stress defined as

$$J_2 = \frac{1}{2}\boldsymbol{s} : \boldsymbol{s} = \frac{1}{6}\left[(\sigma_1 - \sigma_2)^2 + (\sigma_2 - \sigma_3)^2 + (\sigma_3 - \sigma_1)^2\right]$$ ---------- *(C2 : 04)*

$\boldsymbol{\sigma}$ is the Cauchy stress and $\sigma_1, \sigma_2, \sigma_3$ are its principal values, $\boldsymbol{s}$ is the deviatoric part of the Cauchy stress and s_1, s_2, s_3 are its principal values. *Ref [26].*
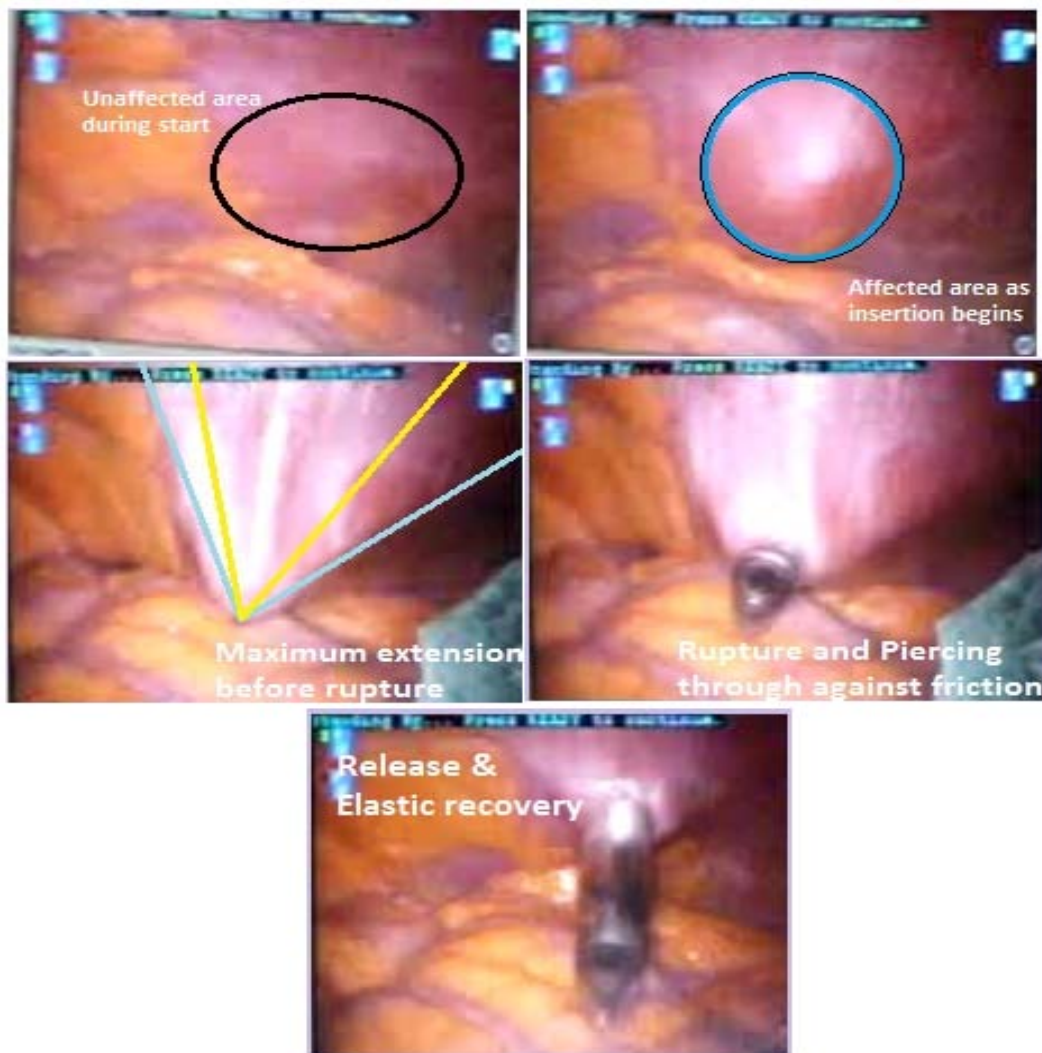
Fig 02.09: *Typical trocar insertion deformations and failure. Ref [24].*

2.7   Insertions Force and Torques

From the expansive properties of abdominal wall tissues force and torques of a typical trocar insertion is estimated. As trocar insertion produces conical deformation, a typical depth of deformation is estimated from the hemispherical deformation of tissue expansion test. Analogous ultimate shear strength is calculated from ultimate expansive strength by reducing it by a factor of $\sqrt{3}$ times in the *Table BBBB.* For a trocar with tip area of 1mm^2, axial force of piercing and torques are calculated in the *Table AAAA.*

Tissue	Ultimate Expansive strength per unit thickness $(kg/cm^2/mm)$	Calculated shear strength $(kg/cm^2/mm)$	Ultimate Expansion (ml) for an aperture of 7 mm diameter	Calculated depth of conical expansion (mm)
Skeletal Muscle	7.9	4.56	0.16	4.3
Fasicas	67.9	39.20	0.07	2.85
Panniculus Adipose	0.712	0.41	0.0461	2.31

Table 02.06: *Expansive properties of abdominal wall tissues. Ref [29].*

Axial force to pierce through a 1 mm thick tissue layer (g/mm)	Torque to shear through a 1 mm thick tissue layer (g mm)	For a radius of Influence of 100 mm, depth of expansion (mm)
79 (0.78 N/mm)	45.61 (0.45 mNm)	61.5
676 (6.62 N/mm)	390.89 (3.82 mN/m)	40.72
7.12 (0.07 N/mm)	4.11 (0.04 mN/m)	33

Table 02.07: *Force and torque requirements for 1mm² tip trocar insertion.*

2.7.1 Device suitability
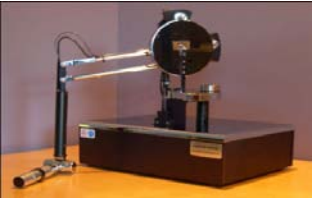
	Phantom premium 1.5 High Force/6 DOF	Phantom premium 1.5 /6 DOF
Workspace	*Translational:* 381 W x 267 H x 191 D mm *Rotational :* Roll 335 degrees	*Translational:* 381 W x 267 H x 191 D mm *Rotational :* Roll 335 degrees
Continuous exertable force and torque	*Translational:* 6.2 N *Rotational:* Roll 48 mNm	Translational: 1.4 N *(**Less than the required force)** Rotational: Roll 48 mNm

Table 02.08: *Workspace, force and torque specifications of Phantom prepmium 1.5. Ref [27].*

With reference to *Table 02.07*, Phantom premium 1.5 High Force/6 DOF completely meets trocar insertion force and torque expected values where as 1.5/6DOF does not meet the requirement of continuously exertable force.

2.8　Equations of Motion

Abdominal soft tissues are nearly incompressible and mass conserved systems. In the process of trocar insertion, body forces are only due to gravity and can be neglected when compared to insertion forces and torques.

Cauchy's equation of motion

for arbitrary volume

and mass conserved system　　$\partial_j \sigma_{ij} + F_i = \rho \dfrac{Dv_i}{Dt}$　　$-----(C2:05)$

for incompressible system　　$\partial_j \sigma_{ij} + F_i = \rho \dfrac{\partial v_i}{\partial t}$　　$-----(C2:06)$

When body force is neglected　　$\partial_j \sigma_{ij} = \rho \dfrac{\partial v_i}{\partial t}$　*or*　$\dfrac{\partial v_i}{\partial t} = \dfrac{1}{\rho}(\partial_j \sigma_{ij})$

$$-----(C2:07)$$

$\sigma = -p\mathrm{I} + \mathrm{T}$

$F_i : body\ force \quad \rho : density$

$\sigma : cauchy\ stress\ tensor$

$p : pressure \quad \mathrm{T} : deviatoric\ stress\ tensor$

18

2.9   Problem Complexity and Alternative

Trocar insertion involves cutting and tearing of tissues and it cannot be modeled as just expansion of a minute hole with some cutting forces for each layer cutting. It is not axisymetric problem either, as the interaction of trocar with tissue is not fixed and it can be anything. Hence the tissues and trocar has to be modeled in full three dimensions to capture the interaction of trocar with tissues and cutting.
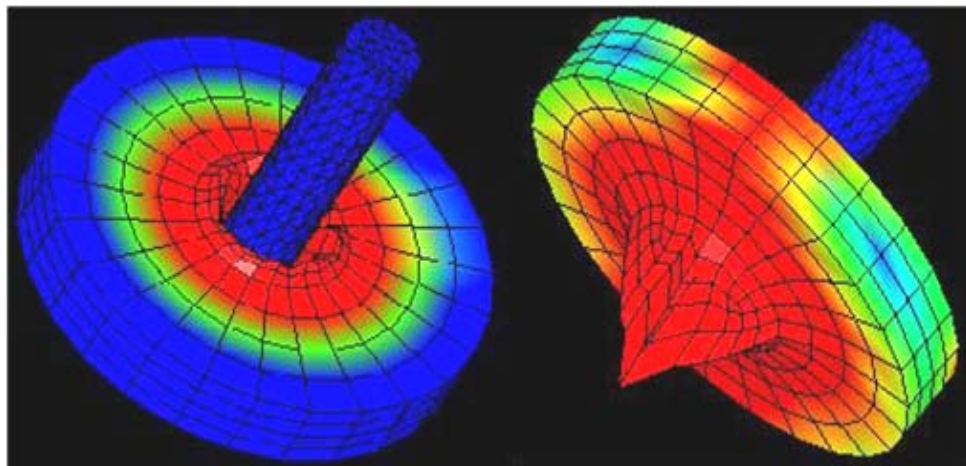
Fig 02.10: *LS – Dyna simulation of linear isotropic hyperelastic rubber to imitate the trocar insertion using only axial force and 12 mmHg initial pressure. Simulation had the disc dimension of 50 mm diameter, 10 mm thick and conical pointed needle 10 mm diameter. Simulation run time on a single core processor was nearly 12 hours. Body-to-body contact algorithm and element erosion on failure methods was used.*

Biological tissues, skin, panniculus adiposes, muscles, fascias are high strain exhibiting non-linear viscoelastic materials. The loading situations such as creep (constant stress loading condition), hysteresis (cycling loading condition), stress relaxation (constant strain loading condition) and temperature (no significant variation of body temperatures) are absolutely insignificant in the trocar insertion procedure. More over these biological tissues show nearly complete elastic recoveries. So, these tissues in this problem can be treated as *NEARLY INCOMPRESSIBLE, NEARLY ISOTROPIC, NON-LINEAR HYPERELASTIC* materials.

CHAPTER: 3

ABDOMINAL WALL ANATOMY AND TISSUE THICKNESS

Introduction

Studying the constitutive tissues (skin, fascia, muscles, nerves, veins & arteries) of anterior abdominal wall is the primary requisite to understand their role in structural integrity and deduce the engineering information such as tissue structural geometry, different layers dimensions, tissue layers orientations and the way different tissue layers are attached to each other. This study will also help in identifying the different topographical regions of significant variations in the abdominal wall anatomy for different regional finite element simulations.

3.2   Surface Anatomy of the Abdomen

Abdomen anatomy is projected onto the surface of abdomen to visualize the relative positions of abdominal organs as they lie within the abdomen. Clinicians do several different ways of subdividing the surface of the anterior abdominal wall, one of such ways are presented here. By subdividing the surface into regions, one person can tell another person exactly where to look for possible problems.

One of the ways of dividing the abdominal surface is into 9 regions. These regions are formed by two vertical planes and two horizontal planes. The two vertical planes are the lateral lines LLL and RLL. These lines are dropped from a point half way between the jugular notch and the acromion process. The two horizontal planes are the transpyloric

plane TPP and the transtubercular plane TTP. The tubercles are the tubercles of the iliac crests.
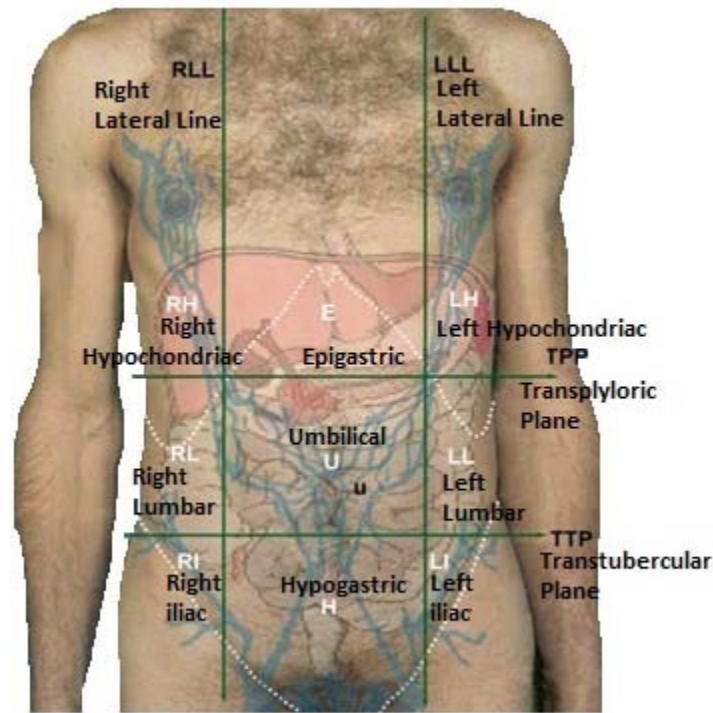
Fig 03.01: *Surface anatomy of abdominal wall with internal organs and veins projected on the wall. Adapted from Ref [37].*

3.3   Layers of the Abdominal Wall

When entering the abdominal cavity to remove or reconstruct something in the abdominal cavity it is essential to know where, specifically you want to enter. Knowing what makes up the wall of the abdomen is helpful in judging how deep one has gone with each knife cut and during trocar insertion.

The layers of the abdominal wall vary, depending on the regions. For instance, it is somewhat different along the lateral sides of the abdomen than it is at the anterior side. It is also somewhat different at its lower regions.

The anatomical layers of the abdominal wall include skin, subcutaneous tissue, superficial fascia, deep fascia, muscle, extraperitoneal fascia, and peritoneum. This anatomy may vary with respect to the different topographic regions of the abdomen. The major source of structural integrity and strength of the abdominal wall is provided by the musculofascial layer. The main paired abdominal muscles include the external oblique muscles, internal oblique muscles, transversus abdominis muscles, and rectus abdominis muscles and their respective aponeuroses, which are interdigitated with each other, and provide core strength and protection to the abdominal wall viscera.
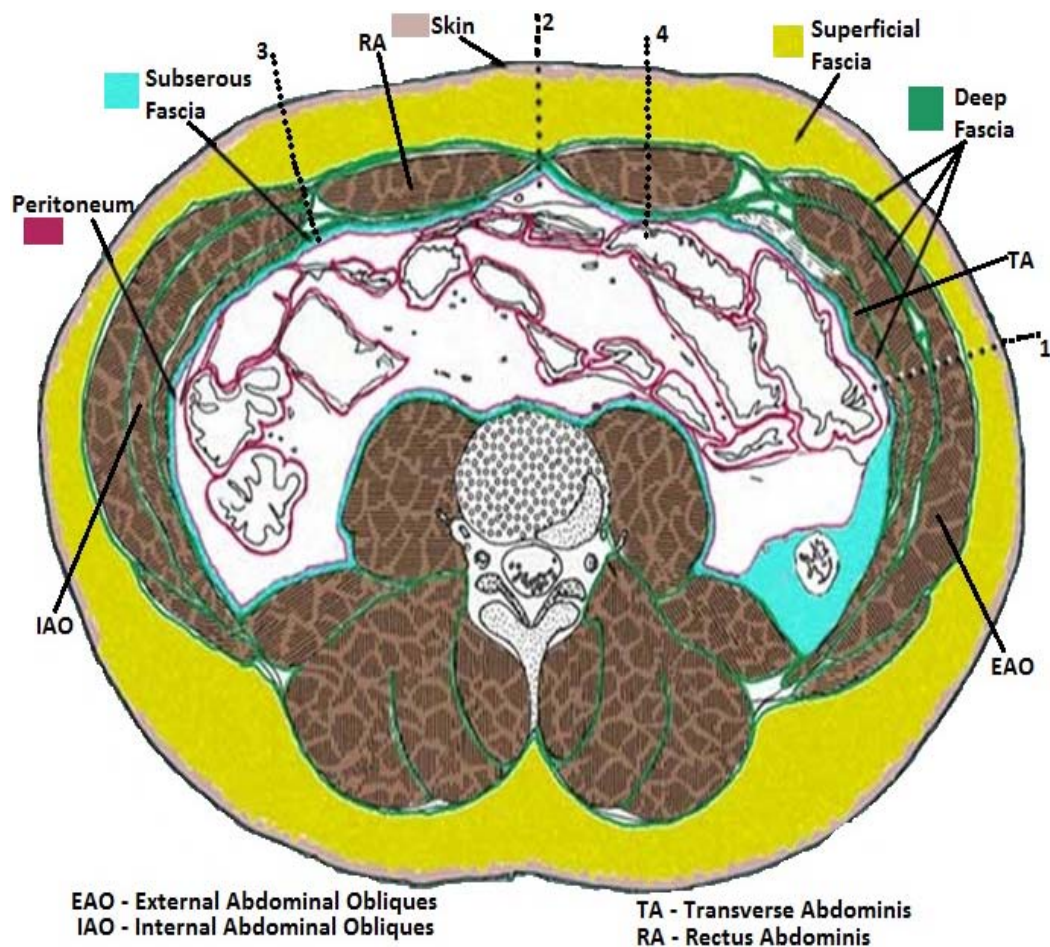
Fig 03.02: *Transverse section of the abdomen showing the different tissue layers of abdominal wall. Adapted from Ref [37].*

Lateral side of the abdomen there is a dotted line (1) passing through the abdominal wall skin, superficial fascia, deep fascia, muscles: external abdominal obliques, internal abdominal obliques, transverse abdominis, subserous fascia, peritoneum. At the anterior wall of the abdomen, in the midline (2) there is no muscle so the trocar would only go through the skin, superficial fascia, deep fascia (in this case a thickened area of deep fascia called the linea alba), subserous fascia and peritoneum. The line (3) at the semi lunaris as to only go through the skin, superficial fascia, deep fascia (in this case a thickened area of deep fascia called at semi lunar line), subserous fascia and peritoneum. Again through the line (4) a trocar would go through skin, superficial fascia, deep fascia, rectus abdominis muscle, subserous fascia and peritoneum.

3.3.1 Skin and Subcutaneous Tissues
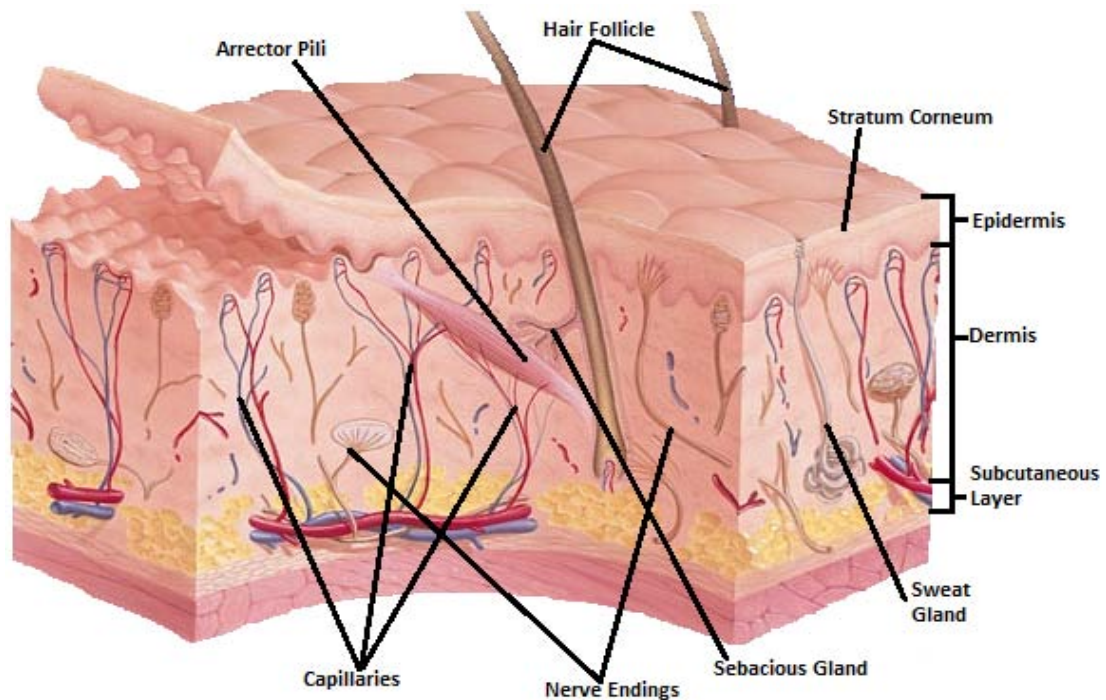
Fig 03.03: *Cut section of skin showing different tissue layers of skin.*
Adapted from Ref [39].

The epidermis is made up of several overlapping layers of skin cells. The outer layer contains dried, flattened cells rich with keratin, a protein also found in hair and fingernails that help retain moisture inside the skin and keep the skin surface waterproof. The lower epidermis is where new skin cells are produced. Epidermis cells are constantly sloughed off and replaced from below. The dermis is a strong, thick, flexible layer beneath the epidermis composed of connective tissue called collagen and elastin. This layer houses a network of tiny blood vessels that help in regulating body temperature, and pain. The dermis layer is also home of hair follicles and sweat glands. Underneath the dermis is the subcutaneous layer, a seam of fat used as fuel reserve as well as for insulation and cushioning. The skin is dotted with millions of tiny cavities called follicles. These pits originate in the dermis and are responsible for growing our body's coat of hair. They also channel to the surface a skin-softening oil called sebum. Capillaries are thin blood vessels that extend throughout the dermis layer and help regulate body temperature. When the body is warm, they widen to increase blood flow and aid heat transfer out of the skin. To warm the body, they narrow, decreasing blood flow and inhibiting heat transfer. Stratum corneum means "horny layer." It is the covering of flattened, dead skin cells the make up the topmost layer of the epidermis. Nerve endings relay messages between the skin and the brain. Nerves in the dermis come in two different forms: touch receptors that detect light touch and pressure receptors that detect pressure and vibrations. Arrector pili are the tiny muscles attached to the base of the hair follicles. They pull the hair upright and produce goose bumps when the body gets cold. Sebaceous glands are attached to each hair follicle. They produce oil called sebum, which moves to the surface and keeps the skin and hair soft and flexible. Every square

inch of skin contains about 650 sweat glands. These tiny ducts emit droplets of perspiration that cool the body as they evaporate. Sweat glands are also used by the body to remove certain waste materials from the blood.

3.3.2 Fascia

Fascia is a layer of fibrous tissue that permeates the human body. It interpenetrates and surrounds muscles, bones, organs, nerves, blood vessels and other structures. Fascia is an uninterrupted, three-dimensional web of tissue that extends from head to toe, from front to back, from interior to exterior

3.3.2.1 Superficial Fascia

The superficial fascia of the abdominal wall is divided into a superficial and a deep layer. It may be as thin as half an inch or less or as thick as 6 inches or more. Above the umbilicus, the superficial fascia consists of a single layer. Below the umbilicus, the fascia divides into two layers: the camper fascia and the scarpa fascia. Camper's fascia is a superficial fatty part that is continuous with the same layer over the rest of the body. Scarpa's fascia is a deep membranous layer that is continuous down into the perineum to surround the reproductive organ and to form a layer of the scrotum. The superficial epigastric neurovascular bundle is located between these two layers. The abdominal subcutaneous fat, which is separated by the scarpa fascia, is highly variable in thickness.
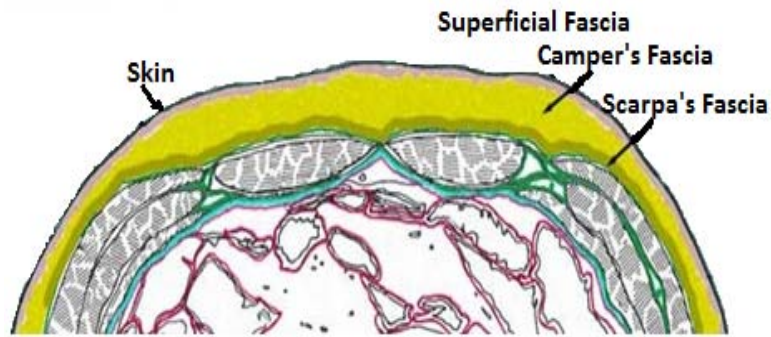
Fig 03.04: *Transverse section of abdomen showing the camper and scarpa fascias of superficial fascia. Adapted from Ref [37].*

3.3.2.2 Deep Fascia

The deep fascia is a thin, tough layer that surrounds and is adherent to the underlying abdominal muscles and all skeletal muscle is surrounded within its own deep fascia. The deep fascia of the abdominal wall is different than that found around muscles of the extremities, however. It is of the loose connective tissue variety. It is necessary in the abdominal wall because it offers more flexibility for a variety of functions of the abdomen. At certain points, this fascia may become aponeurotic and serve as attachments for the muscle to bone or to each other, as is the case at the linea alba.

3.3.2.3 Subserous Fascia

Subserous fasica is a layer of loose connective tissue that serves as a glue to hold the peritoneum to the deep fascia of the abdominal wall or to the outer lining of the gastrointestinal tract. It may receive different names depending on its location, i.e. transversalis fascia when it is deep to that muscle, psoas fascia when it is next to that muscles, iliac fascia, etc.

3.3.2.4 Peritoneal Fascia

Peritoneum is a thin one cell thick membrane that lines the abdominal cavity and in certain places reflects inward to form a double layer of peritoneum. Double layers of peritoneum are called mesenteries, omenta, falciform ligaments, lienorenal ligament, and other inter abdominal structures.

3.3.3 Muscles of the Abdominal Wall

Muscles that make up the anterior and anterolateral abdominal wall are considered. The abdominal wall includes five paired muscles; three flat muscles and two vertical muscles. The three flat muscles are the external oblique, internal oblique, and transversus abdominis. The three layered structure, combined with extensive aponeuroses, works in a synkinetic fashion not only to protect the abdominal viscera but also to increase abdominal pressure. The two vertical muscles are the rectus abdominis and pyramidalis. Fusion of the fascial layers of these muscles forms three distinct fascial lines: the linea alba and two semilunar lines. The linea alba is formed by the fusion of both rectus sheaths at the midline, while the semilunar lines are formed by the union of the external oblique, internal oblique, and transversus abdominis aponeuroses at the lateral border of the rectus abdominis muscle.

In the following figures muscle layers are carefully removed to see the deeper levels. In the deeper layers, there are cutaneous veins and nerves that travel in the layers.
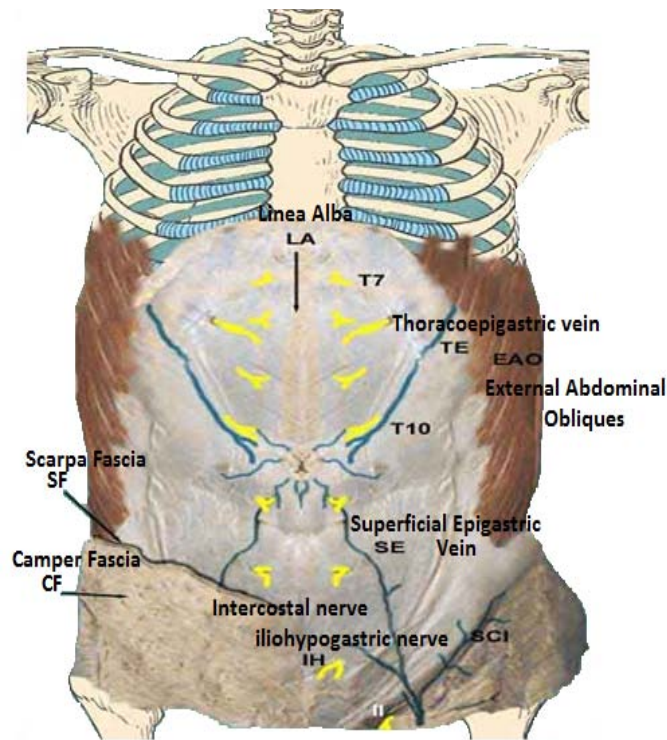
Fig 03.05: *Showing camper fascia, scarpa fascia, external abdominal obliques, linea alba and abdominal veins. Adapted from Ref [37].*

The most superficial layer of anterolateral muscles are the external abdominal obliques. On the right side of the specimen that the lower part of the superficial fascia has been left behind to show its two layers, the fatty layer camper's fascia and the membranous layer scarpa's fascia. Running through the fatty layer are the superficial veins, the superficial epigastric, the paraumbilical veins radiating out from the umbilicus and the thoracoepigastric vein. The cutaneous nerves to the abdomen are mainly continuations of the lower intercostal nerves T7 - T12, i.e. thoracic vertebrae rami branch 7-12. The umbilical region is supplied by the 10th intercostal nerve. The lowermost part of the abdominal wall is supplied by a branch of L1, i.e. lumbar, the iliohypogastric nerve. Its other branch is the ilioinguinal II nerve. The aponeuroses of the external abdominal oblique, internal abdominal oblique, and transverse abdominis muscles converge at the midsagittal part of the abdominal wall to form a white line called linea alba. It is located

28

from xiphoid to pubis. The linea alba is a three dimensional composition of tendon fibers from abdominal wall muscles.

The external oblique muscle is the largest and thickest of the flat abdominal wall muscles. It originates from the lower eight ribs, interlocks with slips of latissimus dorsi and serratus anterior, and courses inferior-medially, attaching via its aponeurosis centrally at the linea alba. Inferiorly, the external oblique aponeurosis folds back upon itself and forms the inguinal ligament between the anterior superior iliac spine and the pubic tubercle. Medial to the pubic tubercle, the external oblique aponeurosis is attached to the pubic crest. Traveling superior to the medial part of the inguinal ligament, an opening in the aponeurosis forms the superficial inguinal ring. The innervation to the external oblique is derived from the lower 6 thoracic anterior primary rami branch and the first and second lumbar anterior primary rami branch.
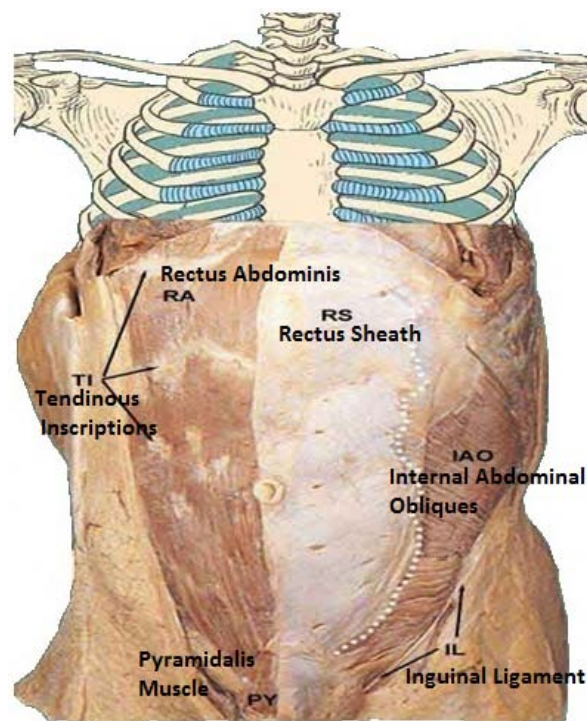
Fig 03.06: Showing rectus abdominis, rectus sheath, internal abdominal obliques, and pyramidalis muscle. Adapted from Ref [37].

In the Fig 03.06, the left external abdominal oblique has been cut away at the white dotted line and removed to show the internal abdominal oblique. Lower cut edge of the external abdominal oblique at the inguinal ligament is also shown. The anterior wall of the rectus sheath has also been removed on the right side in order to show the underlying right rectus abdominis muscle. The rectus abdominis muscle is subdivided into small sections by tendinous inscriptions. A small muscle, pyramidalis muscle, is also shown overlying the inferior end of the rectus abdominis muscle. This small muscles tenses the lower part of the linea alba.

The internal oblique muscle originates from the anterior portion of the iliac crest, lateral half to two-thirds of the inguinal ligament, and posterior aponeurosis of the transversus abdominis muscle. The internal oblique fibers run superior-anteriorly at right angles to the external oblique and insert on the cartilages of the lower four ribs. The anterior fibers become aponeurotic at around the ninth costal cartilage. At the lateral border of the rectus abdominis muscle and above the arcuate line, the aponeurosis splits anteriorly and posteriorly to enclose the rectus muscle to help form the rectus sheaths. However beneath the arcuate line, the internal oblique aponeurosis does not split, resulting in an absent posterior rectus sheath. The inferior aponeurotic fibers arch over the spermatic cord, pass through the inguinal canal and then descend posterior to the superficial ring to attach to the pubic crest. The most inferior medial tendinous fibers fuse with the aponeurotic fibers of the transversus abdominis muscle to form the conjoint tendon, which also inserts on the pubic crest.

The rectus abdominis muscles are paired, long, straplike muscles that are the principal vertical muscles of the anterior abdominal wall. The rectus abdominis is interrupted

throughout its length by three to four tendinous inscriptions, all of which are adherent to the anterior rectus sheath and separated by the linea alba. These inscriptions can be visualized externally in a well-developed individual secondary to fasciocutaneous ligaments. The medial tendon of the rectus abdominis originates from the pubic symphysis and the lateral tendon of the rectus abdominis originates from the pubic crest. It inserts to the anterior surfaces of the fifth, sixth, and seventh costal cartilages and xiphoid process. The lateral border of each rectus muscle and its sheath merge with the aponeurosis of the external oblique to form the linea semilunaris. The rectus abdominis muscle functions as a tensor of the abdominal wall and flexor of the vertebrae. Additionally, this muscle helps to stabilize the pelvis during walking, protects the abdominal viscera, and aids in forced expiration.

The rectus sheath is a strong, semifibrous compartment that houses the rectus muscles, the superior and inferior epigastric vessels, and the inferior five intercostal and subcostal nerves. It is formed by interlacing aponeurotic fibers from the three flat abdominal muscles. The anterior rectus sheath is the union of the external oblique aponeurosis and the anterior layer of the internal oblique.

The linea semilunares can be seen as a pair of linear impressions in the skin that correspond with the most lateral edges of the rectus abdominis. These lines are visible in a person who is physically fit but obscured in a person who is obese. They are formed by the band of aponeuroses of the external oblique, the internal oblique, and the transversus abdominis muscles.

The pyramidalis is a small triangular muscle located anterior to the inferior aspect of the rectus abdominis; the pyramidalis is absent in some people. The pyramidalis originates from the body of the pubis directly inferior to the insertion of the rectus abdominis and inserts into the linea alba inferior to the umbilicus to assist in stabilization of the lower midline.
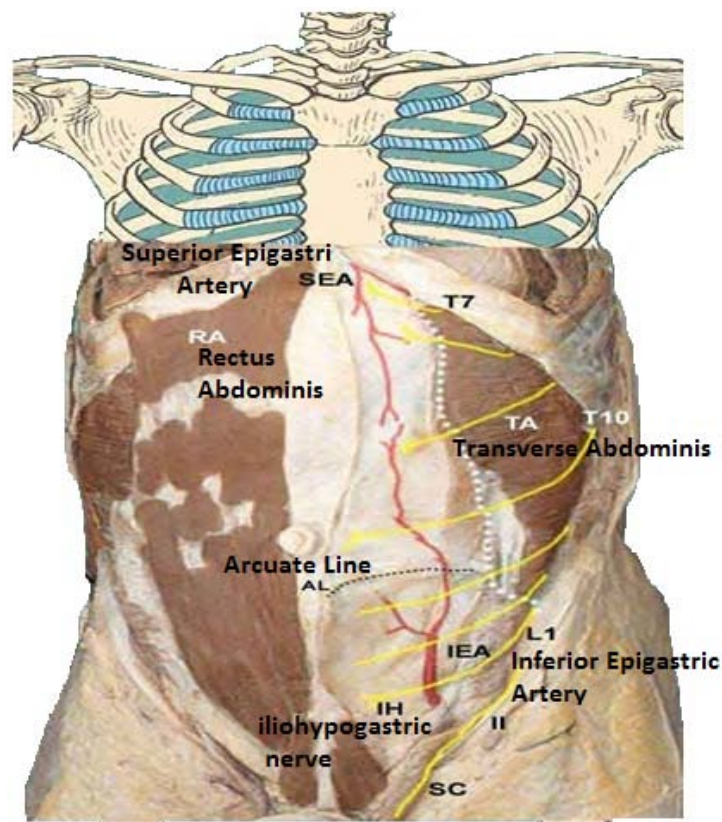
Fig 03.07: *Anatomy showing the transverse abdominis, rectus abdominis, arcuate line, arteries & veins. Adapted from Ref [37].*

In the Fig 03.07, the rectus abdominis muscle, internal abdominal oblique and anterior rectus sheath are removed. The posterior rectus sheath and its lower free margin, the arcuate line are seen. Below arcuate line is the transversalis fascia and running in the fascia is the inferior epigastric artery, a branch of the external iliac artery. This artery enters the rectus sheath posterior to the rectus abdominis muscle and supplies the anterior

abdominal wall. Extending from the top, is a branch of the internal thoracic or mammary artery, the superior epigastric artery. The cutaneous nerves are found to lie between the internal abdominal oblique and the transversus abdominis muscles.

The transversus abdominis muscle is the innermost of the three flat abdominal muscles. The fibers of the transversus abdominis course predominately in a horizontal orientation. It has two fleshy origins and one aponeurotic origin. The first fleshy origin is from the anterior three-fourths of the iliac crest and lateral third of the inguinal ligament, while the second origin is from the inner surface of the lower six costal cartilages where they interdigitate with fibers of the diaphragm. Between the two fleshy origins is the aponeurotic origin from the transverse processes of the lumbar vertebrae. These fibers course medially to the lateral border of the rectus muscle. From about 6.6 cm inferior to the xiphoid process to the arcuate line, the insertion is aponeurotic and contributes to the formation of the posterior rectus sheath. Above the arcuate line, the anterior rectus fascia exists anterior to the rectus muscle, and the posterior rectus fascia is posterior to the rectus muscle. Below the arcuate line, the three aponeuroses merge together to form exclusively the anterior rectus sheath, with little or no posterior sheath. The arcuate line is generally located two fingerbreadths from the umbilicus to midway between the umbilicus and pubis. However, some reports in the literature state that the arcuate line is closer to 75% of the distance between the pubic crest and the umbilicus or 1.8 cm superior to the anterior superior iliac spine.

3.3.4 Vascular Supply and Innervation

The plane between the internal oblique muscle and transversus abdominis muscle contains the neurovascular structures that supply the abdominal muscles. The superior

and inferior deep epigastric vessels enter the rectus muscle superiorly and inferiorly. Transperitoneal vessels enter the rectus in the periumbilical region. The abdominal wall receives its blood supply from direct cutaneous vessels and musculocutaneous perforating vessels. The two subdivisions of perforators course medially and laterally. The lateral branch is usually the dominant branch and contains most of the perforator vessels. The lateral fasciocutaneous perforators pierce the aponeuroses of the internal and external oblique muscles. They may pass through the linea alba and emerge on the lateral aspect of the rectus abdominis.

Sensory innervation to the abdomen is derived from the roots of the nerves T7 to L4. These nerves travel in the plane between the internal oblique and transversus abdominis muscles. Motor innervation is provided by the intercostal, subcostal, iliohypogastric, and ilioinguinal nerves. These nerves must be preserved during abdominal wall reconstruction in order to maintain abdominal wall sensation and muscular function.
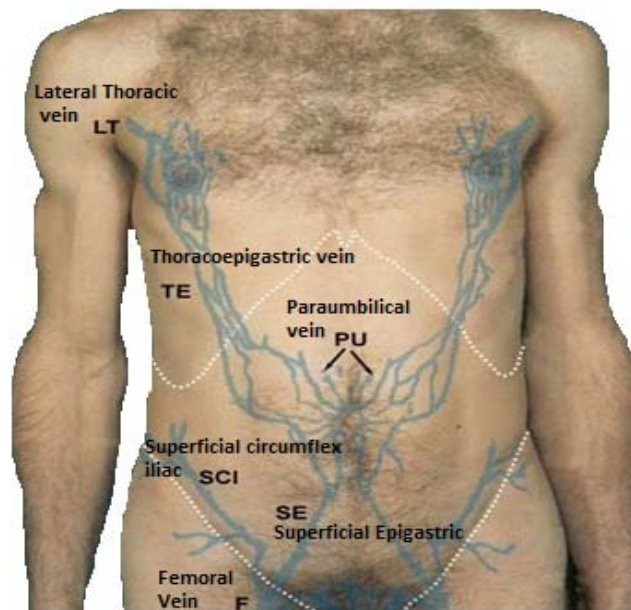
Fig 03.08: *Surface anatomy of the abdominal wall showing various veins. Adapted from Ref [37].*

Superficial veins in the abdominal wall drain into one of two major veins, Subclavian or Femoral and also into a minor, the paraumbilical vein. The paraumbilical vein drains into the portal vein and then through the liver. The lower abdominal wall is drained by way of the superficial epigastric and superficial circumflex iliac veins into the femoral vein. The upper abdominal wall is drained by way of the thoracoepigastric and lateral thoracic veins into the subclavian.

3.4   Abdominal Anatomy Summary

Fig 03.09: *Showing the abdominal wall divided into four different regions for finite element simulations. Adapted from Ref [40].*

Above figure shows the identification of different topographical regions of significant variations in the abdominal wall anatomy for different regional finite element simulations.

REGION - 1

Skin
Superficial Fascia
Deep Fascia
External Abdominal Obliques
Deep Fascia
Internal Abdominal Obliques
Deep Fascia
Transverse Abdominis
Deep Fascia
Subserous Fascia
Peritoneum

REGION - 2

Skin
Superficial Fascia
Deep Fascia (Linea Alba)
Subserous Fascia
Peritoneum

REGION - 3

Skin
Superficial Fascia
Deep Fascia (Semi-lunaris
Subserous Fascia
Peritoneum

REGION - 4

Skin
Superficial Fascia
Deep Fascia
Rectus Abdominis
Deep Fascia
Subserous Fascia
Peritoneum

Fig 03.10: Showing the layers of four different regions for finite element simulations.

SKIN

- **EPIDERMIS** (Overlapping layers of skin cells)
  - Upper layer of dead skin cells
  - Below layer of new cells
- **DERMIS** (Strong, thick, flexible layer of connective tissue composed of collagen & Elastin and houses a network of tiny blood vessels - arteries, veins and nerves)
- **SUBCUTANEOUS LAYER** (This fat layer is highly variable in thickness)

Fig 03.11: Skin anatomy summary.

36

FASCIA

fibrous tissue, 3-D web of tissue that extends from head to toe, from front to back, from interior to exterior

SUPERFICIAL FASCIA

As thin as 1/2 inch to as thick as 6 inches

Single layer above umbilicus - Camper's Fascia (fatty layer)

Neurovascular bundle between Camper's and Scarpa's Fascias

Two layers Camper's fascia (fatty layer) and Scarpa's fascia (membranous layer)

DEEP FASCIA

(deep fascia may become aponeurotic and serve as attachments for the muscle to bone or to muscle to muscle, as is the case at linea alba)

SUBSEROUS FASCIA

(Its a loose connective tissue and serves as a glue to hold the peritoneum to the deep fascia of the abdominal wall or to the outer lining of the gastrointestinal tract)

PERITONEAL FASCIA

(Thin one cell thick membrane that lines the abdominal cavity)

Fig 03.12: Fascia anatomy summary.

MUSCLES
(Abdominal wall inculdes 5 paired of muscles 3- flat & 2 vertical muscles)

3 - Flat Muscles

External abdominal obliques
(Most superficial layer of anterolateral muscles, its largest & thickest of the flat abdominal wall muscles)

Internal abdominal obliques
(Internal oblique fibers run superior-anteriorly at right angles to the external abdominal obliques)

Transversus abdominis
(Innermost of the three flat abdominal muscles, fibers course predominantly in a horizontal orientation)

2 - Vertical Muscles

Rectus Abdominis
(Paired, long, straplike muscles that are the principal vertical muscles of the anterior abdominal wall. It is interrupted throughout its length by 3 to 4 tendinous inscriptions, the inscriptions are adherent to anterior rectus sheath and separated by linea alba

Pyramidalis
(small triangular muscle located anterior to the inferior aspect of the rectus abdominis)

Fusion of fascial layers of these muscles form 3 distinct fasical lines - Linea alba & two semilunaris lines

Linea Alba
(Fusion of both the rectus sheath at the midline, it is a three dimensional composition of tendon fibers from abdominal wall muscles)

Two - Semilunaris lines
(Fusion of external oblique, internal oblique and transverse abdominis aponeuroses, they are pair of linear impressions in the skin that corresponds with the most lateral edges of the rectus abdominis

Fig 03.13: Abdominal wall muscles anatomy summary.

3.5   Tissue Thickness and Regional Variations

Assuming the thickness of subcutaneous tissue and muscles of average mid age group persons as a standard, then the following thickness variation amongst different age group and gender of nearly same Body Mass Index (BMI) are qualitatively derived from, Ref [41].

Age and Sex Variation Parameter : AS_1				
Tissue	**Subcutaneous Fat**		**Abdominal Muscles**	
Sex / Age group	Male	Female	Male	Female
Young (15 -34 years)	0.88	1.08	1.19	0.95
Mid Age (35-54 years)	1	1.53	1	0.79
Elderly (50-80 years)	1.13	1.89	0.81	0.62

Table 03.01: *Variation of abdominal tissues thickness amongst the different age group and gender for same BMI. Derived from Ref [41].*

Within a same age group, tissues thicknesses differ depending on the Body Mass Index (BMI) of the person.

BMI Type Parameter: BT_2	
BMI Category	**Value (Kg/m^2)**
Underweight	< 18.5
Normal weight	18.5 – 24.9
Overweight	25.0 – 29.9
Obesity	BMI of 30 or greater

Table 03.02: *BMI Category classification with numerical values. Adapted from Ref [42].*

$Z = (-1)^N \cdot B$; $B = (N/100)$; where N is an integer random number between 0 and 100.

Maximum Tissue Thickness Parameter: MT₃					
BMI Type	Subcutaneous Fat thickness (mm)	Rectus Abdominis thickness (mm)	Internal Obliques thickness (mm)	External Obliques thickness (mm)	Transverse Abdominis thickness (mm)
Underweight	$10 + Z \cdot 4$	$8 + Z \cdot 2$	$8 + Z \cdot 2$	$5 + Z \cdot 2$	$4 + Z \cdot 2$
Normal weight	$17 + Z \cdot 4$	$14 + Z \cdot 2$	$11 + Z \cdot 2$	$8 + Z \cdot 3$	$7 + Z \cdot 3$
Overweight	$22 + Z \cdot 4$	$13 + Z \cdot 4$	$12 + Z \cdot 2$	$10 + Z \cdot 2$	$8 + Z \cdot 3$

Table 03.03: *A qualitatively maximum tissue thickness for different BMI Categories. Derived from, Ref [41], [43], [44], [45].*

Skin, Deep fascia, Subserous fascia, Peritoneum tissues thickness does not vary significantly with the age, sex and BMI. They show regional thickness variations.

Maximum Tissue Thickness Parameter: MT₄			
Layers	Region - 1 Thickness (mm)	Layers	Region - 2 Thickness (mm)
Skin	2	Skin	2
Deep Fascia – $R_{1,1}$	1.6	Deep Fascia – $R_{2,1}$	4.2
Deep Fascia – $R_{1,2}$	1	Subserous Fascia	2
Deep Fascia – $R_{1,3}$	1	Peritoneum	0.4
Subserous Fascia	2	-	-
Peritoneum	0.4	-	-

Table 03.04: *Regional 1 & 2, maximum thicknesses of skin, deep fascias, subserous fascia and peritoneum. Derived from Ref [30], [37].*

Maximum Tissue Thickness Parameter: MT_4			
Layers	**Region - 3 Thickness (mm)**	**Layers**	**Region - 4 Thickness (mm)**
Skin	2	Skin	2
Deep Fascia – $R_{3,1}$	3.6	Deep Fascia – $R_{4,1}$	1.6
Deep Fascia – $R_{3,2}$	1.6	Deep Fascia – $R_{4,2}$	1.6
Deep Fascia – $R_{3,3}$	1.6	Subserous Fascia	2
Subserous Fascia	2	Peritoneum	0.4
Peritoneum	0.4	-	-

Table 03.05: *Regional 3 & 4, maximum thicknesses of skin, deep fascias, subserous fascia and peritoneum. Derived from Ref [30], [37].*

Regional Percentage Variation Parameter: RV_5			
Layer	**Region – 3 % Variations**	**Layer**	**Region – 4 % Variations**
Skin	B·10	Skin	- B·10
Superficial Fascia	- B·10	Superficial Fascia	- B·10
Deep Fascia – $R_{3,1}$	- B·10	Deep Fascia – $R_{4,1}$	- B·10
Fat	- B·10	Rectus Abdominis	- B·300
Deep Fascia – $R_{3,2}$	- B·10	Deep Fascia – $R_{4,2}$	- B·10
Fat	- B·10	Subserous Fascia	- B·10
Deep Fascia – $R_{3,3}$	- B·10	Peritoneum	- B·10
Subserous Fascia	- B·10	-	-
Peritoneum	- B·10	-	-

Table 03.06: *Regional 3 & 4, within the region type percentage thicknesses variations of the tissue layers. Derived from Ref [30], [37].*

Regional Percentage Variation Parameter: RV_5			
Layer	**Region – 1 % Variations**	**Layer**	**Region – 2 % Variations**
Skin	- B·10	Skin	- B·10
Superficial Fascia	- B·25	Superficial Fascia	- B·10
External Abdominal Obliques	- B·50	Deep Fascia – $R_{2,1}$	- B·10
Deep Fascia – $R_{1,1}$	- B·10	Subserous Fascia	- B·10
Internal Abdominal Obliques	- B·45	Peritoneum	- B·10
Deep Fascia – $R_{2,1}$	- B·10	-	-
Transverse Abdominis	- B·55	-	-
Deep Fascia – $R_{3,1}$	- B·10	-	-
Subserous Fascia	- B·10	-	-
Peritoneum	- B·10	-	-

Table 03.07: Regional 1 & 2, within the region type percentage thickness variations of the tissue layers. Derived from Ref [30], [37].

3.5.1 Sample Tissue Thickness Workout

Given: Sex: Male, Age: 40 and BMI Type: Normal Weight

Required: Tissue layers thicknesses in Region-1

Workout:

AS_1 Parameter = 1 for both subcutaneous fat and muscles

BT_2 Parameter = Normal weight

For random number N=50, B= 0.5, Z = 0.5

MT_3 Parameter

    Max. Subcutaneous fat thickness = 17 + 0.5 x 4 = 19 mm

    Max. Rectus Abdominis thickness = 14 + 0.5 x 2 = 15 mm

    Max. Internal Obliques thickness = 11+ 0.5 x 2 = 12 mm

    Max. External Obliques thickness = 8+ 0.5 x 3 = 9.5 mm

    Max Transverse Abdominis thickness = 7+ 0.5 x 3 = 8.5 mm

MT_4 Parameter: Region -1

    Max. Skin Thickness = 2 mm

    Deep Fascia – $R_{1,1}$ = 1.6 mm

    Deep Fascia – $R_{1,2}$ = 1 mm

    Deep Fascia – $R_{1,3}$ = 1 mm

    Subserous Fascia = 2 mm

    Peritoneum = 0.4 mm

RV$_5$ Parameter: Region -1

Skin	- 5.0 %
Superficial Fascia	- 12.5 %
External Abdominal Obliques	- 25.0 %
Deep Fascia – R$_{1,1}$	- 5.0 %
Internal Abdominal Obliques	- 22.5 %
Deep Fascia – R$_{2,1}$	- 5.0 %
Transverse Abdominis	- 27.5 %
Deep Fascia – R$_{3,1}$	- 5.0 %
Subserous Fascia	- 5.0 %
Peritoneum	- 5.0 %

Therefore final tissue layer thicknesses are as follows

Skin	1.9 mm
Superficial Fascia	16.2 mm
External Abdominal Obliques	7.1 mm
Deep Fascia – R$_{1,1}$	1.5 mm
Internal Abdominal Obliques	9.3 mm
Deep Fascia – R$_{2,1}$	0.9 mm
Transverse Abdominis	6.2 mm
Deep Fascia – R$_{3,1}$	0.9 mm
Subserous Fascia	1.9 mm
Peritoneum	0.4 mm

CHAPTER 4

TISSUE CONSTITUTIVE MODELS

Introduction

For accurate simulation of soft tissues it is important to find realistic biomechanical models which closely imitate the tissue behaviors. At the same time one should reduce the models according to the problem specific needs. Some inevitable assumptions and reductions in models occurring due to limitations of availability of material properties should also be well accommodated to the problem needs. For the trocar insertion problem, owing to the lack of 3D material data and closely analyzing the problem needs some reduction in the available realistic soft tissue models are proposed.

Ref [47] proposes the following soft tissue models. Soft Tissue Model for Fascia, MAT 91. It is transversely isotropic hyperelastic model. The complexity of this model is able to realistically model fascial tissues in 3D. But for the problem of trocar insertion, this model is an overabundance and computationally intensive. Similarly, the Skeletal Muscle Model, MAT S15 is a modified Hill type muscle model which works for different activation levels. As there is no activation of muscles during trocar insertion again the model is an overabundance. The MAT 176, Quasilinear viscoelastic model based on hyperelastic model is more suitable to the problem. It accounts for both larger deformations through hyperelasticity and also viscoelastic nature of the soft tissue. A similar model with some reduction is what is expected of this problem.

4.2   Quasilinear Hyperelastic Viscoelastic Model

The material model MAT 176, Form = 1, is based on hyperelastic model and assumes isotropy and incompressibility. It accounts for both hyperelastic stress and viscoelastic stress, with one dimensional data, as follows

$$\sigma(\varepsilon,t) = \sigma_{hyp}(\varepsilon) + \sigma_{vis}(t) \qquad\qquad ----(C4:01)$$

$$\sigma_{vis}(t) = \int_{0}^{t} G(t-\tau)\frac{\partial\varepsilon}{\partial\tau}d\tau \qquad\qquad ----(C4:01)$$

$$\sigma_{hyp} : hyperelastic\ stress$$
$$\sigma_{vis} : viscoelastic\ stress$$

As the time taken for trocar insertions are small, the time dependence of stresses of the problem is not significant and hyperelastic stresses are more prominent and significant during tissue cutting than the viscoelastic time dependent stresses. The hyperelatic part of the total stress is discussed in chapter 6.

CHAPTER: 5

MATERIAL PROPERTIES TREATMENT

Introduction

Biological materials, organs and tissues, show stable and constant strength values in mechanically stabilized state (MSS). For mechanical stabilization, specimen are put in a physiological saline solution and stored in a refrigerator overnight or longer. Mechanical stabilization is mainly by saturation with water and disappearance of rigor mortis for smooth and skeletal muscles. This MSS of tissues can also be obtained by preconditioning with repetitive loading before testing. Almost all biological testing and already available data are in mechanically stabilized state.

Biological tissues, skin, panniculus adiposes, muscles, fascias are high strain exhibiting non-linear viscoelastic materials. The loading situations such as creep (constant stress loading condition), hysteresis (cycling loading condition), stress relaxation (constant strain loading condition) and temperature (no significant variation of body temperatures) are absolutely insignificant in the trocar insertion procedure. More over these biological tissues show nearly complete elastic recoveries. So, these tissues in this problem can be treated as *NEARLY INCOMPRESSIBLE, NEARLY ISOTROPIC, NON-LINEAR HYPERELASTIC* materials.

According to the problem in hand, there is need for a specific set of material properties and its variations are to be considered. For the current problem, the specific set of properties and variations required are enumerated in the following flow diagram.

```
                    ┌─────────────────────────┐
                    │      TISSSUE TYPE        │
                    │    Parameter: T₁         │
                    └─────────────────────────┘
                              │
                              ▼
┌───────────────────────────────────────────────────────────────┐
│  ┌─────────┐ ┌──────────────┐ ┌──────────┐ ┌────────┐ ┌──────────┐ │
│  │ Tissue-1│ │  Tissue-2    │ │ Tissue-3 │ │Tissue-4│ │ Tissue-5 │ │
│  │  Skin   │ │ Subcutaneous │ │ Skeletal │ │ Fascia │ │Peritoneum│ │
│  │         │ │    Fat       │ │  Muscle  │ │        │ │          │ │
│  └─────────┘ └──────────────┘ └──────────┘ └────────┘ └──────────┘ │
└───────────────────────────────────────────────────────────────┘
```

TISSSUE TYPE
Parameter: T_1

Tissue-1 Skin
Tissue-2 Subcutaneous Fat
Tissue-3 Skeletal Muscle
Tissue-4 Fascia
Tissue-5 Peritoneum

SEXUAL DIFFERENCE
Parameter: S_2

MALE   FEMALE

AGE
Parameter: A_3

Age
Ranging from 10 to 80 years

PERSON BUILT
Parameter: B_4

Under Weight
Normal Weight
Over Weight

Fig 05.01: Flow diagram of the tissue properties and its variations considered for the laparascopic trocar insertion problem.

5.2   Skeletal Muscle Tensile Data Treatment (MSS data only)
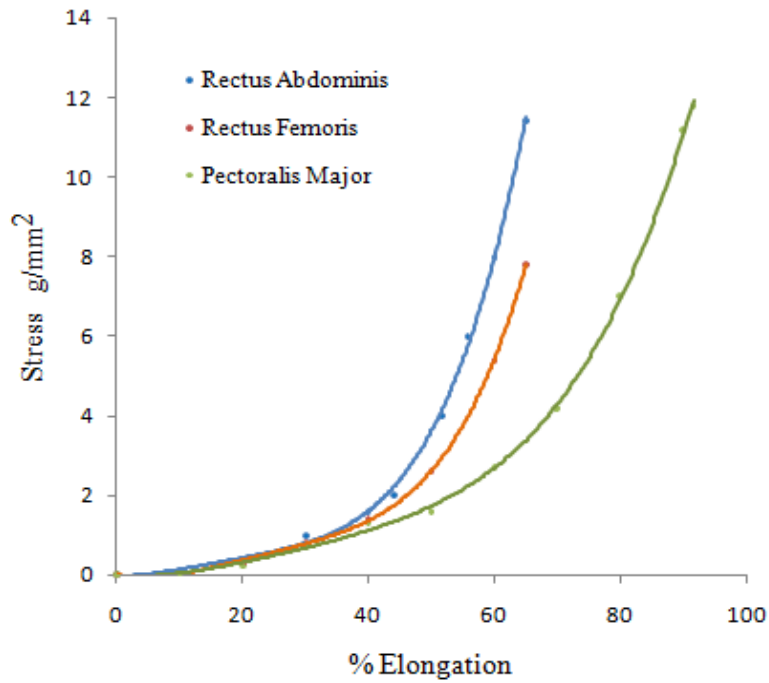
Fig 05.02: *Tensile stress-strain curves of skeletal muscle tissues of 29 years of age persons. Adapted from Ref [29].*
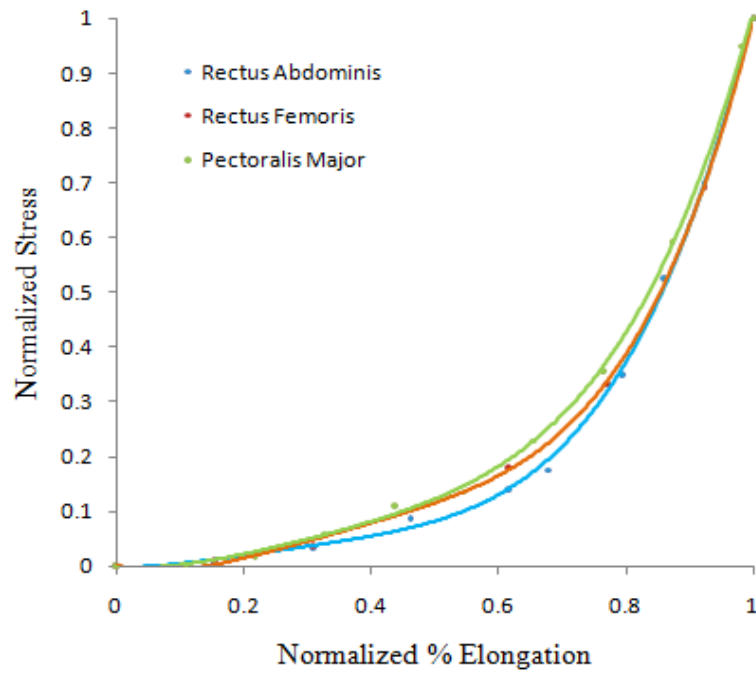
Fig 05.03: *Normalized tensile stress-strain curves of skeletal muscle tissues.*
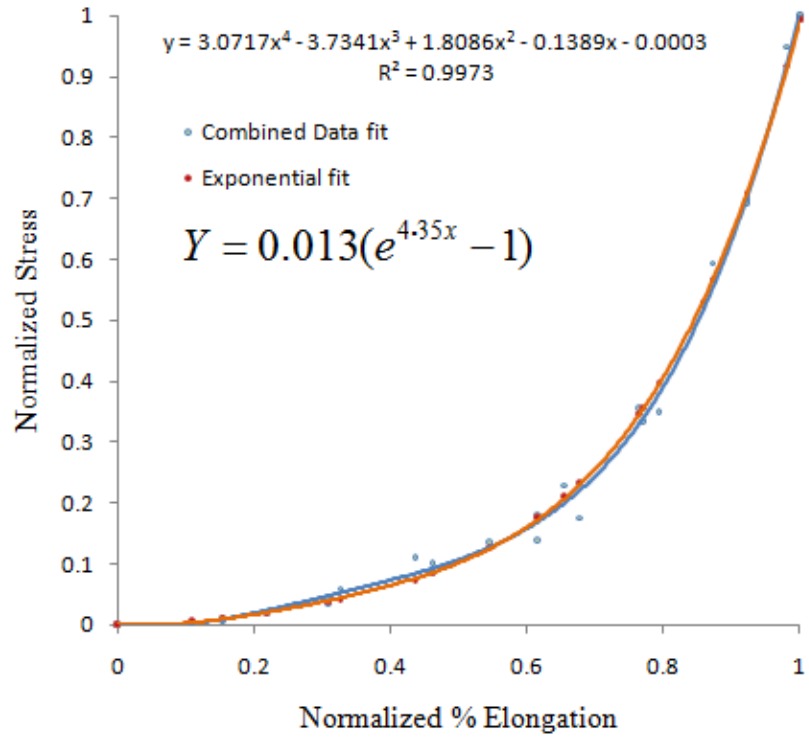
Fig 05.04: *Normalized tensile stress-strain curves of skeletal muscles with polynomial and exponential data fit.*
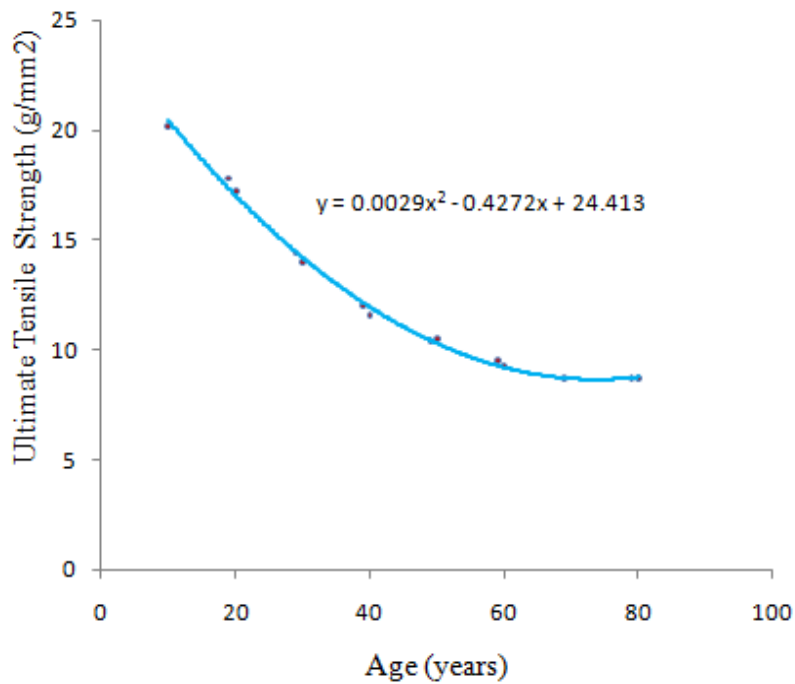
Fig 05.05: *Age difference of Ultimate Tensile Strength (UTS) of skeletal muscle-rectus abdominis muscle.*
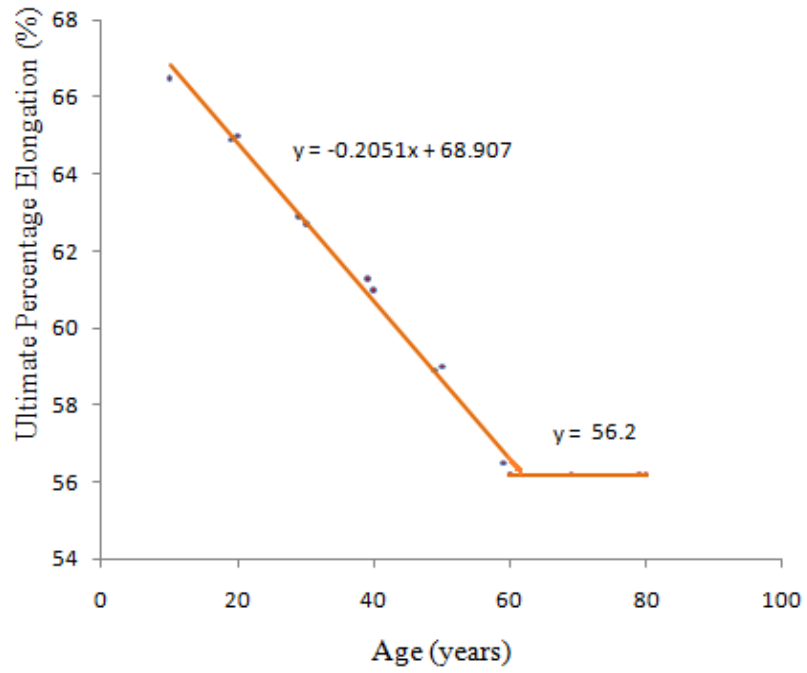
Fig 05.06: Age difference of tensile Ultimate Percentage Elongation (UPE) of
skeletal muscle-rectus abdominis muscle.
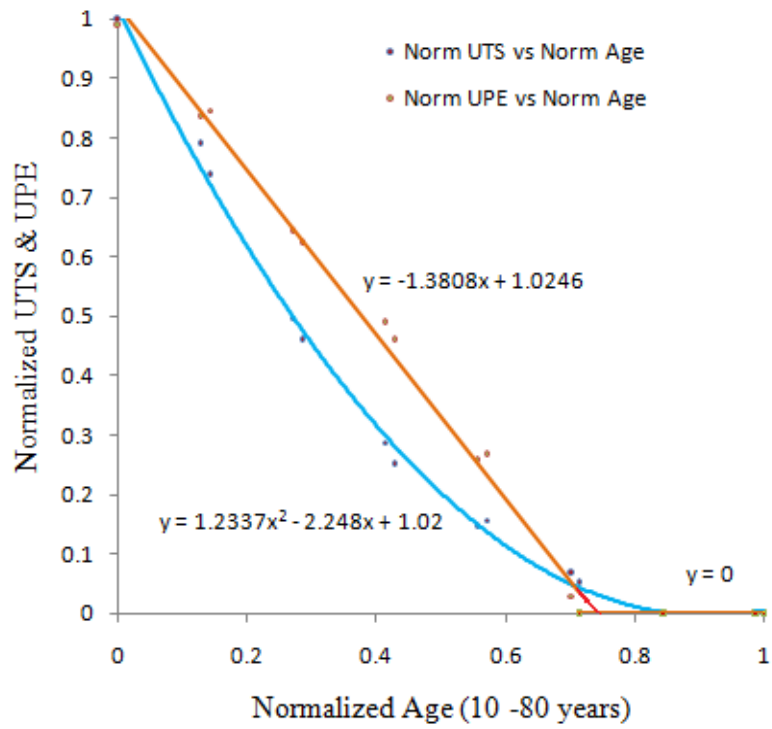
Fig 05.07: Normalized age difference of tensile UTS & UPE of skeletal muscle-
rectus abdominis muscle.

For abdominal skeletal muscles, % Elongation and Stress relation is as follows

$$\% \ Elongation = (UPE) \cdot x \qquad\qquad\qquad ----(C5:01)$$

$$Stress = (UTS) \cdot Y = (UTS) \cdot [0.013(e^{4.35x} - 1)] \qquad ----(C5:02)$$

$$where, \ \ x: fraction \ between \ 0 \ and \ 1$$
$$UPE = T_{1UPE} \ ; \ UTS = T_{1UTS}$$

5.2.1 Tissue Type Parameter (T_1)

Abdominal skeletal muscles, rectus abdominis, external obliques, internal obliques and transverse abdominis show similar mechanical properties with slight variations. Following are the formulas to obtain UTS and UPE for these skeletal muscles. A variation range of $\pm$ 2.8 g/mm^2 for UTS and $\pm$ 12% for UPE form *Ref [29]* are taken.

$$T_{1UTS} = D_{8UTS} + (-1)^N (B \times 2.8) \qquad\qquad ----(C5:03)$$

$$T_{1UPE} = D_{8UPE} + (-1)^N (B \times 12) \qquad\qquad ----(C5:04)$$

$$B = \frac{N}{100} \qquad\qquad\qquad ----(C5:05)$$

$$Where,$$
$$N = N(t) \ is \ a \ random \ number \ between \ 0 \ and \ 100$$
$$generated \ in \ every \ chosen \ time \ step \ \Delta t$$
$$B : random \ fractional \ number \ between \ 0 \ and \ 100$$

5.2.2 Sexual Difference Parameter (S_2)

There is no significant sexual difference in the ultimate strength and ultimate % elongation of skeletal muscles. Hence the parameter equals the age parameter in value.

$$S_{2UTS} = A_{3UTS} \quad\quad\quad\quad ----(C5:06)$$

$$S_{2UPE} = A_{3UPE} \quad\quad\quad\quad ----(C5:07)$$

5.2.3 Age Parameter (A₃)

From the given age of a person expected average UTS and UPE are derived from the plots in the *Fig 05.05*, *Fig 05.06*. It can be observed that within the age range of 10-80 years, younger age, 10 year old show greater UTS and UPE. For any age within the range, UTS and UPE can be calculated as follows.

$$A_{3UTS} = UTS_{80} + (UTS_{10} - UTS_{80}) \times \left[(1.2337 \times a^2) - (2.248 \times a) + 1.02 \right]$$
$$= 8.7 + 11.5 \times \left[(1.2337 \times a^2) - (2.248 \times a) + 1.02 \right]$$
$$----(C5:08)$$

If age < 60
$$A_{3UPE} = UPE_{60} + (UPE_{10} - UPE_{60}) \times \left[(-1.3808 \times a) + 1.0246 \right]$$
$$= 56.2 + 10.3 \times \left[(-1.3808 \times a) + 1.0246 \right] \quad ----(C5:09)$$

If age ≥ 60
$$A_{3UPE} = 56.2 \% \quad\quad\quad\quad ----(C5:10)$$

$$a = \frac{(Age - 10)}{(80 - 10)} \quad\quad\quad\quad ----(C5:12)$$

Where 'a' is a variable between 0 and 1
$$UTS_{10} = 20.2 \, g / mm^2 \quad UTS_{80} = 8.7 \, g / mm^2$$
$$UPE_{10} = 66.5\% \quad\quad UPE_{10} = 56.2\%$$

5.2.4 Person Built Parameter (B_4)

Built of a person affects his/her UTS and tissue layers thickness significantly. The small variations in UPE can be taken care in the tissue type T_1 parameter itself. UTS are greater in thin than thick muscles. Very thin man has UTS, 1.5 times normal man *Ref [29]*. *Table 05.01* gives relations between built of a person its effect on UTS and UPE of skeletal muscle tissues.

Person Built	UTS	UPE	
Under Weight	$B_{4UTS} = 1.5(A_{3UTS})$		
Normal Weight	$B_{4UTS} = A_{3UTS}$	$B_{4UPE} = A_{3UPE}$	$----(C5:12)$
Over Weight	$B_{4UTS} = 0.8(A_{3UTS})$		

Table 05.01: *Person built parameter for under weight, normal weight and overweight.*

5.2.5 Regional Variation Parameter (V_5)

The UTS and UPE variations due to regional differences can be taken care within the variations due to tissue type in T_1 parameter.

5.2.6 Tissue Intrinsic Parameter (I_6)

To imitate the material anisotropy a random number is continuously generated with time for every chosen time step. The variations in the UTS and UPE due to anisotropy are thus accounted with the newly generated random number in the tissue type parameter T_1 with each time step.

5.2.7 Physiological Testing Condition Parameter (P_7)

Skeletal muscles show different mechanical properties *in-vivo* and *ex-vivo* and also depending on time during when in *ex-vivo* condition. UTS of all human muscle tissue in the mechanically stabilized state are nearly 50% lower than that of just after death.

$$P_{7UTS} = 1.8 B_{4UTS} \qquad\qquad ----(C5:13)$$

$$P_{7UPE} = 1.1 B_{4UPE} \qquad\qquad ----(C5:14)$$

5.2.8 Strain Rate Sensitivity Parameter (D_8)

Generally a thousand fold change in strain rate does not exceed a factor of one or two change in stress for given strain, *Ref [25]*. UPE decreases and UTS increases with increasing strain rate. From *Table 02.05*, the typical strain rate for trocar insertion procedure is 0.032 cm s^{-1} and an initial high strain rate of 1.875cm s^{-1}. Taken a 1.2 factor of increase in UTS and 0.8 factor of decrease in UPE for initial high strain rate and with linear variation, D_{8UTS} and D_{8UPE} can be expressed as follows.

$$D_{8UTS} = [1 + 7.37(V_{trocar} - 0.032)] P_{7UTS} \qquad ----(C5:15)$$

$$D_{8UPE} = [1 - 18.43(V_{trocar} - 0.032)] P_{7UPE} \qquad ----(C5:16)$$

$$V_{trocar} : Velocity\, of\, trocar\, in\ \ cms^{-1} units$$

5.2.9 Skeletal Muscle Sample Workout

Given: Sex: Male, Age: 40 and Built Type: Normal Weight

Required: Skeletal muscle properties in Region-1

Workout

Sexual difference parameter (S_2): $S_{2UTS} = A_{3UTS}$ $\qquad$ $S_{2UPE} = A_{3UPE}$

Age group parameter (A_3): $A_{3UTS} = 11.96$ g/mm^2 $\qquad$ $A_{3UPE} = 60.66$ %

Person built parameter (B_4): Normal weight, $B_{4UTS} = 11.96$ g/mm^2 $B_{4UPE} = 60.66$ %

Physiological parameter (P_7): $P_{7UTS} = 1.8\ B_{4UTS} = 21.53$ g/mm^2

$$P_{7UPE} = 1.1\ B_{4UPE} = 66.73 \text{ %}$$

Strain rate parameter (D_8): For normal strain rate $V_{trocar} = 0.032$ cms^{-1}

$$D_{8UTS} = P_{7UTS} = 21.53 \text{ g/mm}^2$$

$$D_{8UPE} = P_{7UPE} = 66.73 \text{ %}$$

Tissue type parameter (T_1): Let random number N=25 at first time step Δt_1

$$T_{1UTS} = D_{8UTS} - (0.25) \cdot (2.8) = 20.83 \text{ g/mm}^2$$

$$T_{1UPE} = D_{8UPE} - (0.25) \cdot (12) = 63.73 \text{ %}$$

Following is the stress-strain relation of region-1 skeletal muscles of normal built 40 years old male at a normal strain rate of 0.032 cms^{-1}.

% Elongation = (63.73) ·x %

Stress = (20.83) · [0.0013($e^{4.35x}$-1)] g/mm^2

$$----(C5:17)$$

5.3   Skin Tensile Data Treatment (MSS date only)
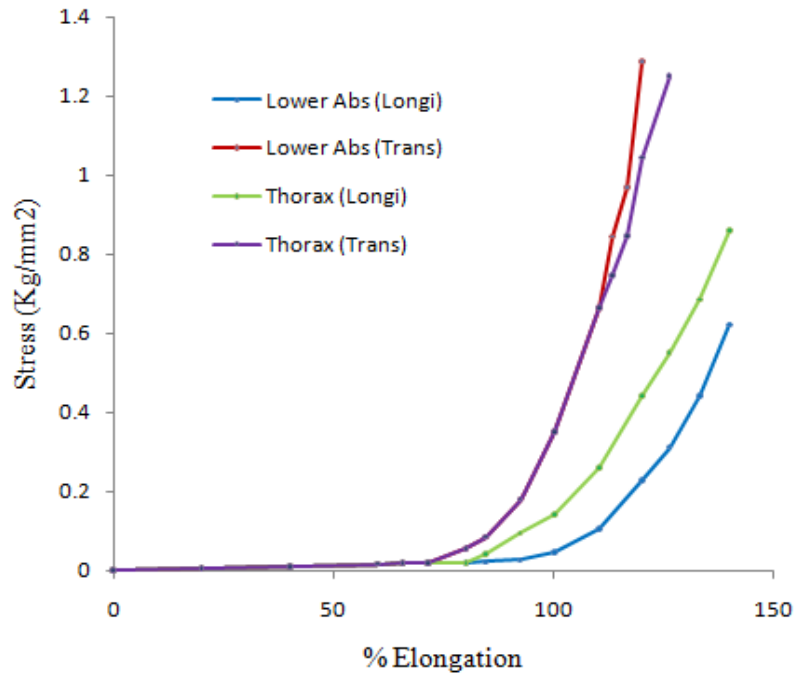
Fig 05.08: *Tensile stress-strain curves of skin tissues of persons 20-29 years age. Adapted from Ref [29].*
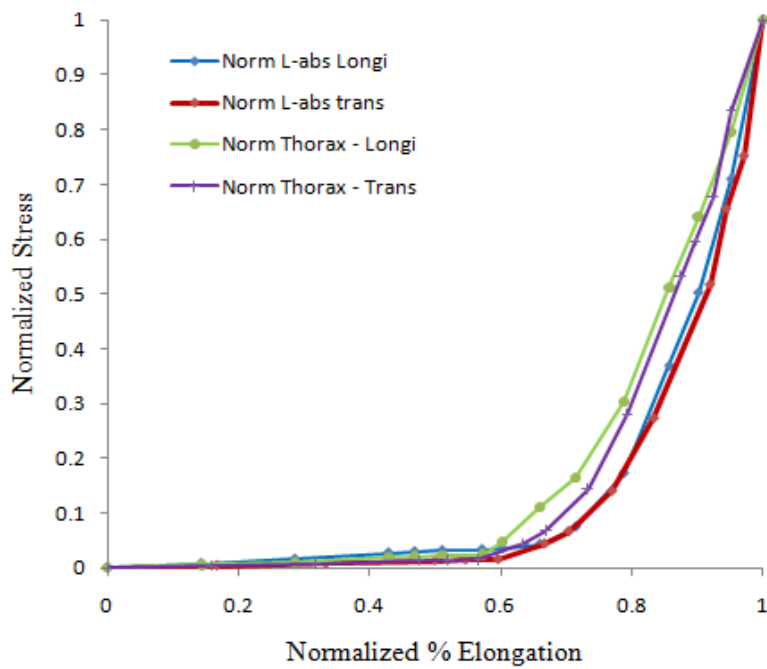
Fig 05.09: *Normalized tensile stress-strain curves of skin tissues.*
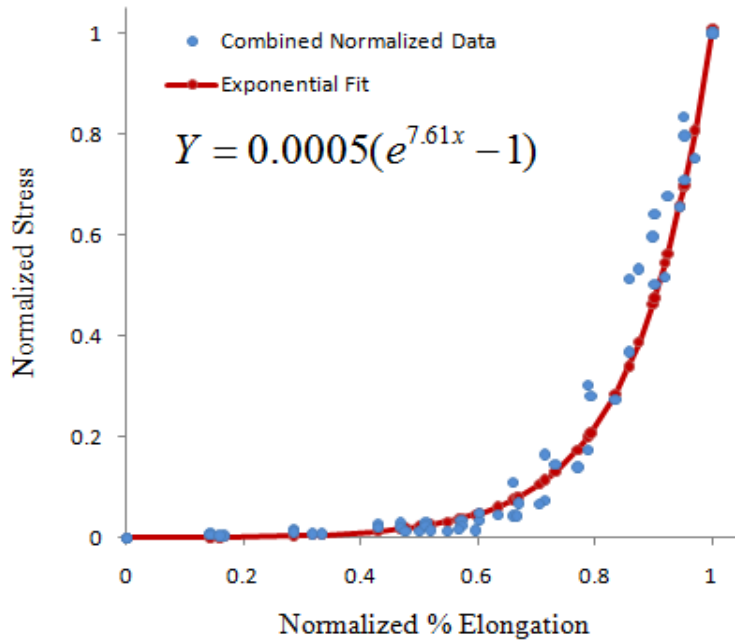
Fig 05.10: *Normalized tensile stress-strain curves of skin and exponential data fit.*

The equation shown in the figure:

$$Y = 0.0005(e^{7.61x} - 1)$$
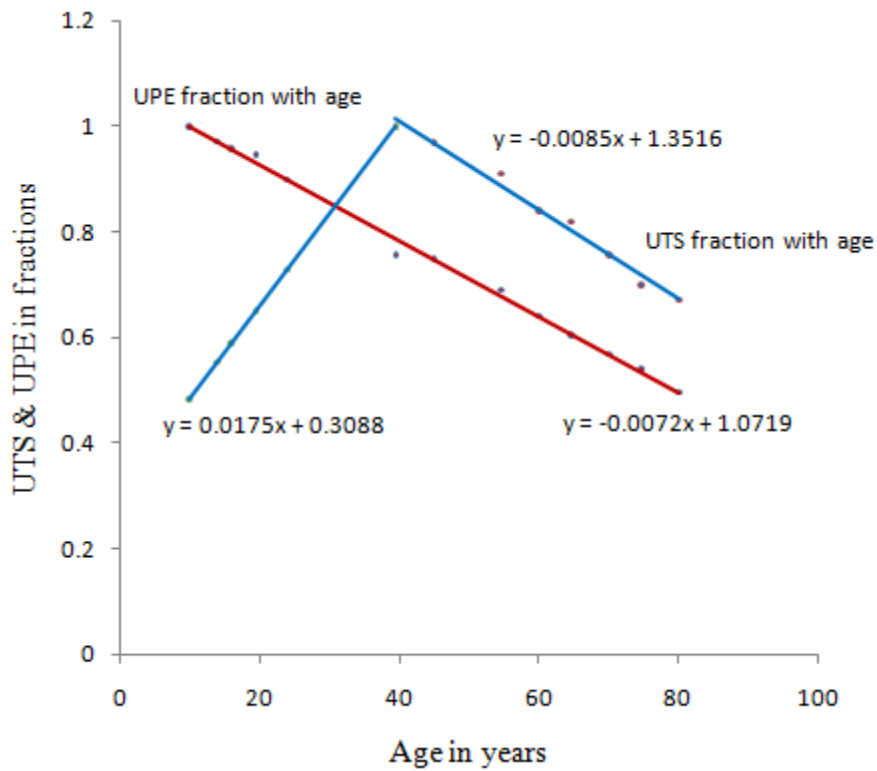
Fig 05.11: *Tensile UTS & UPE in fractions with age of skin tissues.*

Equations shown in the figure:

$y = -0.0085x + 1.3516$

$y = 0.0175x + 0.3088$

$y = -0.0072x + 1.0719$
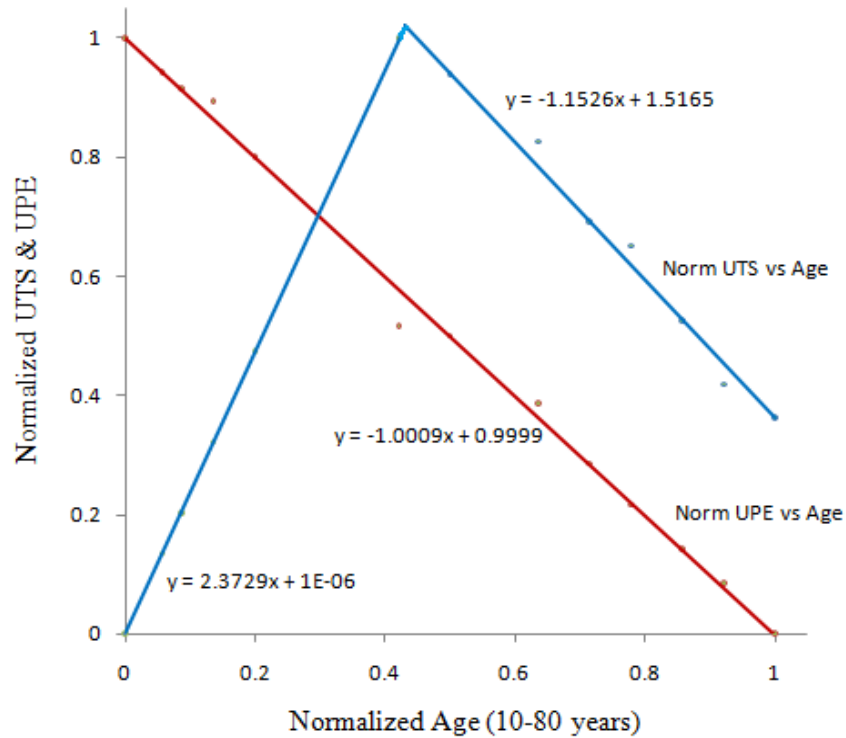
Fig 05.12: *Normalized tensile UTS & UPE with age of skin tissues.*

For abdominal skin tissues, % Elongation and Stress relation is as follows

$$\% \ Elongation = (UPE) \cdot x \qquad\qquad\qquad ----(C5:01)$$

$$Stress = (UTS) \cdot Y = (UTS) \cdot [0.0005(e^{7.61x} - 1)] \quad ----(C5:18)$$

$$where, \ x : fraction\,between\ 0\,and\,1$$
$$UPE = T_{1UPE} \ ; \ UTS = T_{1UTS}$$

5.3.1 Tissue Type Parameter (T_1)

Abdominal skin tissues in the upper abdomen, lower abdomen and lateral abdomen show similar mechanical properties with slight variations. Following are the formulas to obtain UTS and UPE for these skin tissues. A variation range of $\pm$ 0.16 kg/mm^2 for UTS and $\pm$ 15% for UPE form *Ref [29]* are taken.

$$T_{1UTS} = D_{8UTS} + (-1)^N (B \times 0.16) \qquad\qquad ----(C5:19)$$

$$T_{1UPE} = D_{8UPE} + (-1)^N (B \times 15) \qquad\qquad ----(C5:20)$$

$$B = \frac{N}{100} \qquad\qquad ----(C5:05)$$

Where,

$N = N(t)$ is a random number between 0 and 100

generated in every chosen time step Δt

B : random fractional number between 0 and 100

5.3.2 Sexual Difference Parameter (S₂)

Skin from females has a much lower breaking load than that from males, but there is no significant sexual difference in the ultimate strength. UPE of skin in females is greater than in males.

$$S_{2UTS} = A_{3UTS} \qquad \textit{for both} \qquad\qquad ----(C5:06)$$

$$S_{2UPE} = A_{3UPE} \qquad \textit{for male} \qquad\qquad ----(C5:21)$$
$$\quad= (1.15) A_{3UPE} \quad \textit{for female}$$

5.3.3 Age Parameter (A₃)

From the given age of a person expected average UTS and UPE are derived from the plots in the *Fig 05.11 and Fig 05.12.* It can be observed that within the age range of 10-80 years, younger age, 10 year old show greater UPE and 40 year old show greater UTS. From *Ref [29]* 39.5 year old has 1.145 kg/mm^2 UTS and 124.5 % UPE. For any age within the range, UTS and UPE can be calculated as follows.

If $10 \leq age \leq 39.5$

$$A_{3UTS} = UTS_{10} + (UTS_{39.5} - UTS_{10}) \times \left[(2.3729 \times a) + 10^{-6} \right]$$
$$= 0.554 + 0.591 \times \left[(2.3729 \times a) + 10^{-6} \right] \qquad ----(C5:22)$$

If $39.5 \leq age \leq 80$

$$A_{3UTS} = UTS_{80} + (UTS_{39.5} - UTS_{80}) \times \left[(-2.9874 \times a) + 2.9874 \right]$$
$$= 0.757 + 0.388 \times \left[(-2.9874 \times a) + 2.9874 \right] \qquad ----(C5:23)$$

$$A_{3UPE} = UPE_{80} + (UPE_{10} - UPE_{80}) \times \left[(-1.0009 \times a) + 0.9999 \right]$$
$$= 78.4 + 75.7 \times \left[(-1.0009 \times a) + 0.9999 \right] \qquad ----(C5:24)$$

$$a = \frac{(Age - 10)}{(80 - 10)} \qquad\qquad ----(C5:11)$$

Where 'a' is a var*iable between* 0 *and* 1

$$UTS_{10} = 0.554 \quad UTS_{39.5} = 1.145 \quad UTS_{80} = 0.757 \ kg/mm^2$$
$$UPE_{10} = 158.1 \quad UPE_{39.5} = 124.5 \quad UPE_{39.5} = 78.4 \ \%$$

5.3.4 Person Built Parameter (B₄)

There is no significant difference in the ultimate strength and ultimate % elongation of

skin tissue with person built. Hence the parameter equals the age parameter in value.

$$B_{4UTS} = A_{3UTS} \qquad\qquad ----(C5:25)$$

$$B_{4UPE} = A_{3UPE} \qquad\qquad ----(C5:12)$$

5.3.5 Physiological Testing Condition Parameter (P_7)

There are no significant variations in the UTS and UPE of skin tissues from the *in vivo* conditions to the mechanically stabilized testing conditions. The small variations are taken care in the tissue type parameter.

$$P_{7\,UTS} = B_{4\,UTS} \qquad\qquad\qquad ----(C5:26)$$

$$P_{7\,UPE} = B_{4\,UPE} \qquad\qquad\qquad ----(C5:27)$$

5.3.6 Other Skin Parameters

Skin shows orthotropic behavior with more UTS and less UPE in transverse direction than in longitudinal direction. For this trocar insertion problem the average skin tissue property is more suitable and the small Tissue Intrinsic Parameter variation along with other parameters, Regional Variations Parameter (V_5), and Strain Rate Sensitivity Parameter (D_8) show the same variation as that of skeletal muscles and hence the variations of these parameters are accounted with same set of equations.

5.3.7 Skin Sample Workout

Given: Sex: Male, Age: 40 and Built Type: Normal Weight

Required: Skin tissue properties in Region-1

Workout

Sexual difference parameter (S_2): For male $S_{2UTS} = A_{3UTS}$ $S_{2UPE} = A_{3UPE}$

Age group parameter (A_3): $A_{3UTS} = 1.4193$ kg/mm^2 $A_{3UPE} = 121.62$ %

Person built parameter (B_4): Normal weight,

$$B_{4UTS} = 1.4193 \text{ kg/mm}^2 \qquad B_{4UPE} = 121.62 \text{ %}$$

Physiological parameter (P_7): $P_{7UTS} = B_{4UTS} = 1.4193$ kg/mm^2

$$P_{7UPE} = B_{4UPE} = 121.62 \%$$

Strain rate parameter (D_8): For normal strain rate $V_{trocar} = 0.032$ cms^{-1}

$$D_{8UTS} = P_{7UTS} = 1.4193 \text{ kg/mm}^2$$

$$D_{8UPE} = P_{7UPE} = 121.62 \%$$

Tissue type parameter (T_1): Let random number N=25 at first time step Δt_1

$$T_{1UTS} = D_{8UTS} - (0.25) \cdot (0.16) = 1.3793 \text{ kg/mm}^2$$

$$T_{1UPE} = D_{8UPE} - (0.25) \cdot (15) = 117.87 \%$$

Stress strain relation of region-1 skin tissues of normal built 40 years old male at a normal strain rate of 0.032 cms^{-1}.

$$\% \text{ Elongation} = (117.87) \cdot x \%$$

$$\text{Stress} = (1.3793) \cdot [0.0005(e^{7.61x}-1)] \text{ kg/mm}^2 \qquad ---- (C\,5:28)$$

5.4   Fascia Tensile Data Treatment (MSS data only)
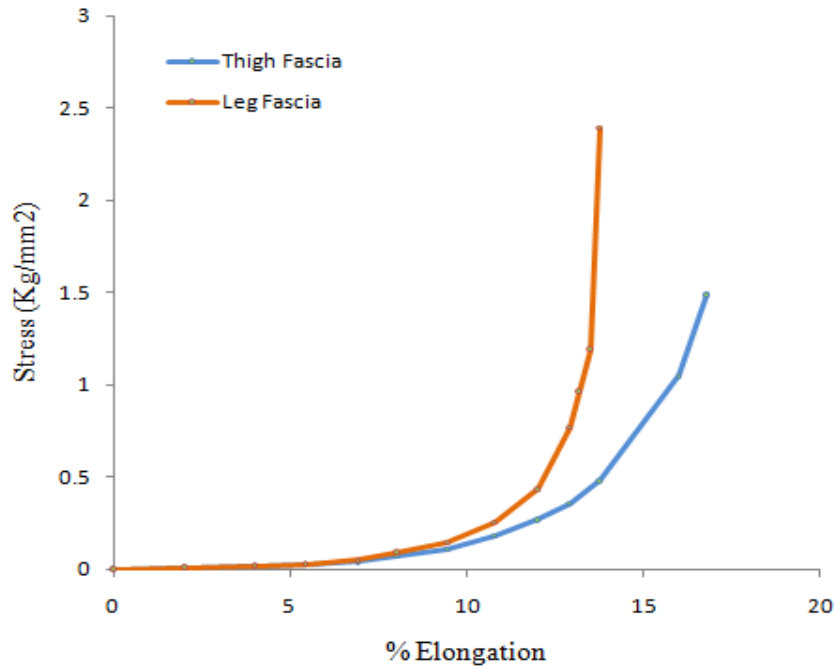
Fig 05.13: *Tensile stress-strain curves in a direction parallel to the course of the fibers, of fascia of persons 30-39 years of age. Adapted from Ref [29].*
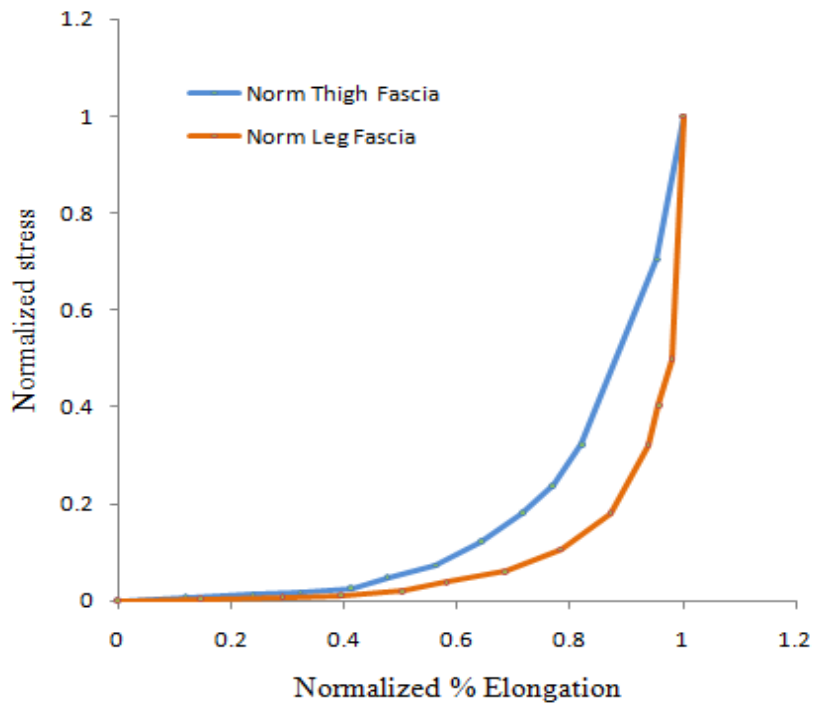
Fig 05.14: *Normalized tensile stress-strain curves of fascia tissues in tension.*
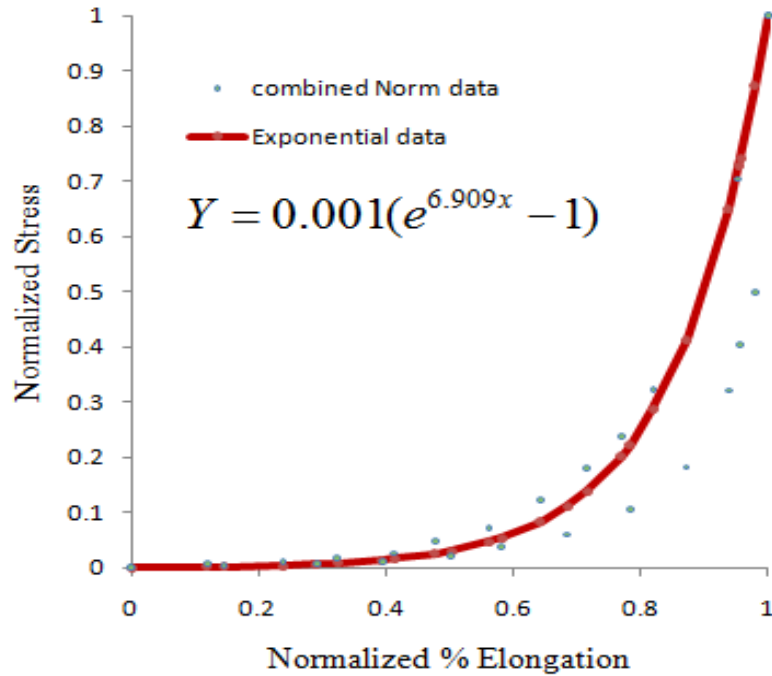
Fig 05.15: *Normalized tensile stress-strain curves of fascia and exponential data fit.*

For fascias, % Elongation and Stress relation is as follows

$$\% \ Elongation = (UPE) \cdot x \qquad\qquad\qquad ----(C5:01)$$

$$Stress = (UTS) \cdot Y = (UTS) \cdot [0.001(e^{6.909x} - 1)] \qquad ----(C5:29)$$

$$where, \ \ x: \ fraction \ between \ 0 \ and \ 1$$
$$UPE = T_{1UPE} \ ; \ UTS = T_{1UTS}$$

5.4.1 Tissue Type Parameter (T_1)

Abdominal fascia tissues in the upper abdomen, lower abdomen and lateral abdomen show similar mechanical properties with slight variations. Following are the formulas to obtain UTS and UPE for these fascia tissues. A variation range of $\pm$ 0.21 kg/mm^2 for UTS and $\pm$ 6% for UPE form *Ref [29]* are taken.

$$T_{1UTS} = D_{8UTS} + (-1)^N (B \times 0.21) \qquad\qquad ----(C5:30)$$

$$T_{1UPE} = D_{8UPE} + (-1)^N (B \times 6) \qquad\qquad ----(C5:31)$$

$$B = \frac{N}{100} \qquad\qquad ----(C5:05)$$

Where,

$N = N(t)$ *is a random number between* 0 *and* 100
generated in every chosen time step Δt

B : *random fractional number between* 0 *and* 100

5.4.2 Age Parameter (A₃)

It is assumed that fascia tissues properties show the same trend of UTS and UPE variations with age as that of the skin tissues. From the given age of a person expected average UTS and UPE are derived from the plots in the *Fig 05.11 and Fig 05.12.* It can be observed that within the age range of 10-80 years, younger age, 10 year old show greater UPE and 40 year old show greater UTS. From *Ref [29]* 34.5 year old has 1.54 kg/mm^2 UTS and 17.4 % UPE. For any age within the range, UTS and UPE can be calculated as follows.

If $10 \leq age \leq 39.5$

$$A_{3UTS} = UTS_{10} + (UTS_{39.5} - UTS_{10}) \times \left[(2.3729 \times a) + 10^{-6} \right]$$
$$= 0.817 + 0.871 \times \left[(2.3729 \times a) + 10^{-6} \right] \qquad ----(C5:32)$$

If $39.5 \leq age \leq 80$

$$A_{3UTS} = UTS_{80} + (UTS_{39.5} - UTS_{80}) \times \left[(-2.9874 \times a) + 2.9874 \right]$$
$$= 1.116 + 0.572 \times \left[(-2.9874 \times a) + 2.9874 \right] \qquad ----(C5:33)$$

$$A_{3UPE} = UPE_{80} + (UPE_{10} - UPE_{80}) \times \left[(-1.0009 \times a) + 0.9999 \right]$$
$$= 10.48 + 10.65 \times \left[(-1.0009 \times a) + 0.9999 \right] \qquad ----(C5:34)$$

$$a = \frac{(Age - 10)}{(80 - 10)} \qquad\qquad ----(C5:11)$$

Where $'a'$ *is a* var*iable between* 0 *and* 1
$$UTS_{10} = 0.817 \quad UTS_{39.5} = 1.688 \quad UTS_{80} = 1.116 \ kg/mm^2$$
$$UPE_{10} = 21.13 \quad UPE_{39.5} = 16.64 \quad UPE_{39.5} = 10.48 \ \%$$

5.4.3 Other Fascia Parameters

Other than the variation in the tissue thickness, there is no significant difference in the tensile properties of fascia with sex, person built, abdominal region of interest, and tissue testing physiological environment. It shows orthotropic behavior as the skin tissue. The Person Built Parameter (B_4), Regional Variation Parameter (V_5), Tissue Intrinsic Parameter (I_6), Physiological Testing Parameter (P_7), and Strain Rate Sensitivity Parameter (D_8) are accounted in the same way as in *section 5.3* of skin tissues. As there is no sexual difference in the properties, the Sexual Difference Parameter (S_2) is accounted as in the *section 5.2.2.*

5.4.4 Fascia Sample Workout

Given: Sex: Male, Age: 40 and Built Type: Normal Weight

Required: Fascia tissue properties in Region-1

Workout

Sexual difference parameter (S_2): For male $S_{2UTS} = A_{3UTS}$ $S_{2UPE} = A_{3UPE}$

Age group parameter (A_3): $A_{3UTS} = 2.0945$ kg/mm^2 $A_{3UPE} = 16.56$ %

Person built parameter (B_4): Normal weight,

$$B_{4UTS} = 2.0945 \text{ kg/mm}^2 \qquad B_{4UPE} = 16.56 \text{ %}$$

Physiological parameter (P_7): $P_{7UTS} = B_{4UTS} = 2.0945$ kg/mm^2

$$P_{7UPE} = B_{4UPE} = 16.56 \text{ %}$$

Strain rate parameter (D_8): For normal strain rate $V_{trocar} = 0.032$ cms^{-1}

$$D_{8UTS} = P_{7UTS} = 2.0945 \text{ kg/mm}^2$$

$$D_{8UPE} = P_{7UPE} = 16.56 \text{ %}$$

Tissue type parameter (T_1): Let random number N=25 at first time step Δt_1

$$T_{1UTS} = D_{8UTS} - (0.25) \cdot (0.21) = 2.042 \text{ kg/mm}^2$$

$$T_{1UPE} = D_{8UPE} - (0.25) \cdot (6) = 15.06 \text{ %}$$

Stress strain relation of region-1 fascia tissues of normal built 40 years old male at a normal strain rate of 0.032 cms^{-1}.

$$
\boxed{
\begin{array}{l}
\text{\% Elongation} = (15.06) \cdot x \text{ %} \\[2mm]
\text{Stress} = (2.042) \cdot [0.001(e^{6.909x} - 1)] \text{ kg/mm}^2
\end{array}
}
\qquad ----(C5:35)
$$

5.5　　　Panniculus Adipose (Fat Tissue) Tensile Data Treatment
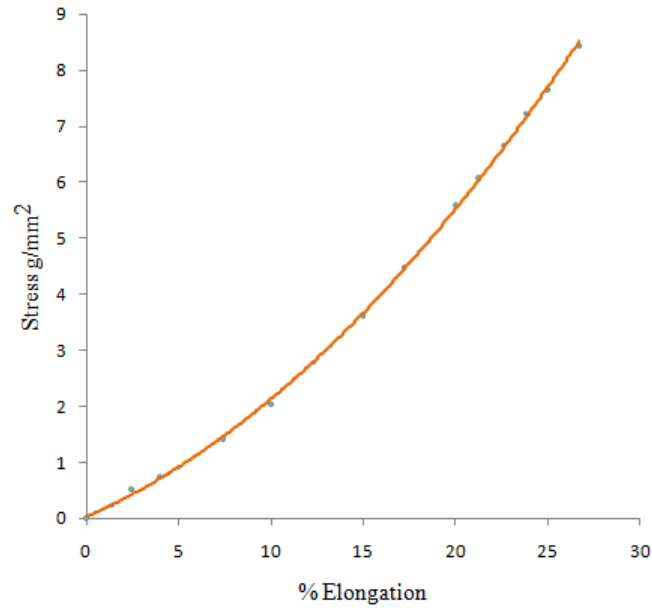
Fig 05.16: *Stress-strain curves in tension of panniculus adipose tissue of persons 29 years age. Adapted from Ref [29].*

$$y = 0.5447x^2 + 0.4617x + 0.0036$$

• Norm Panniculus Adiposus

• Exponential fit
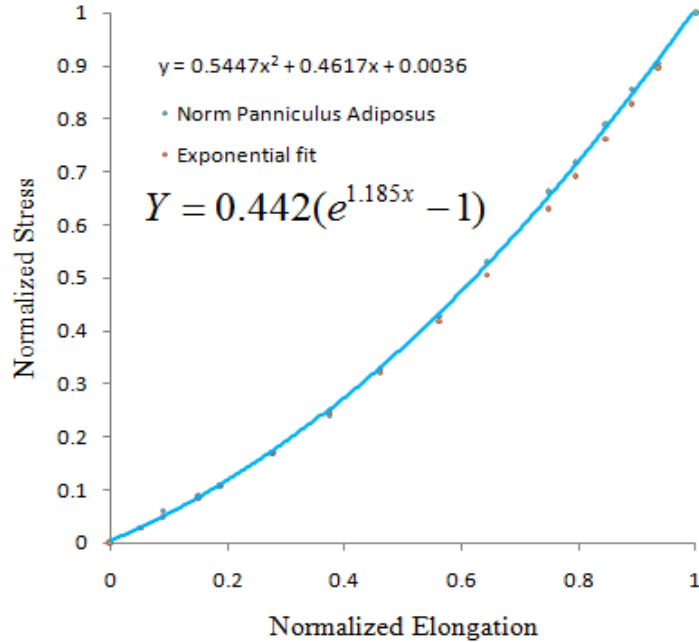
$$Y = 0.442(e^{1.185x} - 1)$$

Fig 05.17: *Normalized stress-strain curves of panniculus adipose and exponential data fit.*

For Panniculus Adipose, % Elongation and Stress relation is as follows

$$\% \; Elongation = (UPE) \cdot x \qquad\qquad ----(C5:01)$$

$$Stress = (UTS) \cdot Y = (UTS) \cdot [0.442(e^{1.185x} - 1)] \qquad ----(C5:36)$$

$$where, \quad x: fraction\, between\; 0\, and\, 1$$
$$UPE = T_{1UPE} \;\; ; \; UTS = T_{1UTS}$$

5.5.1 Tissue Type Parameter (T_1)

Abdominal fat tissues in the upper abdomen, lower abdomen and lateral abdomen show similar mechanical properties with slight variations. Following are the formulas to obtain UTS and UPE for these fat tissues. A variation range of $\pm\, 0.14$ g/mm^2 for UTS and $\pm\, 5\%$ for UPE form *Ref [29]* are taken.

$$T_{1UTS} = D_{8UTS} + (-1)^N (B \times 0.14) \qquad\qquad ----(C5:37)$$

$$T_{1UPE} = D_{8UPE} + (-1)^N (B \times 5) \qquad\qquad ----(C5:38)$$

$$B = \frac{N}{100} \qquad\qquad ----(C5:05)$$

Where,
$$N = N(t)\, is\, a\, random\, number\, between\, 0\, and\, 100$$
$$generated\, in\, every\, chosen\, time\, step\, \Delta t$$
$$B: random\, fractional\, number\, between\, 0\, and\, 100$$

5.5.2 Age Parameter (A_3)

There is no significant variation in the tensile properties of panniculus adipose with age. Fat has an average UTS of 8.44 g/mm^2 and UTS of 26.72 %. The age parameter for fat is a follows.

$$A_{3UTS} = 8.44 \ g/mm^2 \qquad\qquad ----(C5:38)$$

$$A_{3UPE} = 26.72 \ \% \qquad\qquad ----(C5:39)$$

5.5.3 Other Fat Tissue Parameters

Other than the variation in the tissue thickness, there is no significant difference in the tensile properties of fascia with sex, person built, abdominal region of interest, and tissue testing physiological environment. The Sexual Difference Parameter (S_2), Person Built Parameter (B_4), Regional Variation Parameter (V_5), Tissue Intrinsic Parameter (I_6), Physiological Testing Parameter (P_7), and Strain Rate Sensitivity Parameter (D_8) are accounted in the same way as in *section 5.4.3* of fascia tissues.

5.5.4 Fat Tissue Sample Workout

Given: Sex: Male, Age: 40 and Built Type: Normal Weight

Required: Fat tissue properties in Region-1

Workout

Sexual difference parameter (S_2): For male $S_{2UTS} = A_{3UTS}$ $S_{2UPE} = A_{3UPE}$

Age group parameter (A_3): $A_{3UTS} = 8.44$ g/mm^2 $A_{3UPE} = 26.72$ %

Person built parameter (B_4): Normal weight,

$$B_{4UTS} = 8.44 \text{ g/mm}^2 \quad B_{4UPE} = 26.72 \text{ \%}$$

Physiological parameter (P_7): $P_{7UTS} = B_{4UTS} = 8.44$ g/mm^2

$$P_{7UPE} = B_{4UPE} = 26.72 \%$$

Strain rate parameter (D_8): For normal strain rate $V_{trocar} = 0.032$ cms^{-1}

$$D_{8UTS} = P_{7UTS} = 8.44 \text{ g/mm}^2$$

$$D_{8UPE} = P_{7UPE} = 26.72 \%$$

Tissue type parameter (T_1): Let random number N=25 at first time step Δt_1

$$T_{1UTS} = D_{8UTS} - (0.25) \cdot (0.14) = 8.41 \text{ g/mm}^2$$

$$T_{1UPE} = D_{8UPE} - (0.25) \cdot (5) = 25.47 \%$$

Stress strain relation of region-1 fat tissues of normal built 40 years old male at a normal strain rate of 0.032 cms^{-1}.

$$\% \text{ Elongation} = (25.47) \cdot x \%$$

$$\text{Stress} = (8.41) \cdot [0.442(e^{1.185x} - 1)] \text{ g/mm}^2$$

$$---- (C5 : 40)$$

73

CHAPTER 6

REAL-TIME COMPUTATION

Introduction

Real-time finite element analysis limitation is primarily due to overabundance of information provided by standard FE approaches. Mathematics is to be optimized to yield only the information essential for the surgical task then computational time will be drastically reduced. Parallel computation and preprocessing of the model before the simulation begins can also reduce the size of the problem and greatly increase computation speed. Distributed parallel processing to separate graphical rendering from mathematical computation will lead to increase performance speed.

To obtain realistic and stable haptic sensation, the haptic rendering loop must maintain a 1000 Hz (minimum of 300Hz is required) update rate which is much higher than that of 20-30 Hz graphic rendering rate. Parallelizing visual and haptic rendering processes in different threads will meet the respective refresh rates. The trocar insertion simulation requires 3D modeling of the tissues, as the manipulation of the trocar is not fixed. So there is a need to gauge the computational infrastructure. Taking a minimum of 300 Hz updates for haptic rendering, for LU decomposition the number of FLoating point Operations required Per Second (FLOPS) for N number of nodes is given by FLOPS = 0.5(3N*3N)(300). Estimating a 20,000 to 30,000 number of nodes for the problem, couple of NVIDIA GPUs and QUAD CORE workstation is proposed.

Unit	Giga Flops	Number of Nodes
Single Core Processor (1333MHz x 4 Flops)	53	3962
NVIDIA TESLA C2050 GPU	515	12353

Table 06.01: *Different processing units and their 300Hz updatable nodes.*
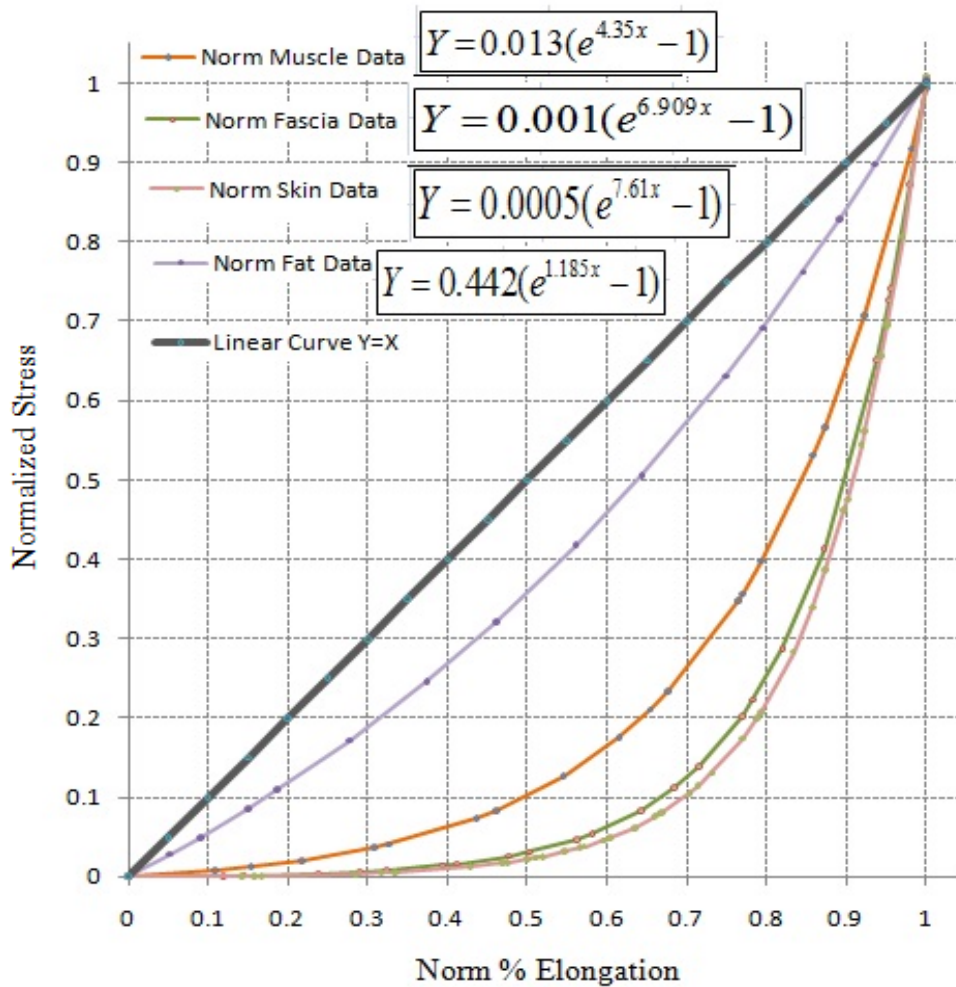
Fig 06.01: *Mapping of tissue tensile curve to pseudo Hookean or Neo-Hookean curve.*
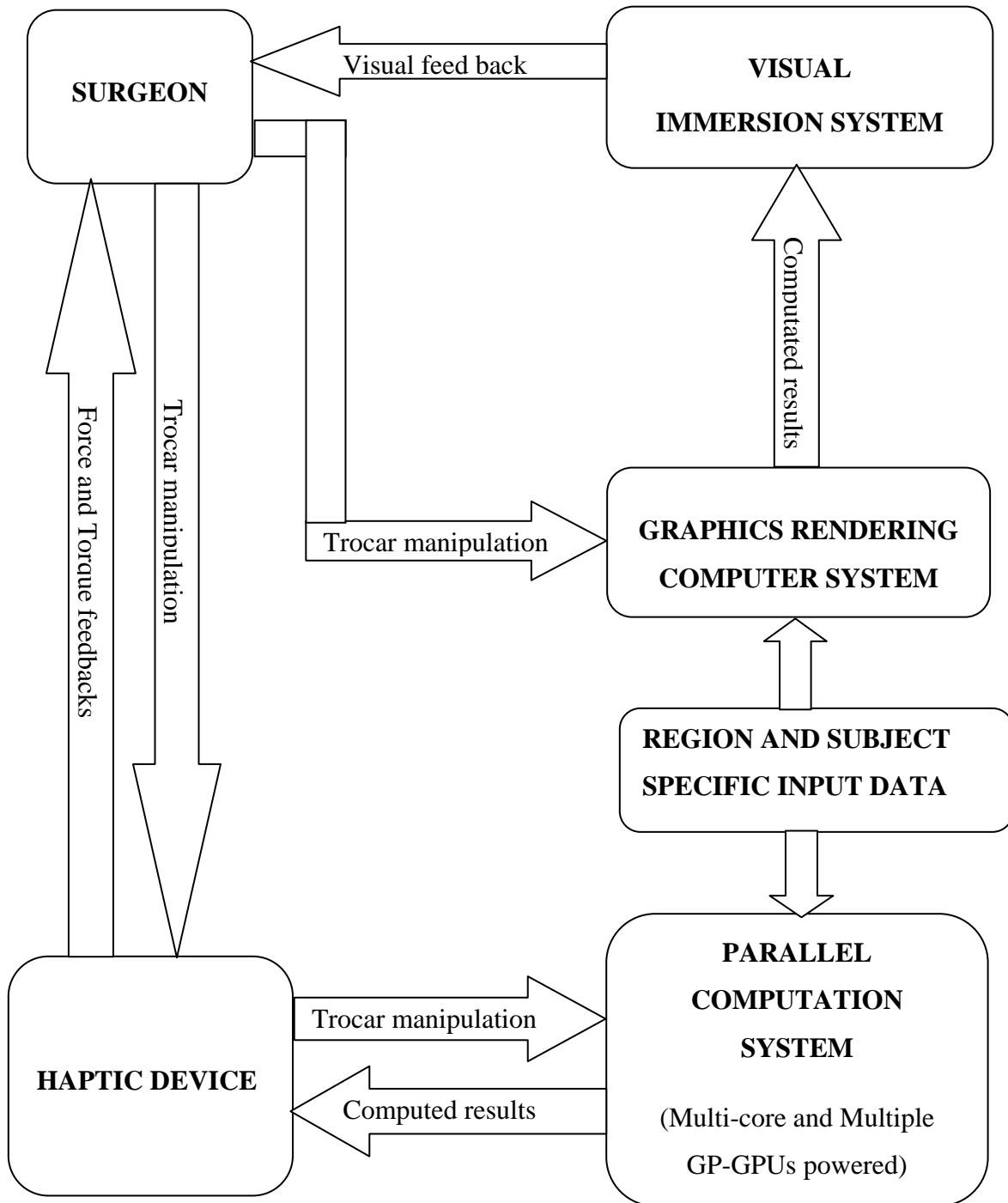
Fig 06.02: *Proposed real-time simulation architecture for torcar insertion.*

6.2   Model Reduction

For real-time computation, tissue tensile curves are mapped to pseudo Hookean or pseudo Neo-Hookean curve as shown in the *Fig 06.01* and the simulation is run to capture the trocar manipulations. As the trocar tissue interactions are captured, the deformations are reversed mapped to original tissue properties to calculate stresses and hence forces and torques. The mapping of all tissue tensile curves to a single curve provides an opportunity to easily address the finite element formulation of different layers of tissue by just a single continuous Galerkin formulation.

6.3   Model Reduction Equations

6.3.1 Green-Lagrange Strain

Deformations of Tissues from finite strain theory

$$displacement\ gradient\ u_{ij} = \frac{\partial(x_i - X_i)}{\partial X_j} = F_{ij} - \delta_{ij}\ ----(C6:01)$$

$$deformation\ gradient\ F_{ij} = \frac{\partial x_i}{\partial X_j}\qquad\qquad ----(C6:02)$$

$$F = RU = VR\qquad\qquad\qquad ----(C6:03)$$

$U, V : right\ and\ left\ stretch\ symmetric\ matrices,$

$\qquad represents\ pure\ strains$

$\qquad Eigen\ values\ \lambda_i(U)\ are\ principal\ stretches$

$R : orthogonal\ matrix\ representing\ pure\ rotation$

Green – Lagrange Strain Tensor (E)

E : does not depend on rigid body rotation
and zero for pure translation

$$E = \frac{1}{2}\left(F^T F - I\right) = \frac{1}{2}\left((RU)^T (RU) - I\right) = \frac{1}{2}\left(U^2 - I\right) = \frac{1}{2}(C - I)$$

$$----(C6:04)$$

$$E_{ij} = \frac{1}{2}\left(u_{ij} + u_{ji} + u_{ki}u_{kj}\right) \qquad ----(C6:05)$$

Stretch ratio in the direction of a unit vector p

$$\hat{\lambda} = \lambda(p) - 1 = \left(p^T F^T F p\right)^{\frac{1}{2}} \qquad ----(C6:06)$$

Deformed infinitisimal volume related to undeformed volume

$$dv = det(F)dV = (\det(C))^{\frac{1}{2}} dV = (\det(U^2))^{\frac{1}{2}} dV \qquad ----(C6:07)$$

6.3.2 Second Piola-Kirchoff Stress Tensor

Stresses in soft tissues from finite strain theory

represented by second piola kirchoff stress tensor (S)
S stress tensor is work conjugate of E strain tensor

$$S = \det(F) F^{-1} \sigma F^{-T} \qquad\qquad ----(C6:08)$$

S :is symmetric tensor

$$(S \cdot \dot{E}) = \det(F)(\sigma \cdot D) = \det(F) tr(\sigma D^T) \qquad ----(C6:09)$$

$$D = \frac{1}{2}\left(L + L^T\right) = symmetric\ part\ of\ velocity\ gradient, L = \frac{\partial v}{\partial x}$$
$$----(C6:10)$$

6.3.3 Strain-Strain Relationship

For hyperelastic material strain energy function (W) exists because
stored strain energy is independent of path of deformation.

For isotropic hyperelastic materials, W is function of

three principal stretch ratios $W(\lambda_1, \lambda_2, \lambda_3)$ or

three right cauchy strain invariants $W(I_1, I_2, I_3)$

$$I_1 = trC = C_{ii} = \lambda_1^2 + \lambda_2^2 + \lambda_3^2 \qquad\qquad ----(C6:11)$$

$$I_2 = \frac{1}{2}\left((trC)^2 - tr(C^2)\right) = \lambda_1^2\lambda_2^2 + \lambda_2^2\lambda_3^2 + \lambda_3^2\lambda_1^2 \qquad ----(C6:12)$$

$$I_3 = \det(C) = \lambda_1^2\lambda_2^2\lambda_3^2 = 1\,(\,for\,incompressible\,\,material\,)$$
$$----(C6:13)$$

$$S = \frac{\partial W}{\partial E} = \frac{\partial W}{\partial\left(\frac{1}{2}(C-I)\right)} = 2\frac{\partial W}{\partial C} \qquad\qquad ----(C6:14)$$

S : Second Poila– Kirchoff stress

C : right cauchy strain tensor

6.3.4 Incompressible Neo-Hookean Model

$$W = C_1(I_1 - 3) \qquad\qquad ----(C6:15)$$

$$I_1 = \lambda_1^2 + \lambda_2^2 + \lambda_3^2 \ ; \ \lambda_1\lambda_2\lambda_3 = 1 \qquad\qquad ----(C6:16)$$

$$\sigma_{11} - \sigma_{33} = \lambda_1\frac{\partial W}{\partial\lambda_1} - \lambda_3\frac{\partial W}{\partial\lambda_3} = 2(\lambda_1^2 - \lambda_3^2)C_1 \qquad ----(C6:17)$$

$$\sigma_{22} - \sigma_{33} = \lambda_2\frac{\partial W}{\partial\lambda_2} - \lambda_3\frac{\partial W}{\partial\lambda_3} = 2(\lambda_2^2 - \lambda_3^2)C_1 \qquad ----(C6:18)$$

For uniaxial extension

$$\lambda_1 = \lambda; \quad \lambda_2 = \lambda_3 = \left(\frac{1}{\sqrt{\lambda}}\right); \quad \varepsilon_{11} = \lambda_1 - 1 \qquad ----(C6:19)$$

$$True\ stress\ \sigma_{11} = 2C_1\left(\lambda^2 - \frac{1}{\lambda}\right) \qquad ----(C6:20)$$

$$Engineering\ stress\ \sigma_{11}^{eng} = 2C_1\left(\lambda - \frac{1}{\lambda^2}\right) \qquad ----(C6:21)$$

6.4   Equations for Forces and Torques calculations

Frictional forces feedback
both due to viscosity and kinetic friction

$$Linear \qquad F_{fric} = \sum(\upsilon_{tis}V_{tro}) + \sum(\mu_{tis}N_{tis}) \qquad ----(C6:22)$$

$$Angular \quad \tau_{fric} = \sum(\upsilon_{tis}r_{tro}^2\omega_{tro}) + \sum(\mu_{tis}r_{tro}N_{tis}) \qquad ----(C6:23)$$

$$\upsilon_{skin} = 0.02\frac{Ns}{mm} \qquad \mu_{skin} = 0.18 \qquad \rho_{skin} = 1.054\,g/ml$$

$$\upsilon_{adipose} = 0.01\frac{Ns}{mm} \qquad \mu_{adipose} = 0.10 \qquad \rho_{adipose} = 0.919\,g/ml$$

$$\upsilon_{muscle} = 0.03\frac{Ns}{mm} \qquad \mu_{muscle} = 0.15 \qquad \rho_{muslce} = 1.06\,g/ml$$

above values from Ref [13,48,49]

6.5   Conclusions

The main objective of Trocar Insertion Haptic Simulator is to generate realistic force and torque feedbacks. The realistic values of forces and torques depend on various parameters of its software and hardware implementations. Available nearly accurate tissue materials properties, approximation of the material models and chosen FE formulation implementation for real time performance makes the force and torque values to differ from the realistic values. So the overall implementation should be aimed at generating force and torque profiles, as close as possible, with all the jerks and spikes of tissue cutting interactions.

Trocar insertion is neither an axisymmetric, plane stress nor a plane strain problem. So the problem can't be simplified to 1D or 2D reduced problem. It needs to be represented in full 3D to capture the trocar–tissue interactions. It can't be solved effectively by preprocessing the data of various solution instances generated using any commercial FEA solvers. So the problem needs its own implementation code.

As this problem is an initial/boundary value problem, the principal radii of abdominal wall geometry, initial tissue stresses and strains require some manipulation to obtain the desired feedback forces and torques. Abdominal wall has many tissue layers and layers can be assumed to be bonded. This leads to material discontinuity. Discontinuous Galerkin formulation can be implemented to capture these discontinuities. On the other hand, mapping all the tissue properties to a single linear curve and reverse mapping at every small time step would need only continuous Galerkin formulation. This method might not represent the tissue properties accurately, but the 3D trocar–tissue interactions

are definitely captured well. There may be need to artificially increasing/decreasing some of the material parameters such as density, Poisson's ratio, tangent young's modulus, during mapping and reverse mapping to represent the tissue properties.

Implicit Integration algorithm gives very close solution but takes more computational time. The alternatives such as, Explicit Integration with or without Nodal Mass Lumping or Quasi-Static formulation takes much less time compared to Implicit Integration. Implicit Integration and Quasi-Static formulation doesn't have any convergence problem as compared to Explicit Integration, where time step chosen plays a key role in convergence. So, an adaptive re-meshing, iterative Quasi–Static formulation with additional separate formulation for frictional force and torque feedback due to visco-elasticity of the tissues would be able to represent the Trocar Insertion problem very well.

APPENDIX – 1: Hiroshi Yamada Book

A Summary of STRENGTH OF BIOLOGICAL MATERIALS

- Hiroshi Yamada, M.D

Biomechanics and Strength of Biological Materials

Biomechanics is the application of the principles of mechanics to biological problems or, in a restricted sense, strength of biological materials. Strength of biological materials is the science dealing with the mechanical properties of biological materials, i.e., organs and tissues of human and animal bodies.

A1.2 Strength Tests of Biological Materials

In testing the strength characteristics of biological materials (organs and tissues) one should be certain, if possible, that the test materials is in mechanically stabilized state, i.e., the state in which stable and constant strength values are obtained. In order to reach the mechanically stabilized state, intact organs, from which the test specimens are made, are removed from the cadavers, put in a physiological saline solution, and stored in a refrigerator overnight or longer. Skeletal muscle, after removal from cadavers, generally must be stored more than two nights before strength tests are made. Mechanically stabilized state for all organs is caused mainly by saturation with water plus disappearance of rigor mortis for smooth and skeletal muscles.

Tissue/Organ	Duration
Bone	Several months
Cartilage	3 days
Ligamentum nuchae	1 day
Muscles	2 days
Fascia	3 days
Tendons	5 days
Heart	3 days
Blood vessels	4 days
Cornea & Sclera	2 days
Red blood corpuscles	3 days
Trachea	3 days
Esophagus	3 days
Stomach	3 days
Intestines	3 days
Amnion	Within 24 hours
Umbilical cord	Within several hours
Nerves	4 days
Skin	3 days
Hair	1 year
Nails	2 days

Table A1.01: *Showing duration of mechanical stabilized state for various tissues.*

Organs	Average number in each decade
Locomotor organs (bone,cartilage,muscle,tendon)	3.6
Circulatory organs (heart, blood vessels, corpuscles)	7.6
Respiratory & digestive organs (larynx, trachea, teeth, esophagus, stomach, small and large intestines)	6.8
Urogenital organs (Kidney, ureter, urinary bladder)	8.5
Nervous system (nerve, dura mater	4.8
Integuments (skin, nails)	4.8
Sense organs (cornea, sclera, tympanic membrane)	4.8

Table A1.02: *Average number of subjects in each decade for which mechanical property were determined (The estimate overall average was 6 persons per decade for all organs).*

Strength tests were based on 15 to 20 specimens for every system of every subject. The average value given in the tables for the various mechanical properties in each age group was the average for all specimens tested. The average value for the mechanical properties of adults was based on the average for all the adult decades (over 20 years of age). Mechanical properties were found for Japanese cadavers only.

A1.2.1   Tension Test

The test specimen of skeletal muscle consisted of a strand of a secondary bundle of muscle fibers 3 cm long with a cross-sectional area of 15-40 mm^2. The strain was measured over a gauge length of 10 mm. The test specimens of membranous organs and tissues were strips each with a reduced middle region 10 mm in length, 2-3 mm in width, and a length-width ratio of 3:1. Test specimen from a cord-like organ was strand of tendon bundle 3cm long with a cross-sectional area of 0.5-0.8 mm^2 a secondary bundle of nerve fibers 3 cm long with a cross sectional area od 0.5-0.2 mm^2 and a hair 3-4 cm long. The strain was measured over a gauge length of 10-20 mm.

Mechanical properties measured were the following

- ➢ Tensile breaking load (kg, g), cord like organs in their original condition
- ➢ Tensile breaking load per unit width (kg/mm, g/mm)

  - ▪ Ultimate tensile strength (kg/mm2, g/mm2) $\times$ thickness (mm)

- ➢ Ultimate tensile strength (kg/mm^2, g/mm^2)
- ➢ Ultimate percentage elongation (%)

  - ▪ $\dfrac{\text{breaking elongation (mm)}}{\text{gauge length or original length of reduced region}} \times 100$

- ➢ Stress- strain curve
- ➢ Proportional limit (kg/mm^2, g/mm^2)
- ➢ Elastic limit (kg/mm^2, g/mm^2)
- ➢ Elastic modulus (kg/mm^2, g/mm^2)

  - ▪ $\dfrac{\text{Stress (kg/mm}^2,\ \text{g/mm}^2)\ \text{within elastic limit}}{\text{percentage elongation (\%) at above stress} \div 100}$

> ➢ Percentage of elastic recovery just before rupture (%)

$$\text{• } \frac{\text{recovered percentage elongation (\%)}}{\text{percentage elongation (\%) just before ruputure}}$$

> ➢ Creep limit (kg/mm^2, g/mm^2)

> ➢ Rupture pattern

In all data the $\pm$ shows the standard error.

A1.2.2   Expansion Test

Most membranous organs, generally test pieces are square 15 mm. Basic pressure of 0.1 kg/cm^2 at 7 mm aperture (Mullen tester).

Mechanical properties measured were the following

> ➢ Ultimate expansive strength (kg/cm^2)

> ➢ Ultimate expansive strength per unit thickness (kg/cm^2/mm)

$$\frac{\text{Ultimate expansive strength (kg/cm}^2)}{\text{thickness (mm)}}$$

> ➢ Ultimate expansion (ml)

> ➢ Pressure-expansion curve

> ➢ Elastic limit (kg/cm^2)

> ➢ Percentage of elastic recovery just before rupture (%)

$$\frac{\text{recovered expansion (ml)}}{\text{expansion (ml) just before rupture}} \times 100$$

> ➢ Creep limit (kg/cm^2)

> ➢ Rupture pattern

A1.2.3　　　Tearing Test

Test specimen was a strap with a small cut at one end. Tension tester machines used to carry out tearing tests. The parts of the specimen on both sides of the cut in the end of specimen were fastened in the jaws of the testing machine. The tearing load was average of the peak loads in the intermittent tearing.

Mechanical properties measured were the following

> ➢　Tearing load (kg, g)

> ➢　Tearing strength (kg/mm, g/mm) = Tearing load (kg, g) / Thickness (mm)

A1.2.4　　　Shearing Test

Test specimens of membranous organs were rectangular straps 2cm wide 2.5cm long. The shearing jig for testing membranous organs included a specimen holder with a 1.5com span and a compression tool 1.5com thick and 2.5com wide with a shearing edge at an inclination angle f 80^0. Single shearing methods were used for membranous organs.

Mechanical properties measured were the following

> ➢　Shearing breaking load per unit width (kg/mm)

> ➢　Ultimate shearing strength (kg/mm^2)

$$\frac{\text{shearing breaking load (kg)}}{\text{cross-sectional area (mm}^2)}$$

A1.2.5　　　Effect of Test Condition on Strength Values

For soft tissues and organs strength varies with the time between death and testing, there is no standard procedure for testing. Materials placed in physiological saline solution and

stored overnight in a refrigerator have constant strength values for different postmortem times before testing.

Species	Material	Mechanical properties
Dog, rabbit, Man	Skeletal muscle	TBL (MSS) = 0.65 (JAD) UTS (MSS) = 0.50 (JAD) UPE (MSS) = 0.60 (JAD)
Cattle	Tendon	UTS (MSS) = 0.80 (JAD) UPE (MSS) = 1.05 (JAD)
	Artery	TBL/UW (MSS) = 0.90 (JAD) UTS (MSS) = 0.90 (JAD) UPE (MSS) = 1.25 (JAD)
Rabbit	Nerve	TBL (MSS) = 0.95 (JAD) UTS (MSS) = 0.85 (JAD) UPE (MSS) = 1.00 (JAD)
	Intestine	TBL/UW (MSS) = 0.90 (JAD) UTS (MSS) = 1.20 (JAD) UPE (MSS) = 0.90 (JAD)
	Skin	TBL/UW (MSS) = 0.95 (JAD) UTS (MSS) = 0.95 (JAD) UPE (MSS) = 0.95 (JAD)
Cat	Sclera	TBL/UW (MSS) = 0.95 (JAD) UTS (MSS) = 0.90 (JAD) UPE (MSS) = 1.20 (JAD)

Table A1.03: *Strength values for soft tissue organs tested in the mechanically stabilized state are different from those tested just after death.*

A1.3   Ligaments

Umbilical ligament, median – is a fibrous cord like remains of the obliterated umbilical artery, running cranial ward beside the bladder to the umbilicus. Cord like remains of a fetal vessel or other structure that has lost its original lumen.

A1.3.1   Tensile Properties of Elastic Ligaments

From ligamentum nuchae, found around the neck of 20 cattle. Ultimate tensile strength of the tissue is proportional to the thickness of the elastic fibers. Elastic tissue exhibits perfect elasticity, i.e. 99% to 100% recovery. Creep limit is 90% to 95% of UTS. Values in table A1.4 and figure A1.1 are for fresh wet elastic ligamentous tissue from the ligamentum nuchae.

Type	Average Thickness(μ)	Ultimate Tensile Strength (kg/mm^2)	Ultimate percentage elongation (%)
Restiform portion	63	0.32 ± 0.054	160 ± 3.4
Flat portion	60	0.20 ± 0.042	128 ± 3.0
Conjunct portion	57	0.16 ± 0.052	99 ± 1.1

Table A1.04: UTS and UPE of ligamentum nuchae.
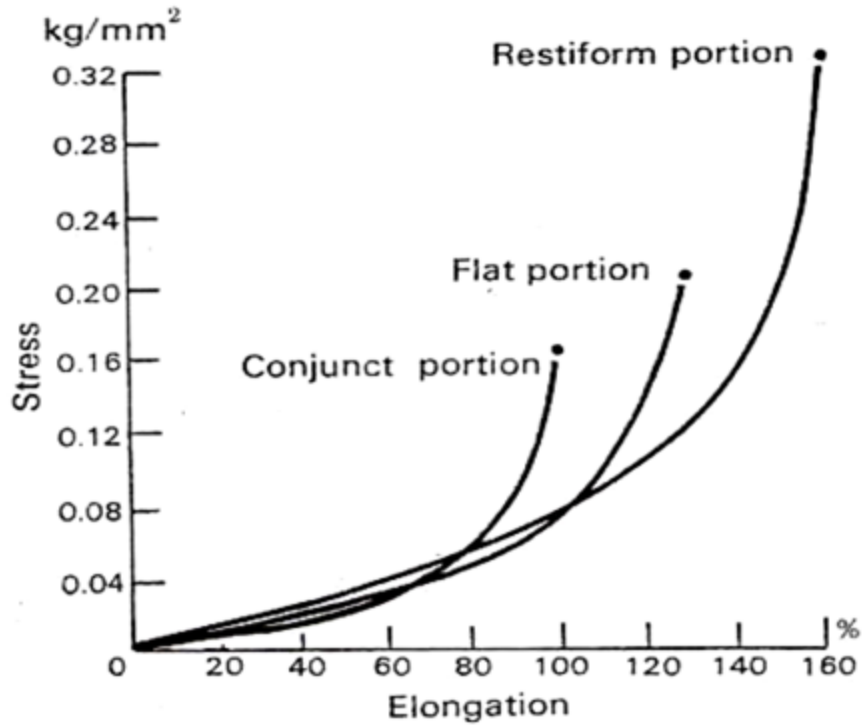
Fig A1.01: *Stress-strain curves in tension of elastic ligamentous tissue from the ligamentum nuchae of cattle.*

A1.3.2   Muscles

The relative strength decreases with age. There is no significant sexual difference in the ultimate strength of skeletal muscle. UTS of all human and animal muscle tissue in the mechanically stabilized state is 50% of that just after death, 10-19 age group has UTS = 38 g/mm^2 just after death and adults have UTS = 22 g/mm^2 just after death. UTS are greater in thin than thick muscles and in extensor than in flexor muscles. Very thin man UTS = 1.8 times normal man.

Age group (years)	UTS (g/mm^2)	UPE (%)
10 - 19	19 ± 1.2	65 ± 1.2
20 - 29	15 ± 0.6	64 ± 1.1
30 - 39	13 ± 1.0	62 ± 0.7
40 - 49	11 ± 0.6	61 ± 0.9
50 - 59	10 ± 0.5	61 ± 1.5
60 - 69	9 ± 0.3	58 ± 1.8
70 - 79	9 ± 0.3	58 ±1.8

Table A1.05: *Age differences in the tensile properties of skeletal muscle tissue from the rectus abdominis muscle in a mechanically stabilized state (48 hours after postmortem).*

UTS are greatest in the sartorious muscle and least in rectus femoris and gastrocnemius muscles. % elastic recovery, 36% - immediately after removal of stress and just before rupture, 43% - with elastic after effect, 90% - recovery in intact muscles, immediately after death and after removal of stress is 90% with elastic after effect it is 100%.

Classification	Muscle	UTS (g/mm^2)
Muscle of mastication	Masseter	13
Muscle of trunk	Sternocleidomastoidesu	19
	Trapezius	16
	Pectoralis major	13
	Rectus abdominis	14
Muscles of upper extremity	Biceps brachii	17
	Triceps brachii	15
	Flexor carpiradialis	21
	Brachioradialis	18
Muscles of lower extremity	Psoas major	12
	Sartorius	30
	Gracilis	20
	Rectus femoris	10
	Vatus medialis	15
	Adductor longus	13
	Semimembranous	13
	Gastrocnemius	10
	Tibialis anterior	22

Table A1.06: *Ultimate tensile strength (g/mm^2) of skeletal muscle tissue from various muscles of people 20 to 39 years of age (Just after death, average UTS = 32 g/mm^2, UPE = 60-70% for all muscles except gastrochemius = 105%).*
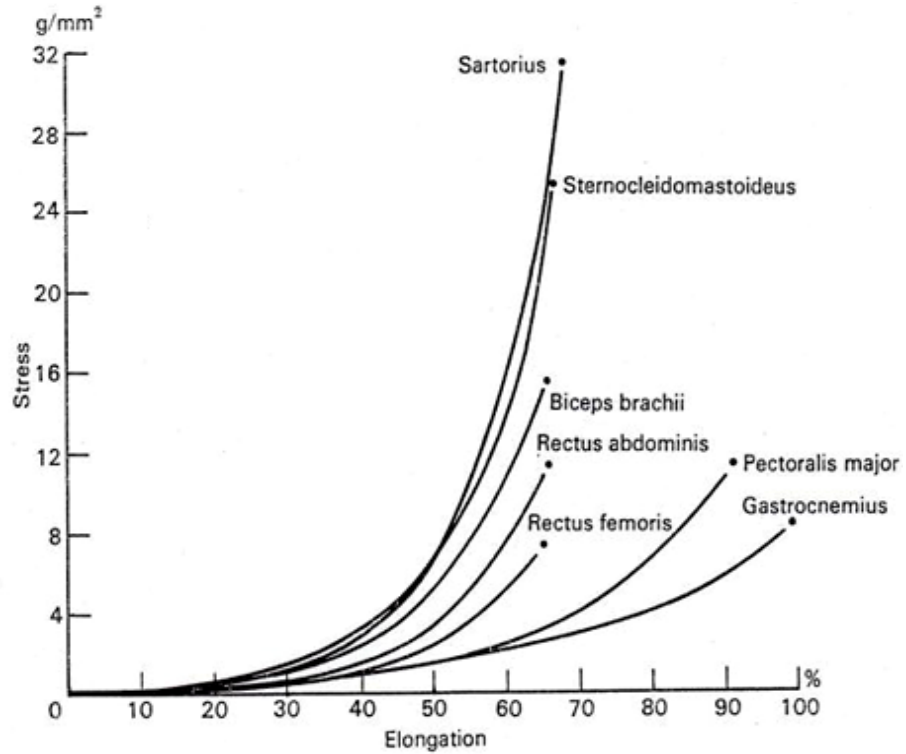
Fig A1.02: Stress-strain curves in tension of skeletal muscle of persons 29 years of age.

A1.3.3 Tensile Properties of Skeletal Muscle of Animals

UTS of rectus abdominis of dogs are much greater than rabbit & cat. Human skeletal muscle has UTS approximately equaling that of rabbits & cats.

Rabbits	UTS (g/mm^2)
Rectus abdominis	11
Masseter	19
Sartorius	15
Soleus	9
Semitendinosus	8

Table A1.07: Ultimate tensile strength of rabbits.

A1.3.4   Expansive Properties of Skeletal Muscle

Parameter	value
Ultimate expansive strength (kg/cm^2)	11 ± 0.47
Ultimate expansive strength per unit thickness (kg/cm^2/mm)	7.9
Ultimate Expansion	0.156 ± 0.0057 ml for an area of 7 mm in diameter

Table A1.08: Mechanical properties of rabbit's obliquus externus abdominis muscle.
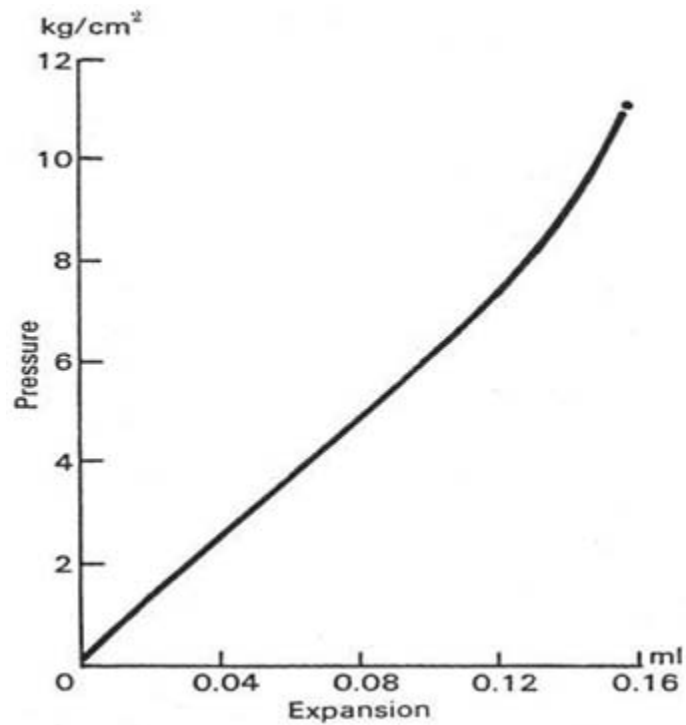
Fig A1.03: Pressure-expansion curve of obliquus externus abdominis muscle of rabbits.

A1.3.5   Tearing Properties of Skeletal Muscle

The tearing load of skeletal muscle tissue from the obliquus externus abdominis muscle of dogs is 0.89 ±0.07 kg and the tearing strength is 0.36 ± 0.03 kg/mm.

A1.3.6   Fasica

Human stress-strain curve in tension, in a direction parallel to the course of the fibers, of fascia of 30-39 years of age. In oblique direction tensile breaking load and UTS is one third that of in parallel direction and UPE is 1.2 times that of parallel direction. No significant sexual difference in any of the tensile properties.

	Tensile Breaking load (kg/mm) (direction parallel to course of fibers)	UTS (kg/mm^2)	UPE (%)
Fascia of thigh	1.14 ± 0.17	1.47 ± 0.21	16.7 ± 0.52
Fascia of leg	1.04 ± 0.14	1.14 ± 0.17	14.4± 0.51
Average	1.09	1.39	15.6

Table A1.09: *Mechanical properties of human thigh and leg fascias in direction parallel to course of fibers.*
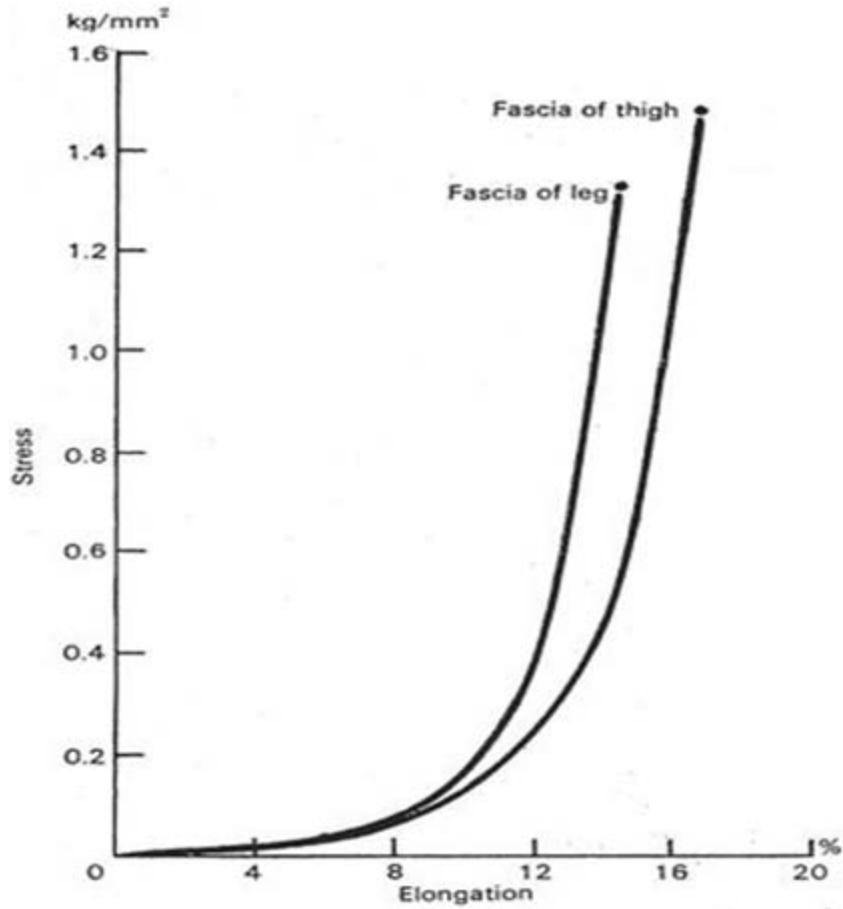
Fig A1.04: *Stress-strain curves in tension, in a direction parallel to the course of the fibers, of fascia of persons 30 to 39 years of age.*

Human fascia of the thigh and the leg in both directions has an ultimate tensile strength equal to that of the lumbodorsal fascia of rabbits.

	Tensile Breaking load (kg/mm)	UTS (kg/mm^2)	UPE (%)
Longitudinal	0.48	0.82±0.14	59±5.6
Transverse	0.20	2.0±0.11	46±3.9

Table A1.10: *Lumbodorsal fascia of several rabbits.*
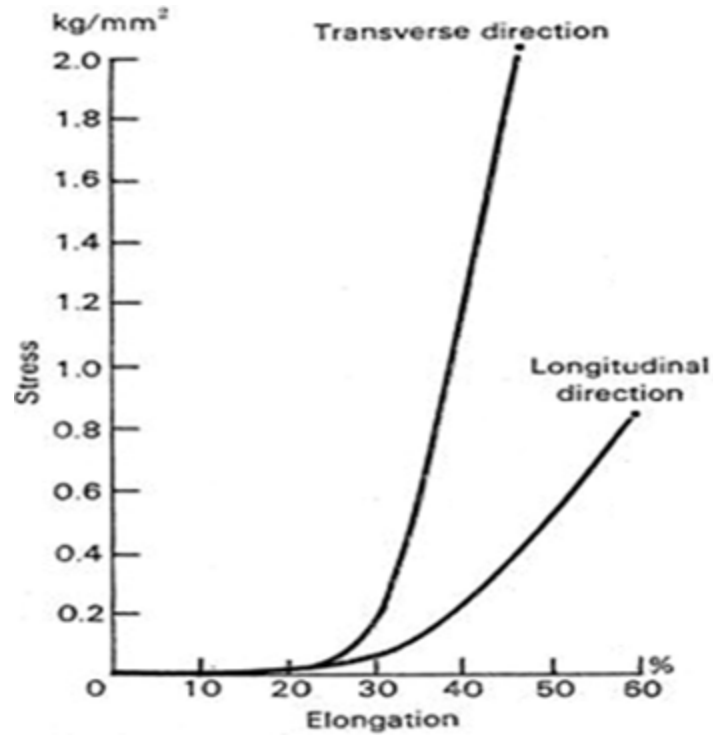
Fig A1.05: *Stress-strain curves in tension of lumbodorsal fascia of rabbits.*

A1.3.7 Expansive Properties of Fascia (human – thigh and leg)

No significant differences were found in the expansive properties of fascias. Ultimate expansion for an area 7mm in diameter is 0.08ml for fascia of thigh and 0.06±0.001 ml for fascia of the leg.

	Ultimate expansive strength (kg/cm^2)	Ultimate expansive strength per unit thickness (kg/cm^2/mm)
Thigh	53±2.2	67.7±1.2
Leg	53±2.2	67.6±1.8
Average	52	67.6

Table A1.11: *Expansive properties of human thigh and leg fascia.*
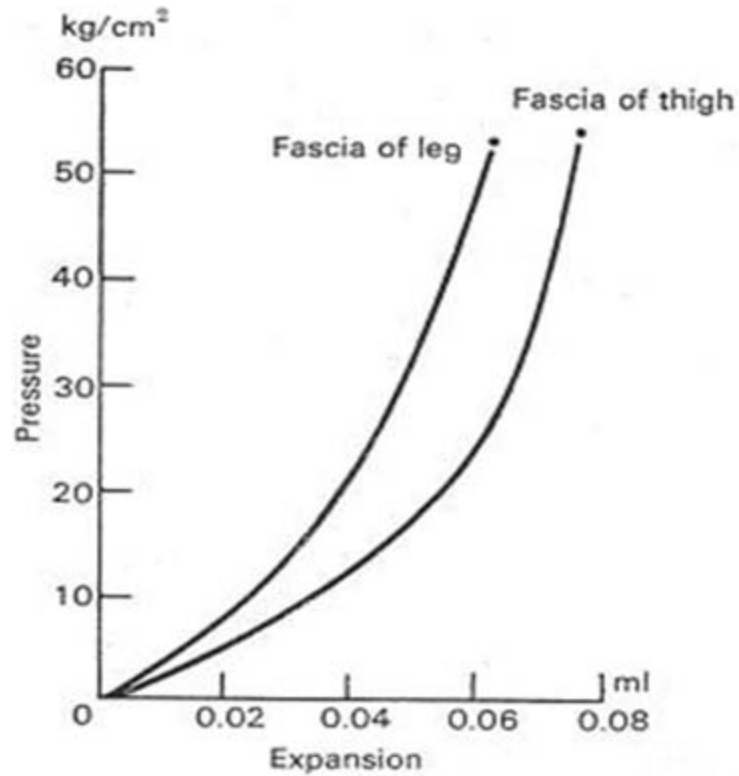
Fig A1.06: *Pressure-expansion curves of fascia of persons 30 to 39 years of age.*

A1.3.8　　　　Expansive Properties (rabbits – thigh & lumbodorsal fascia)

Human fascia has an ultimate expansive strength per unit thickness equal to rabbits. For 7 mm diameter area aperature, ultimate expansion is 0.072±0.0019 ml (lumbodorsal fascia), 0.083±0.0049 ml (fascia of thigh). Creep limit corresponds to 60% of the ultimate strength for the lumbodorsal fascia.

	Ultimate Expansive strength (kg/cm^2)	Ultimate Expansive strength per unit thickness (kg/cm^2/mm)
Lumbodorsal fascia	26.3±1.0	78
Thigh fascia	26.3±1.0	68
Average	25.6	73

Table A1.12: *Expansive properties thigh and lumdorsal fascias of rabbits.*
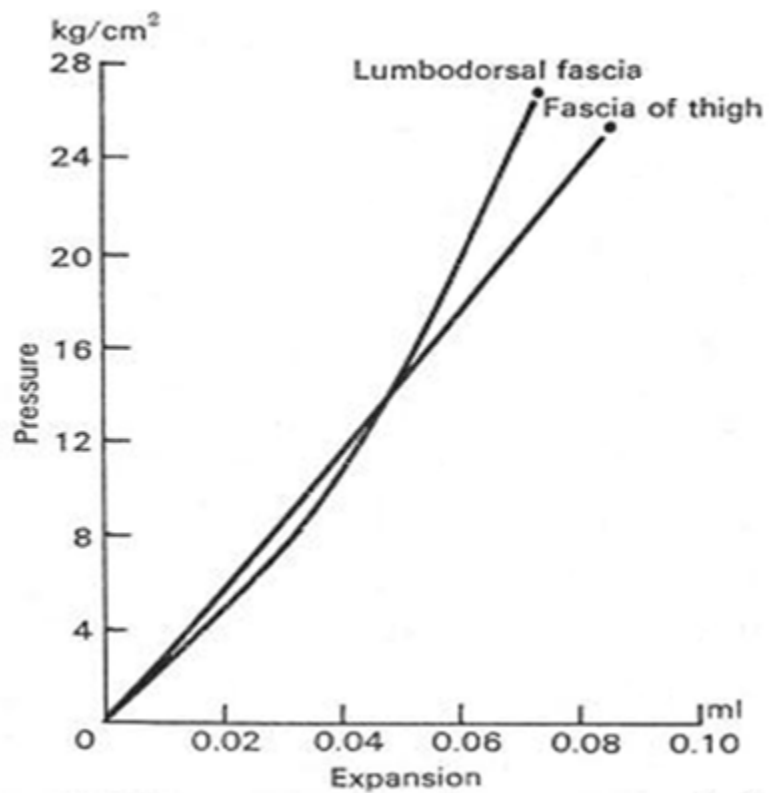
Fig A1.07: *Pressure-expansion curves of fascia of rabbits.*

A1.3.9   Aponeuroses

A sheet like fibrous membrane, resembling a flattened tendon, that serves as a fascia to bind muscles together or as means of connecting muscle to bone. Anterior abdominal aponeuroses are located just on top of the rectus abdominis musle. It has for its borders the external oblique, pectoralis muscle, and the latissimus dorsi.

	Ultimate Expansive Strength (kg/cm^2)	Ultimate Expansive strength per unit thickness (kg/cm^2/mm)	Ultimate Expansion for an area of 7 mm diameter (ml)
Aponeurotic tissue of central tendon	11.4±0.6	44	0.037±0.0025
Aponeurotic tissue of sheath of rectus abdominis	3.9±0.18	43	0.029±0.0014

Table A1.13: Expansive properties of aponeuroses.
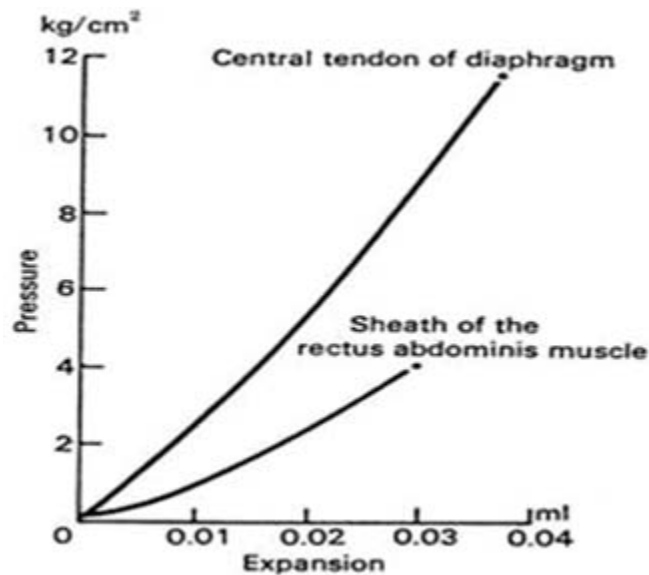
Fig A1.08: Pressure-expansion curves of aponeurotic tissue.

A1.4.1   Arteries

Mixed arteries: quantity of elastic and of the smooth muscle tissue is approximately equal. These are external & internal carotid arteries, axillary artery, common iliac artery, external & internal iliac arteries, femoral artery, visceral arteries (coronary artery, celiac artery, superior and inferior mesenteric arteries etc).

Age group (years)	Tensile Breaking load per unit width (g/mm)		Ultimate tensile strength (kg/mm^2)		Ultimate percentage elongation (%)	
	Longitudinal	Transverse	Longitudinal	Transverse	Longitudinal	Transverse
20-29	142	158	0.18	0.20	105	76
30-39	168	143	0.20	0.17	86	76
40-49	150	108	0.18	0.13	82	66
50-59	150	96	0.14	0.09	82	63
Average	152	120	0.17	0.14	87	69

Table A1.14: *Tensile properties of mixed arterial tissue from human femoral artery.*

The initial elongation limit is about 30% of the ultimate strength for both longitudinal and transverse. Creep limit in longitudinal direction, is about 55% and, in the transverse direction, 40% of the ultimate strength. In both the directions the elongation at creeping rupture is about five-sixths of the ultimate elongation in normal test.
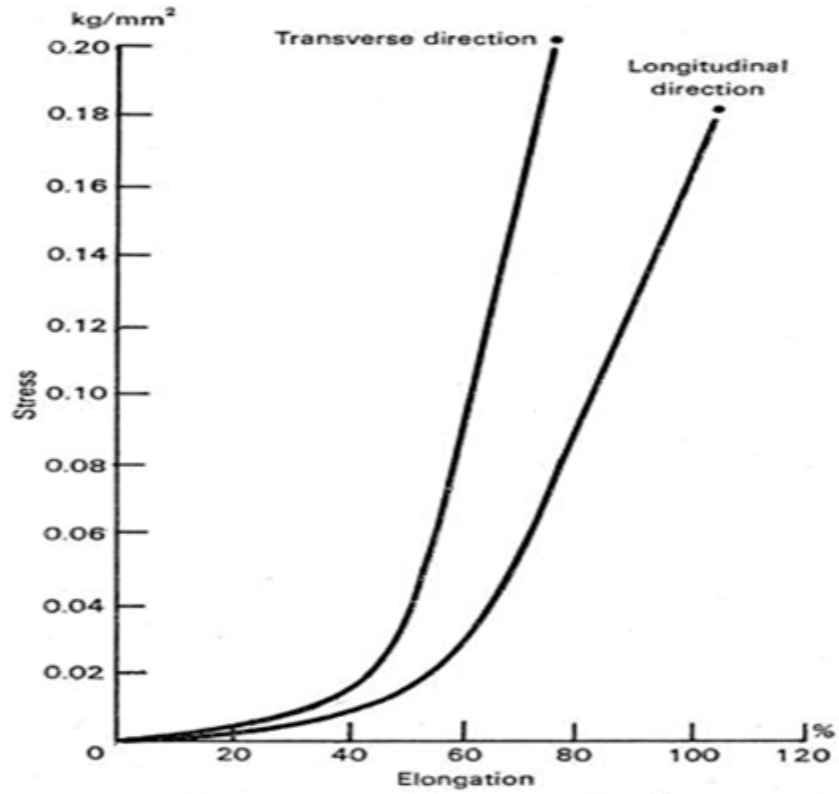
Fig A1.9: *Stress-strain curves in tension of femoral arterial tissue of persons 20-29 years of age.*

A1.4.2 Veins

Age group	Inferior vena cava		Femoral		Popliteal	
	Longitudinal	**Transverse**	**longitudinal**	**Transverse**	**longitudinal**	**Transverse**
20-39	102	245	159	211	116	180
40-59	87	224	149	217	116	197
60-69	68	224	149	224	116	158
Avg	89	232	153	216	116	182

Table A1.15: *Tensile breaking load per unit width (g/mm) of veins.*

Age group	Inferior vena cava		Femoral		Popliteal	
	Longitudinal	Transverse	longitudinal	Transverse	longitudinal	Transverse
20-39	0.15	0.36	0.24	0.32	0.20	0.31
40-59	0.11	0.28	0.21	0.31	0.17	0.29
60-69	0.08	0.27	0.20	0.29	0.15	0.20
Avg	0.12	0.31	0.22	0.31	0.18	0.27

Table A1.16: *Ultimate Tensile Strength (kg/mm^2) of veins.*

Age group	Inferior vena cava		Femoral		Popliteal	
	Longitudinal	Transverse	longitudinal	Transverse	longitudinal	Transverse
20-39	98	58	97	79	112	77
40-59	77	47	72	67	97	77
60-69	70	44	72	56	81	77
Avg	84	51	82	70	100	77

Table A1.17: *Ultimate percentage elongation of veins.*
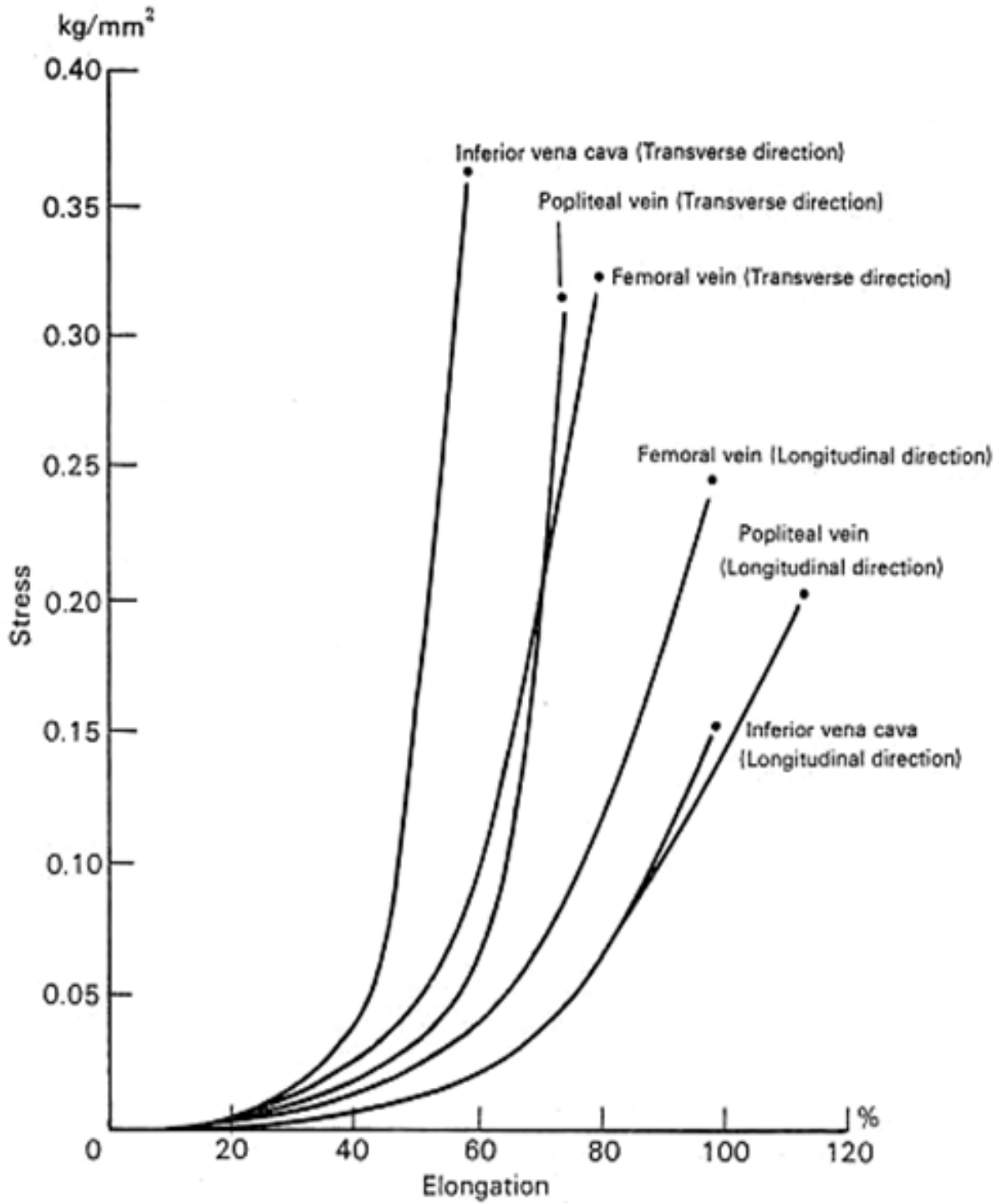
Fig A1.10: *Tension stress-strain curves of venous tissues of persons of 20-39 years of age.*

A1.6.1   Umbilical Cord

Average breaking load of the intact umbilical cord is 3 times the body weight in mature fetuses.

Lunar months	Tensile Breaking load (kg)	Tensile Breaking load (kg) of weakest portion	Ultimate tensile strength (g/mm^2)	Ultimate % elongation
4	0.6±0.08	0.3±0.05	26±1.2	36±1.8
5	1.8±0.12	0.9±0.05	40±2.2	41±1.8
6	3.5±0.24	2.5±0.25	62±3.7	44±1.2
7	4.9±0.12	3.6±0.19	78±3.1	47±1.7
8	6.5±0.28	4.8±0.20	99±4.2	50±1.6
9	7.8±0.22	5.1±0.27	120±3.5	55±1.3
10	9.4±0.31	5.8±0.22	139±6.1	57±2.4
Terminus	10±0.3	6.5±0.2	150±5	59±2

Table A1.18: *Tensile properties of human fetuses.*
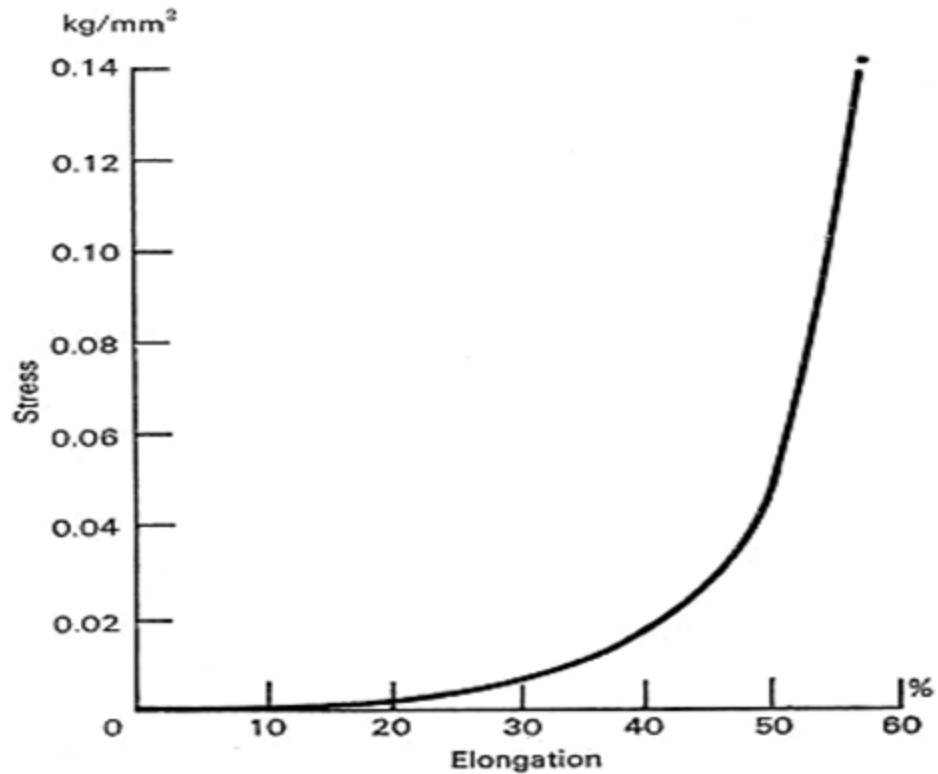
Fig A1.11: *Stress-strain curve in tension of the umbilical cord in the 10th lunar month of pregnancy.*

A1.7.1   Nerves

The strength during the first two decades of life is 90% of the adult strength. Ultimate percentage elongation of bundles of nerve fibers shows no age changes from the first decade of life up to the 60-69 age groups. Elastic limit is 75% of the ultimate strength. Percentage of elastic recovery is 97% just before rupture and immediately after removal of stress.

	Ultimate tensile strength (kg/mm^2)	Ultimate percentage elongation
Femoral	1.30±0.009	18.5±0.14
Intercostal	1.30±0.013	18.4±0.08

Table A1.19: *Tensile properties of secondary bundles of human nerve fibers (20-39 year age group).*
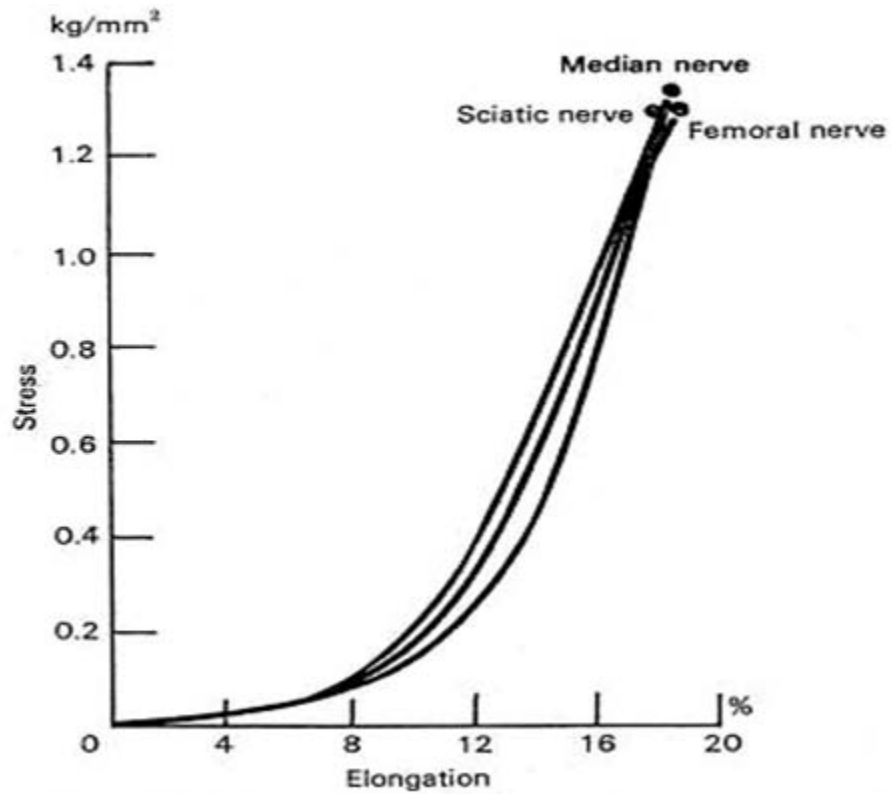
Fig A1.12: *Stress-stain curves in tension of nerves of persons 20 to 39 years of age.*

A1.7.2 Skin

Region	Tensile breaking load per unit width (kg/mm)		Ultimate tensile strength (kg/mm^2)		Ultimate percentage elongation	
	30-49 year	Adult Avg	30-49 year	Adult Avg	30-49 year	Adult Avg
Upper Abdomen	2.4	2.1	1.13	1.02	126	98
Lower Abdomen	2.2	2.0	1.16	1.04	123	95

Table A1.20: *Average values for the tensile properties, in the longitudinal and transverse directions of human skin.*

Skin from females has a much lower breaking load than that from males, but there is no significant sexual difference in the ultimate strength. Generally tensile breaking load and ultimate strength are much greater in transverse than in longitudinal direction. UPE is greatest in people from 10-29 years age and least in 70-79 years age. Between 10-39 years of age the UPE of skin in females is greater than in males although there is no significant difference after 40 years. As a whole, the elongation is greater in transverse direction than in longitudinal direction.

Age group year	Tensile Breaking load per unit width (ratio)	Ultimate tensile strength (ratio)	Ultimate percentage elongation (ratio)
10-29	0.70	0.65	1.00
30-49	1.00	1.00	0.80
50-59	0.78	0.91	0.73
60-69	0.70	0.82	0.64
70-79	0.46	0.70	0.57

Table A1.21: *Age differences in the tensile properties of human skin, tabulated in ratio.*
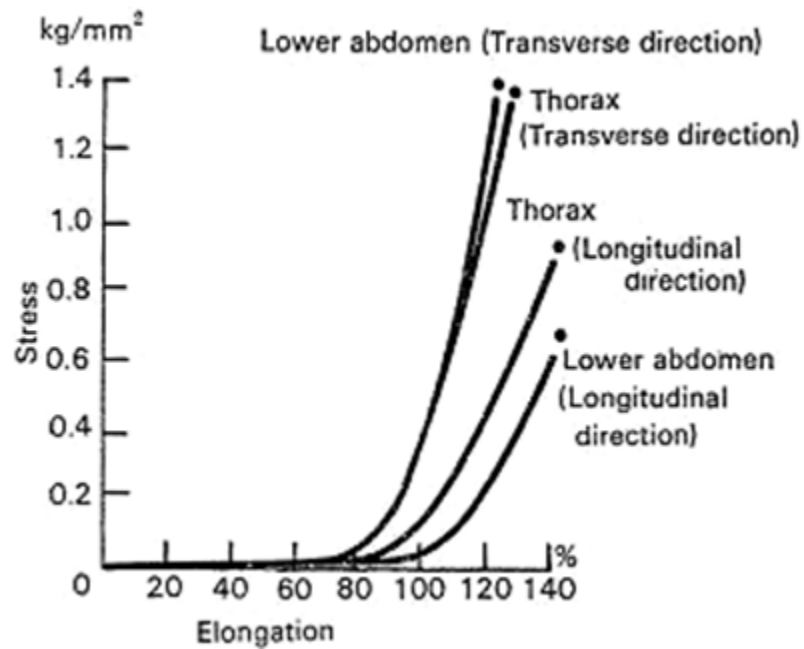
Fig A1.13: *Stress-strain curves in tension of the skin of persons 20 to 29 years of age.*

A1.7.3   Panniculus Adiposus

Panniculus adiposus have an ultimate tensile strength of 8 ± 0.4 g/mm^2, ultimate percentage elongation of 26 ± 0.7 percentage, ultimate expansive strength per unit thickness of 0.71 ± 0.023 kg/cm^2/mm and an ultimate expansion for an area 7 mm in diameter of 0.046 ± 0.0015 ml.
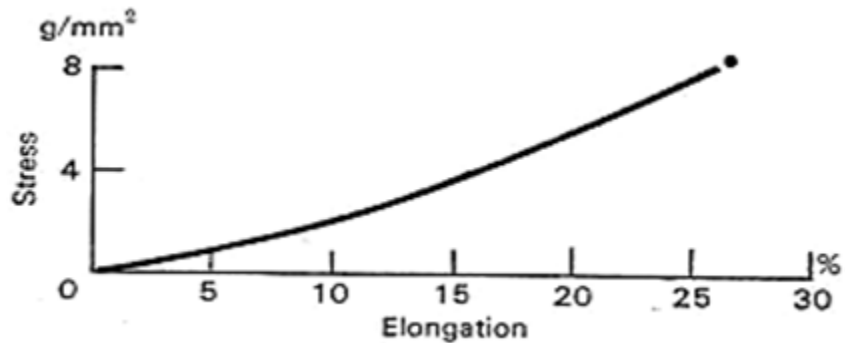
Fig A1.14: *Stress-strain curve in tension of the panniculus adiposus of pigs.*
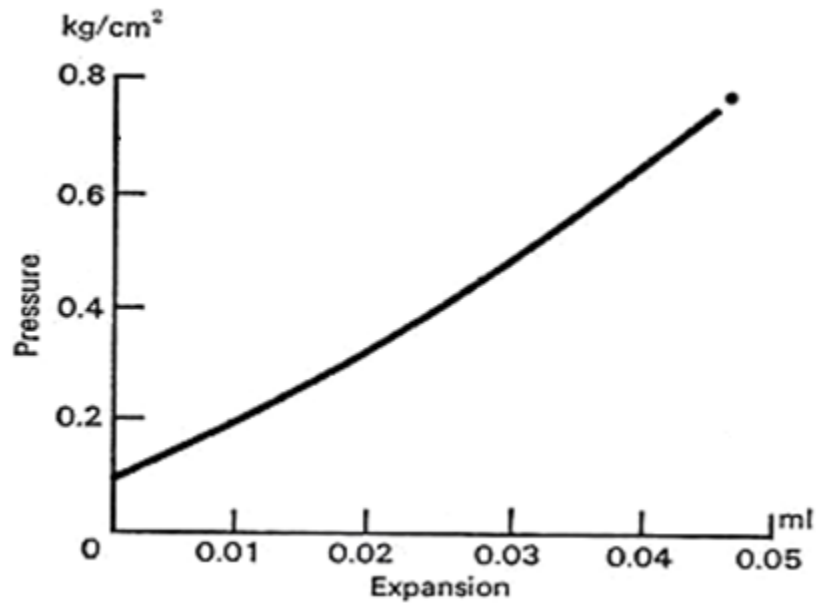
Fig A1.15: *Pressure-expansion curve of the panniculus adiposus of pigs.*

112

Age group	Average co-efficient of variation (%)
20-29	21
30-39	22
40-49	23
50-59	24
60-69	25
70-79	26

Table A1.22: *Average co-efficient of variation, at the 95% limits, of the mechanical property values of all organs according to age group.*

Age group	Average co-efficient of confidence (%)
20-29	8
30-49	9
50-69	10
70-79	11

Table A1.23: *Average co-efficient of confidence, at the 95% limits, of the mechanical property values of all organs according to age group.*

Age group (year)	UTS	UPE
10-19	1.27	1.02
20-29	1.00	1.00
30-39	0.87	0.97
40-49	0.73	0.95
50-59	0.67	0.95
60-69	0.60	0.91
70-79	0.60	0.91

Table A1.24: *Ratios for age changes in tensile properties of human skeletal muscle.*

20-29 age group is taken as standard for comparison because maximum value of mechanical properties are found in this group (but in some case 10-19 age group show higher values).

APPENDIX – 2: Data Book - Abe et al.

A Summary of

DATA BOOK ON MECHANICAL PROPERTIES OF LIVING CELLS, TISSUES AND

ORGANS

H.Abe, K.Hayashi, M.Sato (Eds), Springer, New York, 1996.

A2.1 Skeletal Muscle Mechanical Properties

Force–Length Relation

• Load–extension curve • Maximum isometric tension	• Frog • Semitendinosus muscle	• Isolated muscle fiber • Resting state

Materials
- Frogs, *Rana nigromaculata*
- Semitendinosus muscle
- Small bundle of fast muscle fibers prepared from ventral caput

Testing Methods and Experimental Conditions
- Relation between force and extension of the resting muscle was measured in Ringer's solution at 10°C
- Standard length of 14 mm in all preparations

Data

	Maximum isometric tension P_0 ($\times 10^{-3}$ N)	Cross-sectional area (mm^2)
a, whole muscle	410	1.0~2.5
b, two-bundle preparation	42	0.82
c, two-bundle preparation	74	0.38
d, single fiber	2.8	0.016
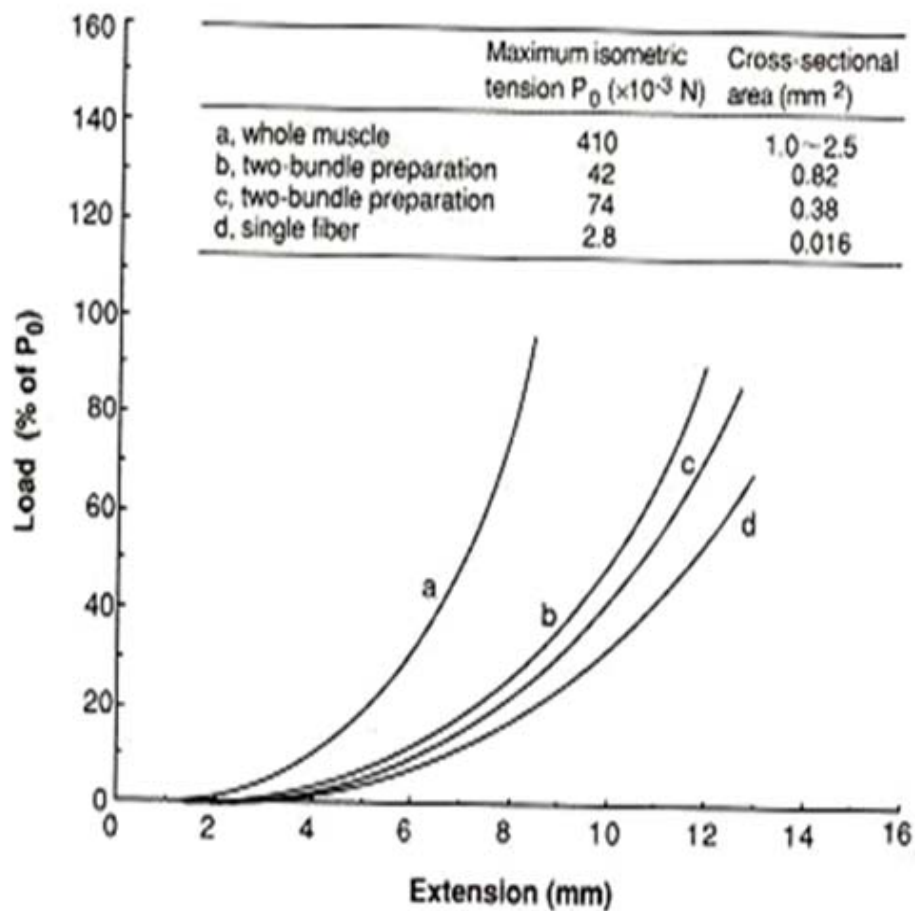
Force–Length Relation

| • Force–extension relation
• | • Frog
• Semitendinosus muscle | • Isolated muscle fiber
• Series elastic component |

Materials
- Frogs, *Rana nigromaculata*
- Semitendinosus muscle
- Small bundle of fast fibers prepared from ventral caput

Testing Methods and Experimental Conditions
- Temperature, 10°C
- Tension–extension curve of the series elastic component (SEC) was directly determined by a controlled quick-release method
- Two kinds of preparations, short tendons and normal long tendons, were used

Data
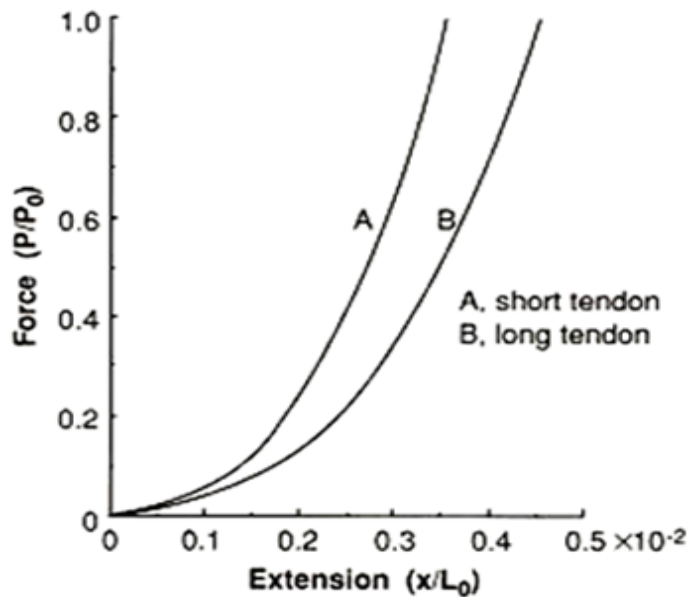
Comments
- P, tension; P_0, maximum isometric tension; x, extension; L_0, standard length.
- In the short tendon preparation, the extension of SEC was about 3.5% L_0 at the tension of P_0 but it was 4.5% L_0 in the long tendon preparation.
- The tension–extension curves are expressed by
  $P/P_0 = 2.9X + 51.8 X^2 + 1.9 \times 10^4 X^3$ for short tendon preparation, and
  $P/P_0 = 2.3X + 31.4 X^2 + 0.9 \times 10^4 X^3$ for long tendon preparation.
  where $X = x/L_0$.

117

Force–Length Relation

• Stress–sarcomere length •	• Frog • Semitendinosus muscle	• Isolated muscle fiber • Resting state

Materials
- Frogs, *Rana pipiens*
- Intact whole semitendinosus fiber

Testing Methods and Experimental Conditions
- Resting muscle in phosphate-buffered Ringer's solution
- Temperature, 11.2°, 16.3°, and 26.2°C

Data
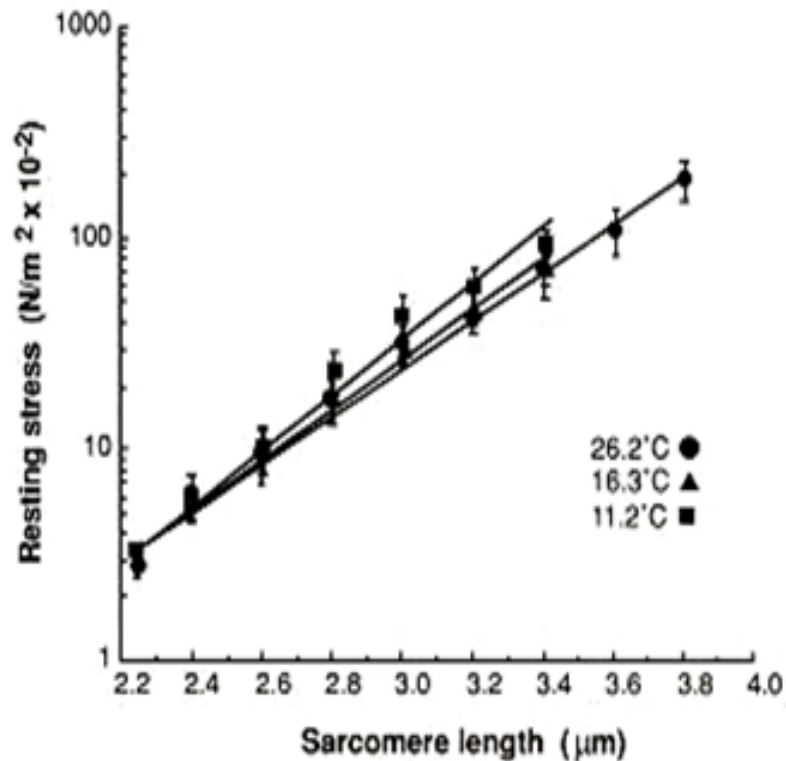
Comments
- The data fit to $\sigma = a \cdot \exp(b\epsilon)$, where σ = resting stress, ϵ = sarcomere strain, a and b = constants.
- The mean static resting stress at resting length for the three temperatures was 290 ± 18 N/m² (mean ± SE).

Force–Length Relation

• Tension–sarcomere length •	• Rabbit • Adductor magnus muscle	• Isolated muscle fiber • Resting state

Materials
- Rabbits (adult)
- Mechanically skinned single fiber prepared from six different muscle tissues (adductor magnus [AM], psoas [PS], longissimus dorsi [LD], sartorius [SA], soleus [SO], semitendinosus [ST])

Testing Methods and Experimental Conditions
- Stress–strain relation under relaxing conditions
- Temperature, 24°C

Data

○ Immediately after each stretch
● After 2.5 min of stress–relaxation

Tension (×10⁻⁵ N) vs Sarcomere Length (μm)
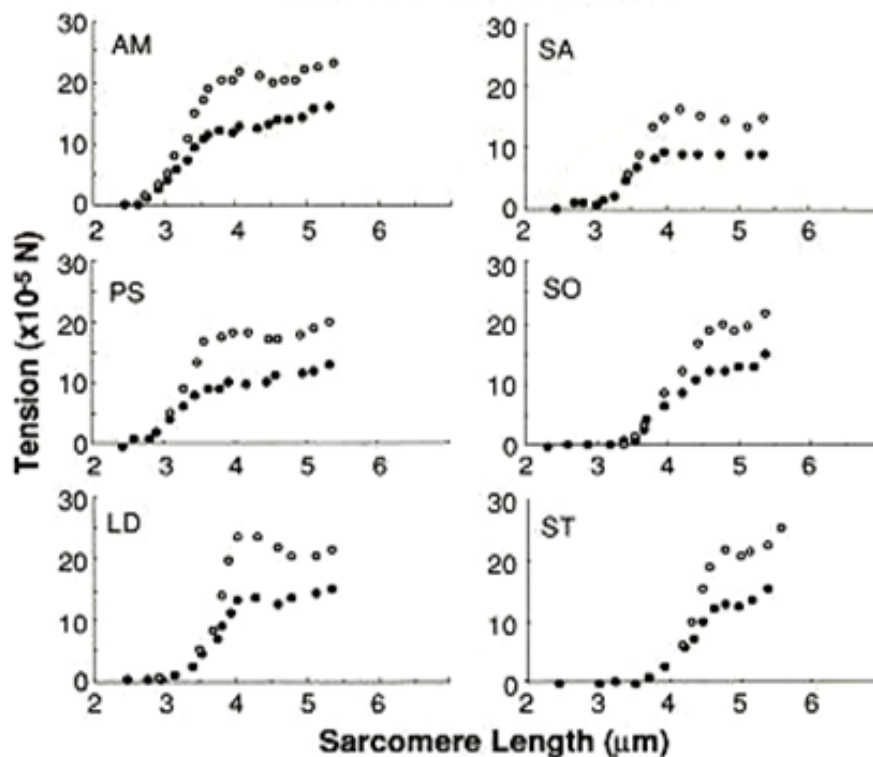
Comments
- The stress–strain relation under relaxing conditions is due to the reversible extension of a segment of titin (connectin) between the Z line and the ends of thick filaments.
- The data suggest that skeletal muscle cells may control and modulate elasticity and compliance and the elastic limit of the sarcomere by selective expression of specific titin size isoforms.

119

Force–Length Relation

• Stress–sarcomere length • Initial elastic modulus	• Frog • Semitendinosus muscle	• Isolated muscle fiber • Resting state

Materials
- Frogs, *Rana pipiens* (6.3–8.5 cm from nose to vent)
- Intact and mechanically skinned single fiber from semitendinosus muscle

Testing Methods and Experimental Conditions
- Resting muscle in normal or calcium-free Ringer's solution
- Room temperature, 20°–22°C

Data
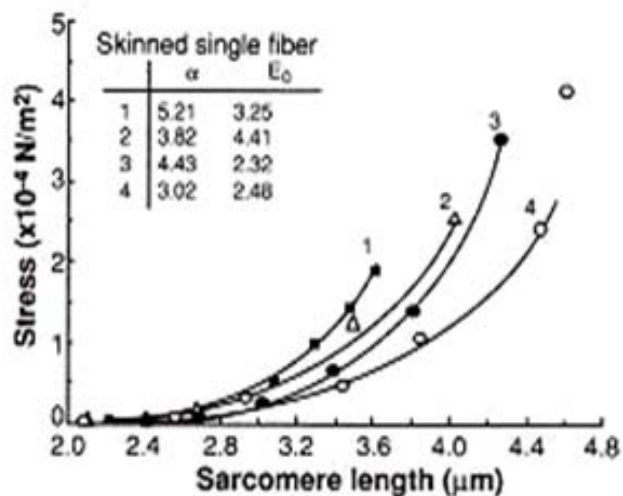
Preparation	Number of samples	Exponent α	Initial elastic modulus E_0 ($\times 10^3$ N/m^2)
Whole muscle	11	4.28 ± 0.19	2.6 ± 0.25
Intact single fiber	10	4.04^a	9.8^a
Skinned single fiber	12	4.13 ± 0.10	5.4 ± 0.75

Date are given as mean ± SE.

[a] No SEs are reported because these values were obtained from a single analysis of pooled data.

Comments
- Stress–strain relation was expressed by

$$\sigma = (E_0/\alpha)(\exp(\alpha\varepsilon) - 1)$$

σ, stress (force per cross-sectional area); E_0, initial elastic modulus; α, empirical constant; ε, sarcomere strain.

Force–Velocity Relation

| • Force–power relation | • Frog | • Isolated muscle fiber |
| | • Anterior tibialis muscle | |

Materials

- Frogs, *Rana temporaria*
- Single living fiber from anterior tibialis muscle

Testing Methods and Experimental Conditions

- Shortening velocity was measured applying isotonic release
- Fibers were tetanized by electrical stimulation
- Experiments were carried out at 1.0°–2.5°C
- Force–velocity relation was determined for fibers in fatigue, which was produced by reducing the interval between isometric tetani to 15 or 30 s

Data
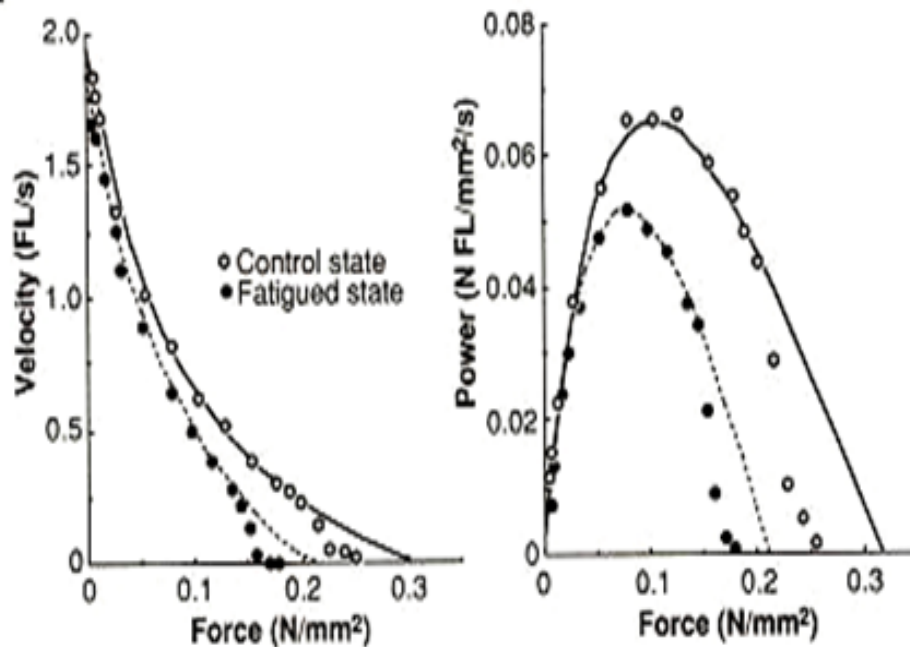
Comments

- Fatigue reduced isometric force (P_0) by $25.8 \pm 1.6\%$ (mean $\pm$ SE, $n = 13$) and depressed the maximum velocity of shortening by $10.2 \pm 2.2\%$. The force–velocity relation became less curved, a/P_0 (Hill's (1938) parameter) being increased by $29.5 \pm 8.8\%$. Thus, power was less affected than isometric force or V_{max}.

121

Force–Velocity Relation

• Force–power relation	• Human	• Training effect
•	• Flexor muscle	•

Materials
- Human
- Flexor muscle around elbow

Testing Methods and Experimental Conditions
- Force–velocity relationship at the maximal effort was measured in elbow flexion using different weights, and effects of training on the relationship were studied
- A subject of each group flexed the elbow with load of 0%, 30%, 60%, and 100% of P_0 (maximum tension) at maximal effort 10 times a day, 3 days a week for 12 weeks
- Force and velocity were calculated at the wrist

Data
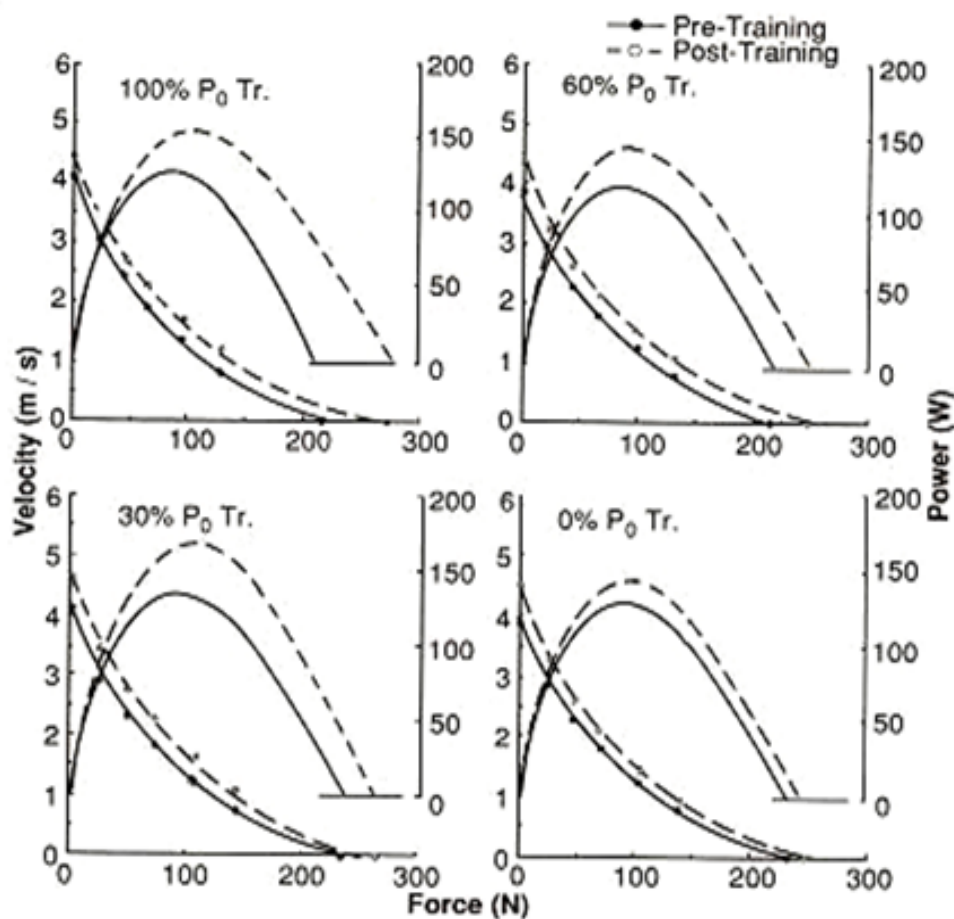
Force–Velocity Relation

• Force–power relation •	• Human • Leg extensor muscle	• •

Materials
- Human (non–athlete, skier, runner, football player)
- Leg extensor muscle

Testing Methods and Experimental Conditions
- Force–velocity relationship at the maximal effort was measured in knee extension using a lever-pulley with different weights
- Velocity is the tangential velocity of the ankle, and force is applied at the point 0.3 m from the knee

Data
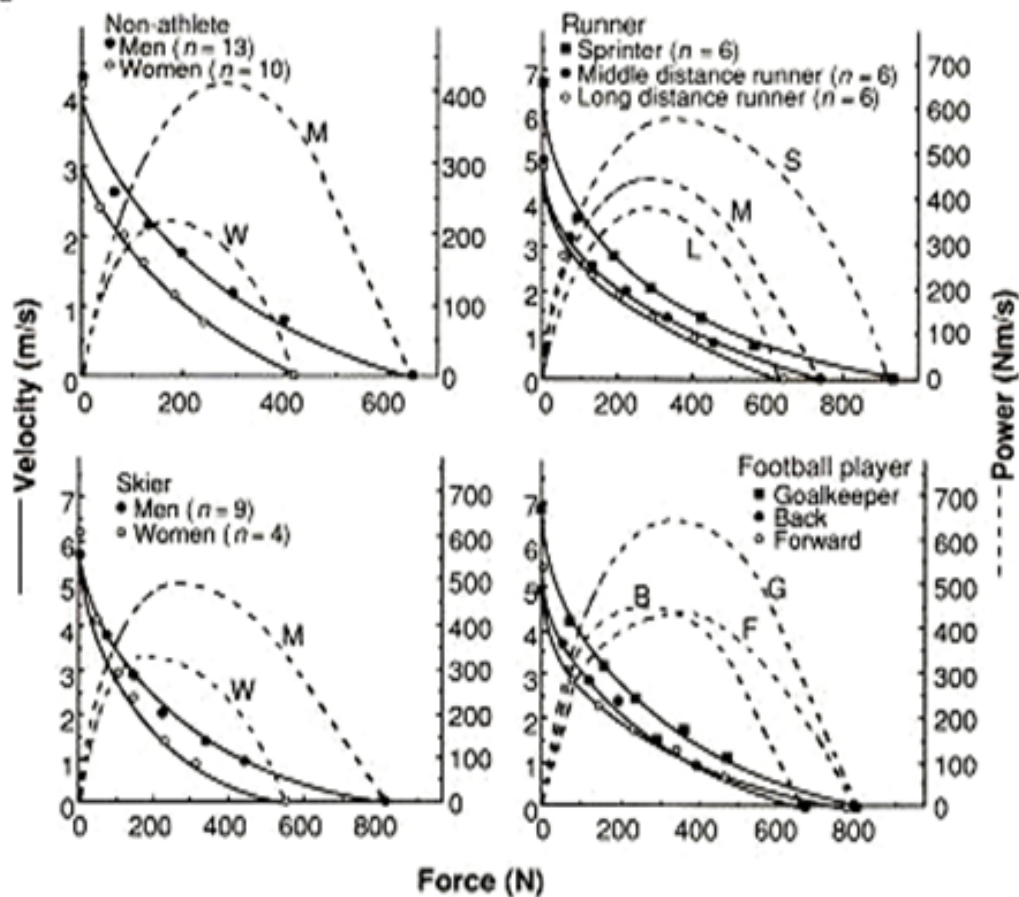
Force–Velocity Relation

|		
• Force–velocity relation •	• Frog • Anterior tibialis muscle	• Isolated muscle fiber •

Materials
- Frogs, *Rana temporaria*
- Single living fiber from anterior tibialis muscle

Testing Methods and Experimental Conditions
- Shortening velocity was measured applying isotonic release
- Fibers were tetanized by electrical stimulation
- Experiments were carried out at 1.0°–3.3°C

Data
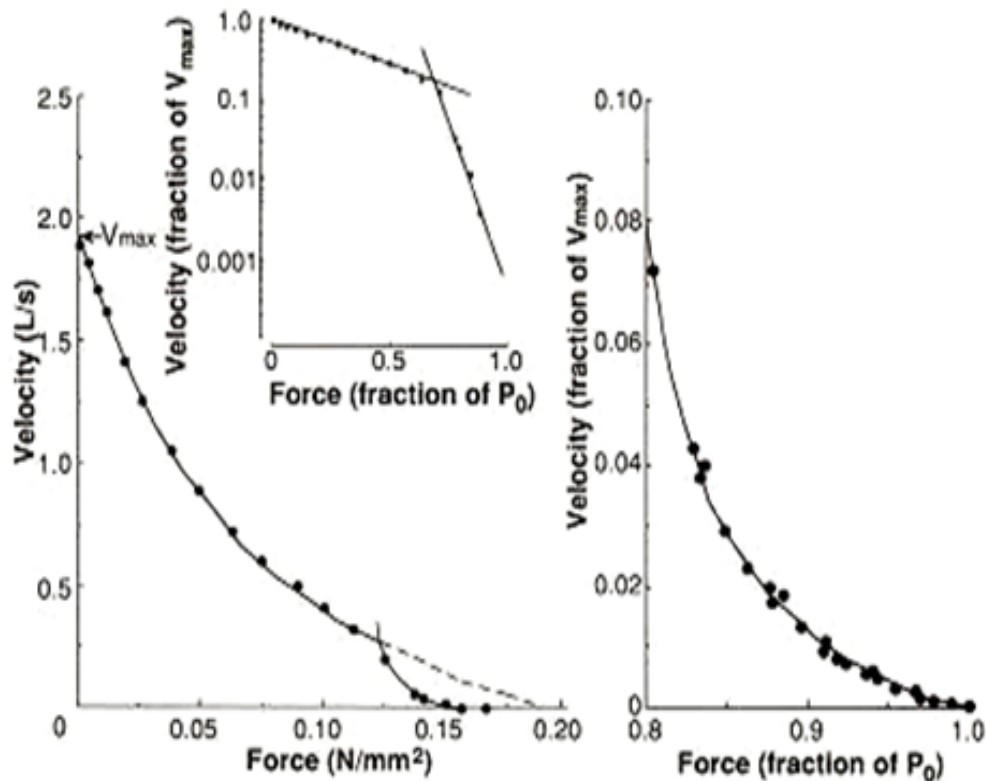
Comments
- The force–velocity relation had two distinct regions, each one exhibiting an upwards concave shape, that were located within the ranges 0%–78% and 78%–100% of the measured isometric force (P_0), respectively. The two portions of the force–velocity relation could be fitted well by hyperbolic functions or by single exponential functions.

124

Force–Velocity Relation

• Force–velocity relation	• Frog	• Isolated muscle fiber
•	• Iliofibularis muscle	•

Materials

- Frogs, *Xenopus laevis*
- Single living twitch and slow fibers from iliofibularis muscle

Testing Methods and Experimental Conditions

- Shortening velocity was measured by subjecting the fibers to isotonic release or afterloaded shortening
- Twitch fibers were tetanized by electrical stimulation. Slow fibers were activated by applying high K (30–75 mM) solutions
- Experiments were carried out at 5°–20°C for twitch fibers, and 21°–24°C for slow fibers

Data
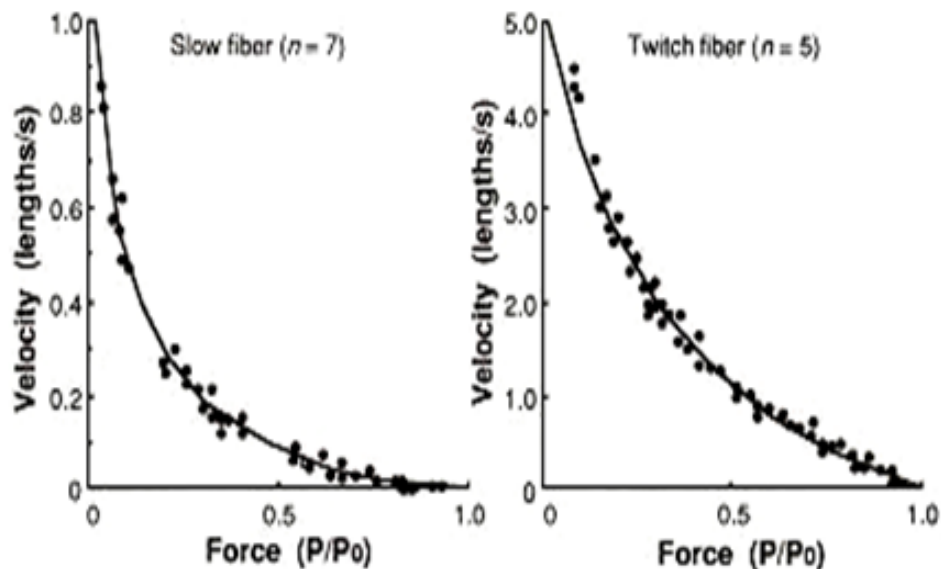
Comments

- Force–velocity data for slow fibers could be represented by a hyperbola with the constants $a = 0.10P_o$, $b = 0.11$ lengths/s; extrapolated V_{max} was 1.10 lengths/s.
- Force–velocity data for twitch fibers were reasonably well fitted by the hyperbola with the constants $a = 0.38P_o$, $b = 1.97$ lengths/s; extrapolated V_{max} was 5.20 lengths/s.
- Calculations based on AF Huxley's (1957) model for muscle contraction indicated that cross-bridge turnover rate was about 15 times lower in slow than in twitch fibers.

Force–Velocity Relation

• Force–velocity relation	• Frog	• Isolated muscle fiber
•	• Sartorius muscle	•

Materials

- Frogs, *Rana temporaria* or *Rana esculenta*
- Whole sartorius muscle

Testing Methods and Experimental Conditions

- Shortening velocity was determined applying isotonic release
- Fibers were tetanized by electrical stimulation
- Experiments were carried out at 0°C

Data
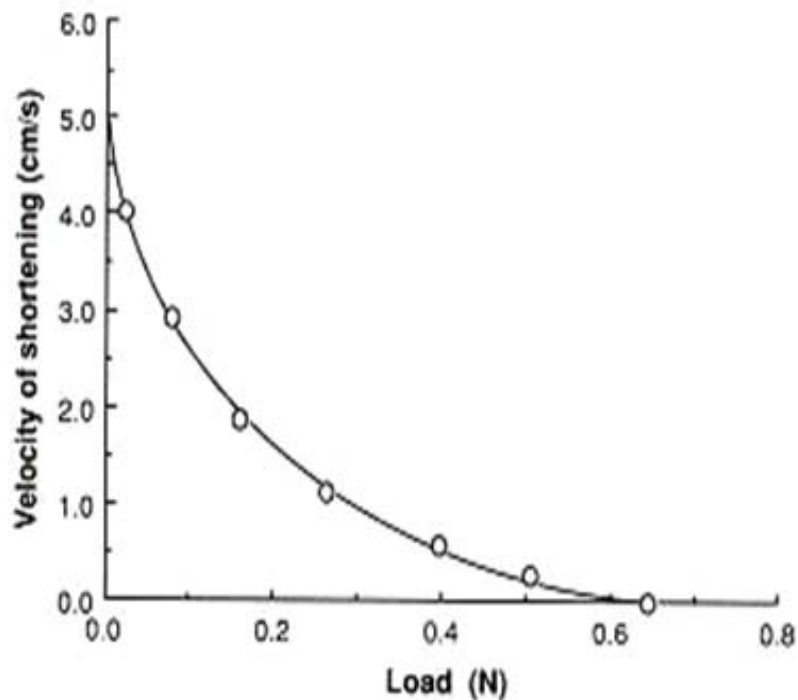
Comments

- Each circle denotes the mean of two observations in a series and reverse.
- The relation between speed of shortening, v, and load, P, is described by $(P + a)(v + b) =$ constant.

Force–Velocity Relation

• Force–velocity relation	• Frog	• Isolated muscle fiber
•	• Sartorius muscle	•

Materials
- Frogs, *Rana temporaria* or *Rana esculenta*
- Whole sartorius muscle

Testing Methods and Experimental Conditions
- Shortening velocity was determined applying isotonic release
- Loads greater than isometric tension were also applied
- Fibers were tetanized by electrical stimulation
- Experiments were carried out at $0°–20°C$

Data

A_1, *Rana temporaria* $(11.8°C)$
A_2, *Rana temporaria* $(0°C)$
B , *Rana esculenta*
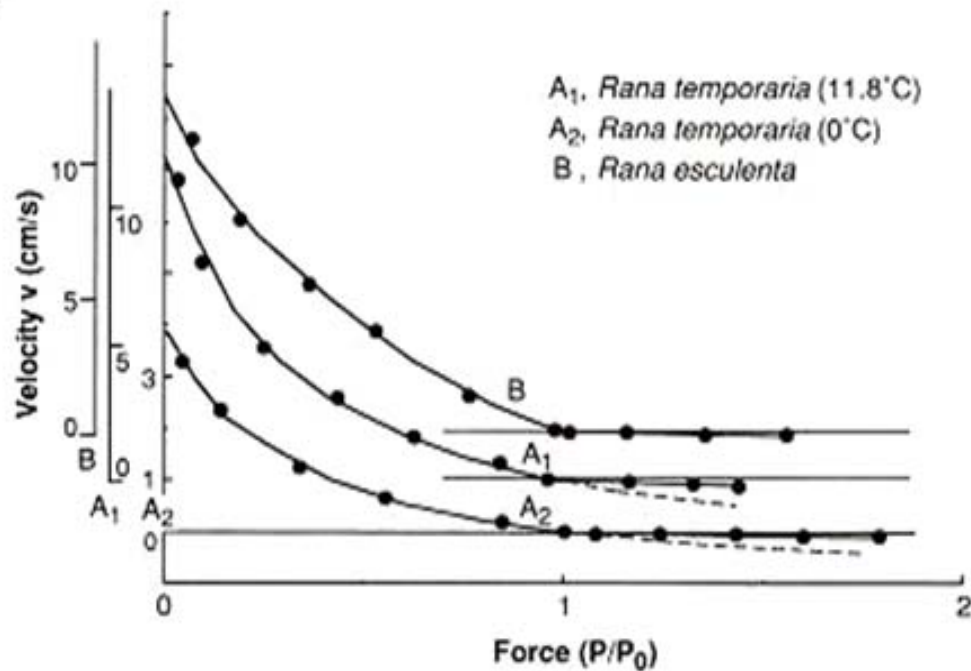
Comments
- The broken lines give the theoretical P–v relation for lengthening, using the constants a and b derived from the speeds of shortening.
- The observed relation between applied force and speed of isotonic shortening is satisfactorily described by Hill's hyperbolic equation $(P + a)(v + b) = constant$.
- The relation between a force greater than isometric and the resulting speed of "reversible" lengthening was determined. The observed velocities are considerably smaller than calculated from theory. If the applied force exceeds the isometric tension by 70–100%, the muscle "relaxes" rapidly.

Force–Velocity Relation

• Force–velocity relation	• Frog	• Isolated muscle fiber
•	• Semitendinosus muscle	•

Materials
- Frogs, *Rana nigromaculata*
- Semitendinosus muscle
- Small bundle of fast muscle fibers prepared from ventral caput

Testing Methods and Experimental Conditions
- Load–velocity relations were measured at different levels of contraction in Ringer's solution at 10°C

Data

Force (P/P₀)
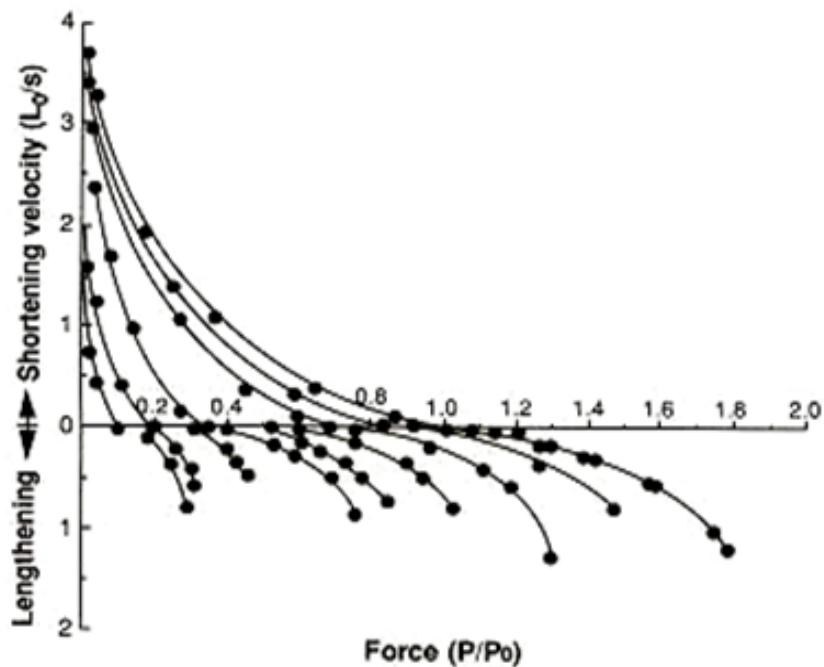
Comments
- Force–load–velocity relation (length region of 0.8 ~ 1.2 L_0):

  $(P + \alpha)(v + b) = b(F + \alpha)$ for shortening, where $\alpha = (a/P_0)F$, $a/P_0 = 0.25$, and $b = 0.9L_0/s$.

  $(P - 2F - \alpha')(v - b') = b'(F + \alpha')$ for lengthening, where $\alpha' = (a'/P_0)F$, $a'/P_0 = 0.4$, and $b' = 0.85L_0/s$.

  P_0, maximum isometric tension; F, contractile force (tension at $v = 0$); a and b, dynamic constants (shortening); a' and b', dynamic constants (lengthening); P, load; v, velocity (positive for shortening); L_0, standard length.

128

Force–Velocity Relation

| • Force–velocity relation
• | • Human
• Flexor muscle | •
• |

Materials
- Human
- Flexor muscle around elbow

Testing Methods and Experimental Conditions
- Force–velocity relationship at the maximal effort was measured in flexion of the elbow using different weights
- Force and velocity were measured at the hand

Data

Top-left graph: $a / P_0 = 0.33$, Velocity (m/s) vs Force (N)

Top-right graph: $a / P_0 = 0.48$, Velocity (m/s) vs Force (N)

Bottom-left graph: $a / P_0 = 0.42$, Velocity (m/s) vs Force (N)

Bottom-right graph: $a / P_0 = 0.37$, Velocity (m/s) vs Force (N)
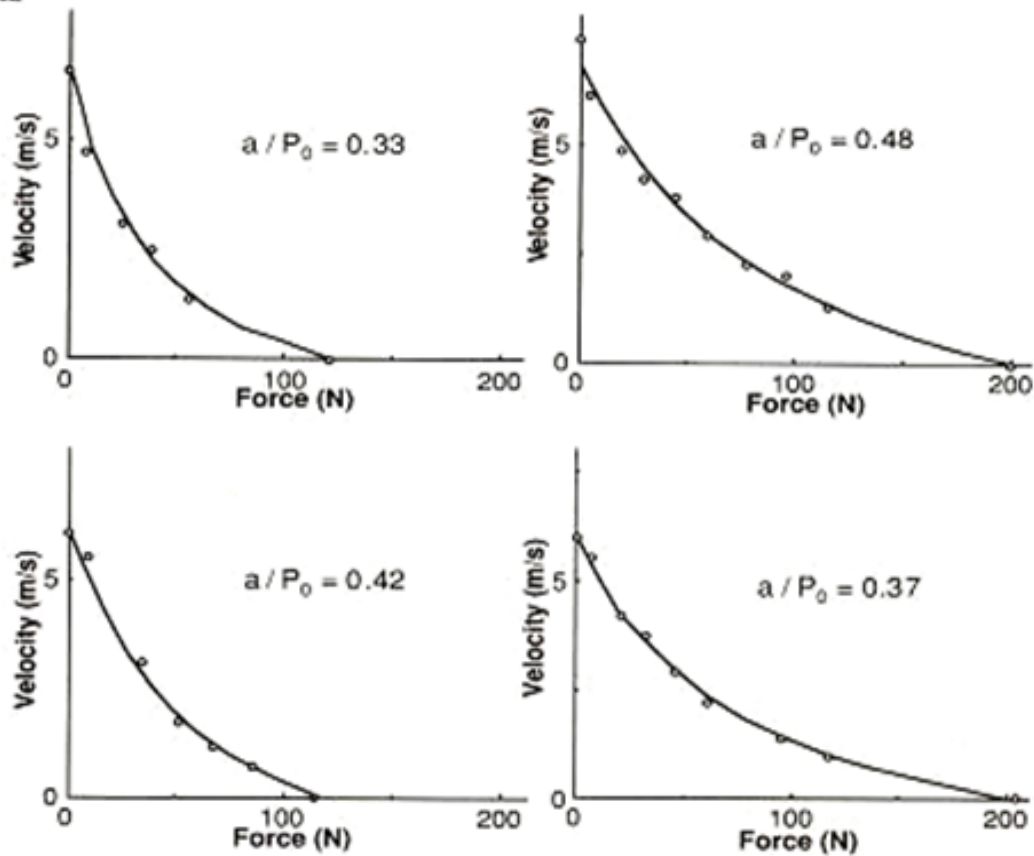
Comments
- P_0, force exerted at zero speed; a, constant of Hill's equation.
- Five muscles were involved in the movement of flexion of the elbow.

Force–Velocity Relation

<table>
<tr><td>• Force–velocity relation
•</td><td>• Human
• Gastrocnemius muscle</td><td>•
•</td></tr>
</table>

Materials
- Human
- Gastrocnemius muscle

Testing Methods and Experimental Conditions
- Force–velocity relationship at the submaximal effort (indicated by constant EMG) was measured in plantar flexion of the foot using a dynamometer
- Force–velocity curves were plotted at four different levels of submaximal excitation

Data
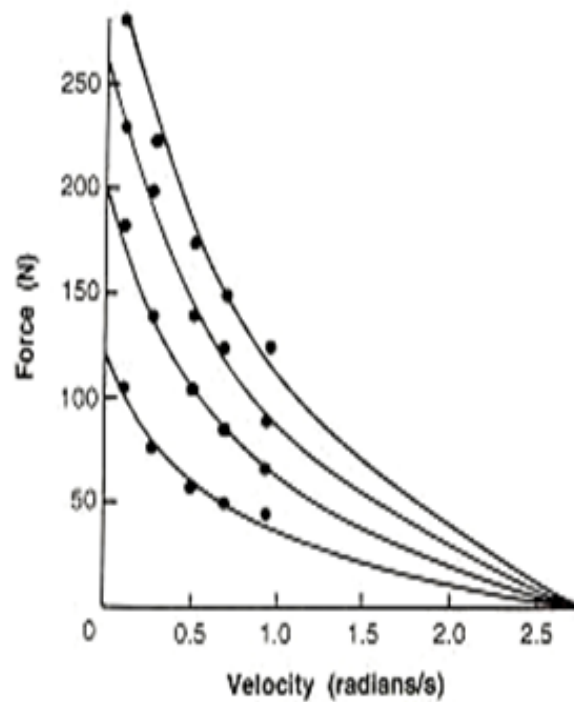
Comments
- Forces are approximately 1/10 of forces calculated in the tendon.

Force–Velocity Relation

| • Force–velocity relation | • Rabbit | • Isolated muscle fiber |
| • | • Psoas muscle | • ATP concentration |

Materials
- Rabbits
- Single fiber or bundle from glycerinated psoas muscle

Testing Methods and Experimental Conditions
- Shortening velocity was obtained using an isotonic release technique
- Fibers were activated by the addition of ATP ($2.5\,\mu M$ – $5\,mM$)
- Experiments were carried out at $10^{\circ}C$

Data

131
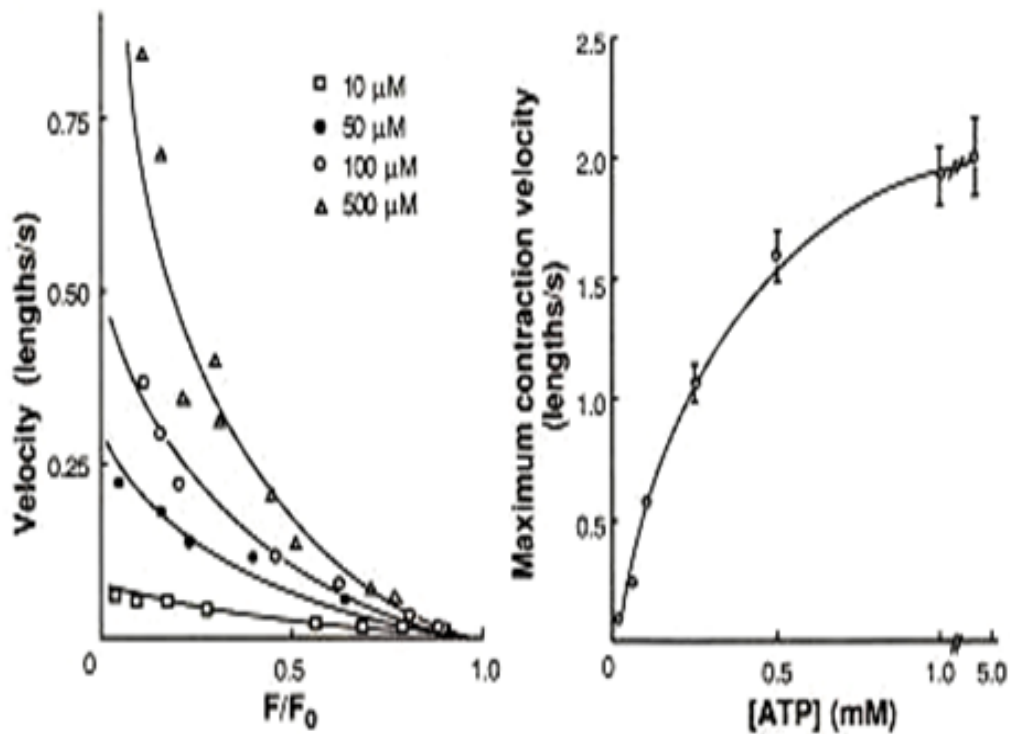
Force–Velocity Relation

| • Force–velocity relation | • Rat | • Isolated muscle fiber |
| • | • Extensor digitorum longus | • |

Materials
- Rats (male)
- Extensor digitorum longus (EDL, fast-twitch muscle)

Testing Methods and Experimental Conditions
- Shortening velocity was measured by subjecting the fibers to isotonic releases or afterloaded shortening
- Twitch fibers were tetanized by electrical stimulation
- The sequence in which data were collected was 35°, 30°, 20°, and 35°C (closed triangles)

Data
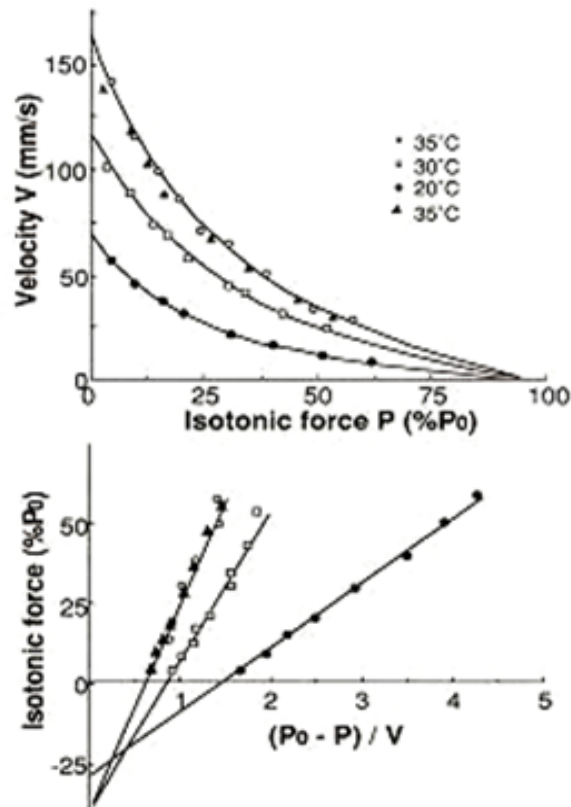
Comments
- The maximum velocity of shortening decreased with cooling in both EDL (fast twitch) and soleus (slow twitch, not illustrated) muscles. The calculated Arrhenius activation energy for maximum velocity of shortening was around 40–45 kJ in both muscles.

Force–Velocity Relation

• Torque–velocity relation •	• Human • Extensor muscle	• •

Materials

- Human
- Knee extensor muscle

Testing Methods and Experimental Conditions

- Torque–velocity relationship at maximal contraction was measured in knee extension using an isokinetic loading dynamometer (Cybex)
- Force–velocity performances of 15 subjects were normalized with respect to the maximum torque

Data
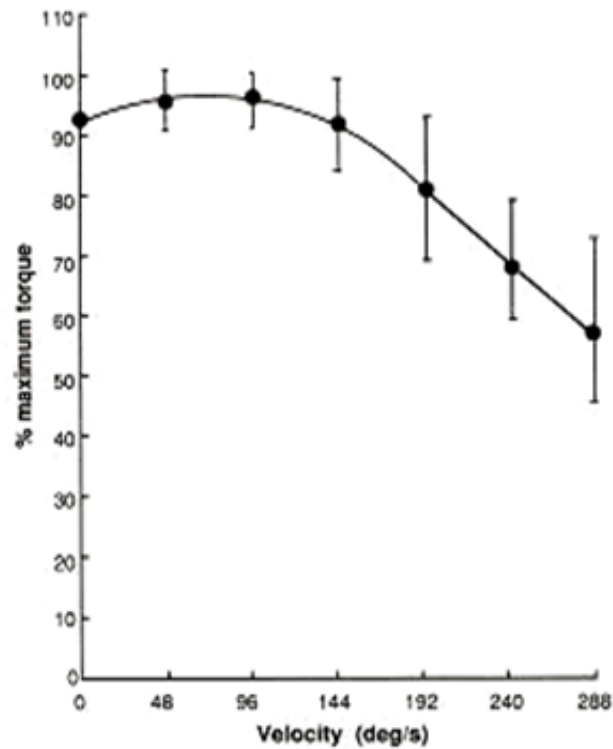
Step–Stretch Response

• Tension •	• Toad • Sartorius muscle	• Isolated muscle fiber •

Materials

- Toads
- Sartorius muscle (33 mm, 45 mg)

Testing Methods and Experimental Conditions

- Stretching a muscle by 3 mm (from 30 to 33 mm) at various moments after maximal shock
- Latent period, 30 ms
- Stretch 3 mm at times 35, 64, 132, 260, 420, 740, and 1020 ms, and remain at the length for 15 – 20 ms

Data
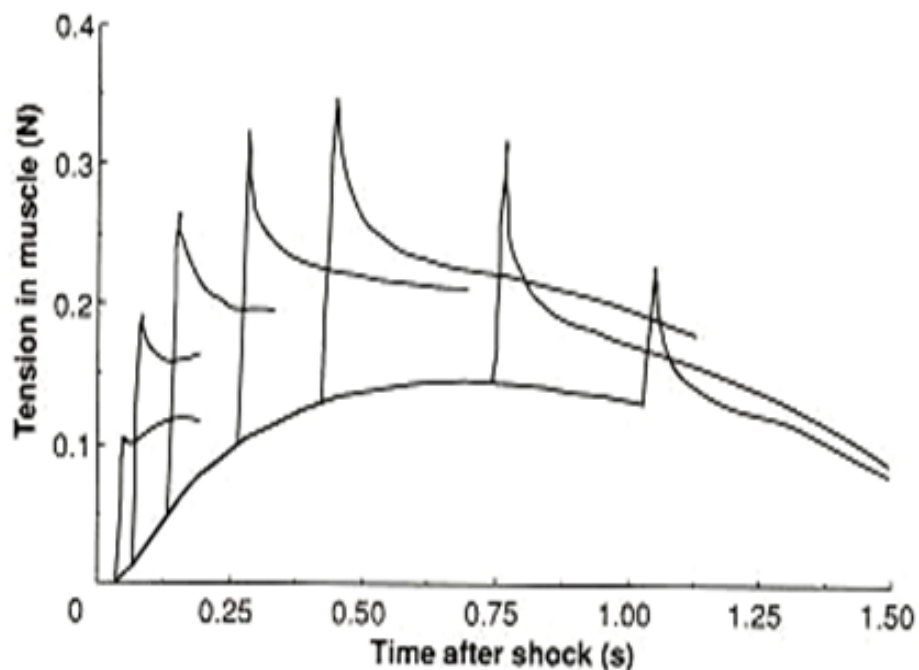
Comments

- 0.3 N tension is equivalent to 0.23 MN/m².
- Tension remains considerably above the isometric twitch tension at the terminal length.
- This is an activation of the contractile machinery and seems to indicate the existence of a parallel elastic component of contracting muscle.

Stiffness

| • Compliance
• Extension | • Rat
• Gracilis anticus muscle | • Isolated muscle fiber
• |

Materials
- White Wistar rats (male; age, 50 days; weight, 140–165 g)
- Gracilis anticus muscle (rest length, 2.7 cm; weight, 60 mg)

Testing Methods and Experimental Conditions
- Krebs–Ringer solution, pH 7.3; temperature, 17.5°C
- Modified Wilkie's quick-release method, releasing from isometric condition to some fixed isometric load
- Muscle stimulation: current density = 0.08 amp/cm^2, train of 322 ms pulses with a pulse separation of 10.5 ms

Data

Muscle	Compliance (cm/dyne $\times 10^{-6}$)	Normalized compliance ($L_0/P_0 \times 10^2$)	Normalized extension at P_0
Cat papillary [a]			
L_0=1.4 cm	5 at P_0	3.6	0.1L_0
P_0=10 g	50 at 0.2P_0	36	
Rat anterior tibialis [a]			
L_0=2.5 cm	0.25 at P_0	4.4	0.05L_0
P_0=440 g	1.5 at 0.1P_0	26.4	
Rat gracilis anticus			
L_0=2.7 cm	1.1 at P_0	1.3	0.07L_0
P_0=30 g	17 at 0.1P_0	19.5	
Frog illiofibularis [a]			
L_0=2.5 cm	1.1 at 0.6P_0	2.0	0.03–0.05L_0
P_0=48 g	5 at 0.1P_0	9.6	
Frog sartorius [a]			
L_0=3 cm	1.6 at 0.7P_0	2.4	0.04L_0
P_0=45 g	20 at 0.02P_0	30.0	
Frog sartorius [a]			
L_0=2.8 cm	0.5 at P_0	2.0	0.04L_0
P_0=120 g	6 at 0.1P_0	26	

[a] A comparison of the series elastic components reported for different striated muscles.

Comments
- A basic similarity was observed among striated muscles both in normalized compliance and normalized total extension.
- There is little variability in the normalized results when different muscles are compared.

Stiffness

| • Stiffness
• | • Human
• Flexor pollicis longus | •
• |

Materials
- Human
- Flexor pollicis longus muscle

Testing Methods and Experimental Conditions
- The thumb was stretched with a torque motor and the steady force was maintained in executing three types of task
- Both force and displacement were measured at the tip of the thumb
- Stretch-evoked stiffness was calculated as the stretch-evoked force per unit of stretch where stretch-evoked force was obtained by subtracting tonic force from the mean force computed over the interval 75–115 ms after the perturbation onset

Data
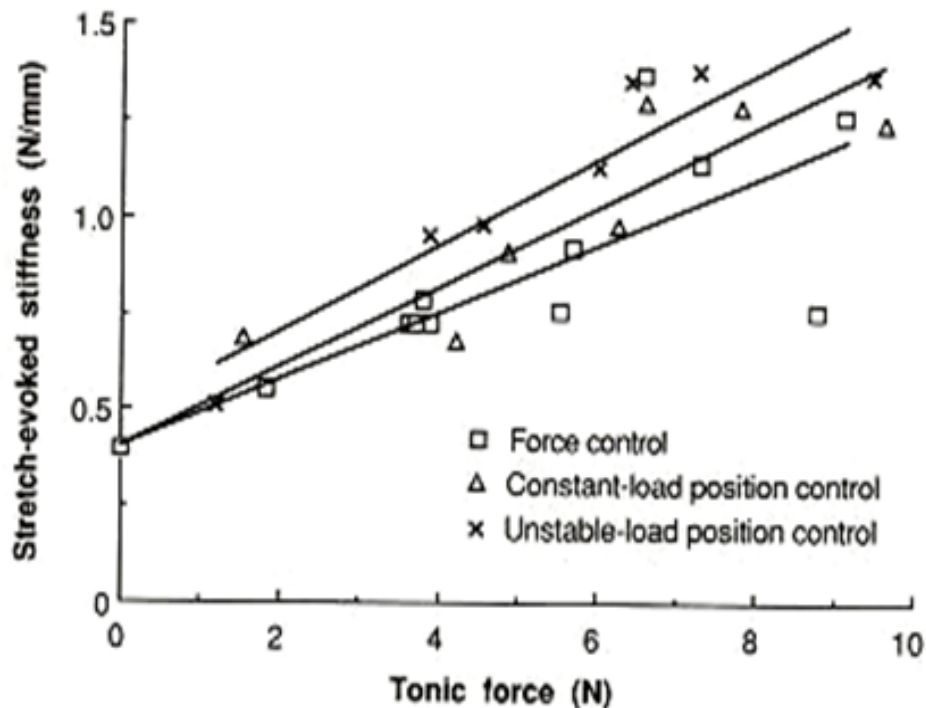
Comments
- The stretch-evoked stiffness around the joint increased with increasing flexing force, and with the level of contraction of flexor and extensor muscles for a given flexing force.

136

A2.2 Smooth Muscle Mechanical Properties

Force–Velocity Relation

• Active force • Shortening velocity	• Rabbit • Urinary bladder	• Quick release • Hill's equation

Materials
- Rabbits weighing 2.5–3 kg
- Urinary bladder
- Transferred to oxygenated Krebs' solution, left in this medium for 1 h at 4°C, and filled with 10 ml Krebs solution

Testing Methods and Experimental Conditions
- A bundle of longitudinal muscle mounted in the bath
- Medium and temperature change to suppress spontaneous contractile activity: accommodated for 1 h at 37°C in a bubbled physiological salt solution, temperature lowered to 25°C, and medium changed to an oxygenated tris solution at 25°C
- Force–velocity relations obtained by the quick-release technique at different times during the twitch
- Single square wave pulses (5 ms, 100 V) at a frequency of 0.03–0.06 Hz to stimulate the muscle
- The results were fitted to Hill's equation: $V(P + a) = b(P_0 - P)$. P, tension in muscle; V, velocity of contraction; a, b, P_0, constants

Data
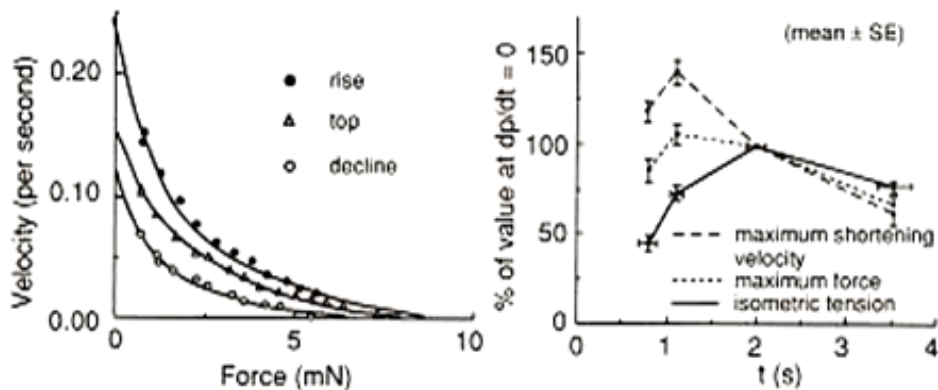
Comments
- Left diagram: Force–velocity relations. Full lines show the fits to Hill's equation.
- Right diagram: Maximum shortening velocity (V_{max}), extrapolated maximum tension (P_0) and isometric tension expressed as percent of their respective values at the peak.
- V_{max} and P_0 reach their highest values during the rising phase of the twitch.
- V_{max} declines rapidly with time and at the peak of the twitch it is only about 70% of the maximum value.

Force–Velocity Relation

• Isometric contraction • Length–tension relation	• Dog • Ureter	• Single twitch • Hill's equation

Materials
- Adult dogs weighing 25–35 kg
- Middle portions of ureter

Testing Methods and Experimental Conditions
- Cylindrical specimen removed to a aerated, modified Krebs' solution at 25°C
- Single twitch, length–tension relation, and force–velocity relation
- Before testing, preconditioned by repeated loading and unloading to stabilize its mechanical properties and stimulated by square waves during this period

Data
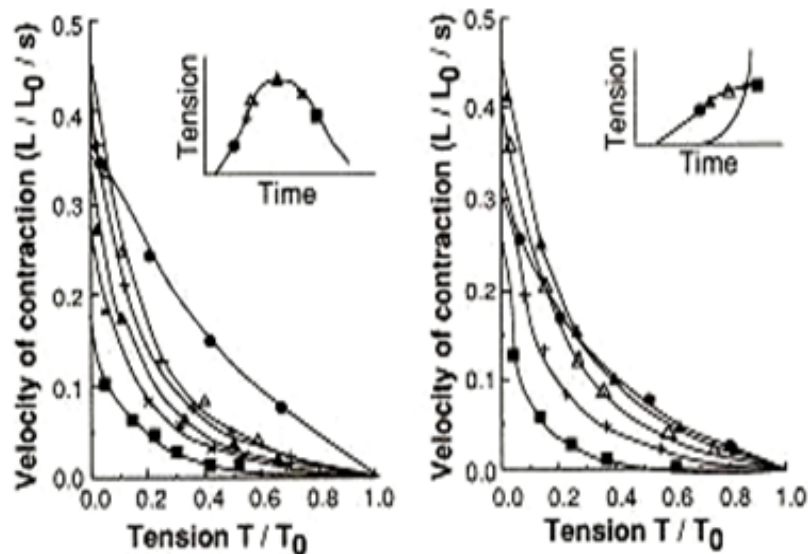
Comments
- Left diagram: Force–velocity relations for different times of release after stimulation.
- Right diagram: Force–velocity relations at a given time after stimulation for different levels of stretch.
- Measurements were analyzed using the hyperbolic Hill's equation.
- Maximum velocity of shortening occurred at 75–100 ms after release.
- Maximum velocity of contraction reached a peak for releases made in a region of stretch where the length was in the range of 0.85–0.90 L_{max}, where L_{max} is the length which the largest active tension can be developed.

Force–Velocity Relation

• Isometric tension • Isotonic contraction	• Rat • Portal vein	• Quick release •

Materials
- Rats weighing 250–400 g, Sprague–Dawley strain
- Portal vein of 3–5 mm in length

Testing Methods and Experimental Conditions
- Force–velocity relation of longitudinal smooth muscle determined at different stages of highly uniform contractions induced by appropriate alteration of the ionic environment
- The experiments were performed by the method of isotonic quick release
- Temperature, 37°C

Data
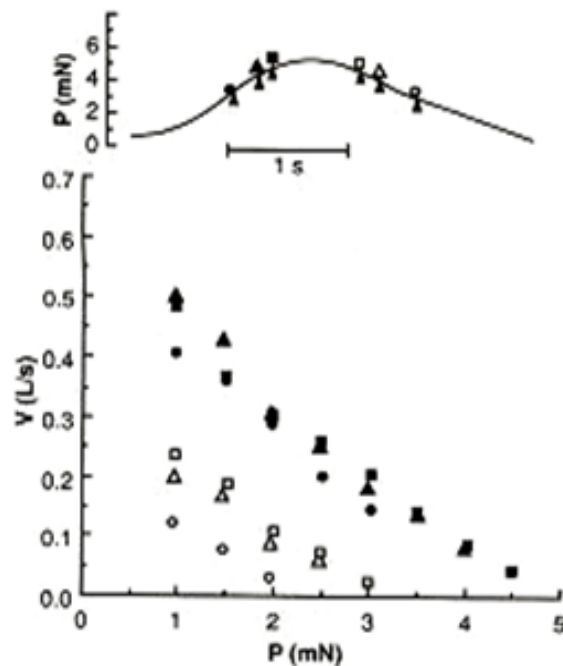
Comments
- Upper diagram: Isometric tension. Different symbols indicate time of release.
- Lower diagram: Force–velocity curves. Symbols corresponding to time of release as shown in upper diagram.
- During the rising phase the curves are not much different at the three force levels.

Force–Velocity Relation

• Isometric tension • Maximum velocity	• Guinea pig • *Taenia coli*	• Quick release • Hill's equation

Materials
- Guinea pigs weighing 0.25–0.5 kg
- *Taenia coli*

Testing Methods and Experimental Conditions
- Specimen mounted in the test chamber filled with aerated Krebs' solution at 36°–37°C, and restored to the in situ length
- Quick-release experiment
- Specimen stimulated with AC field at 50–100 Hz
- Force–velocity relation obtained

Data

Curve #	Isometric force (mN)
1	125 (= Fm)
2	92
3	60
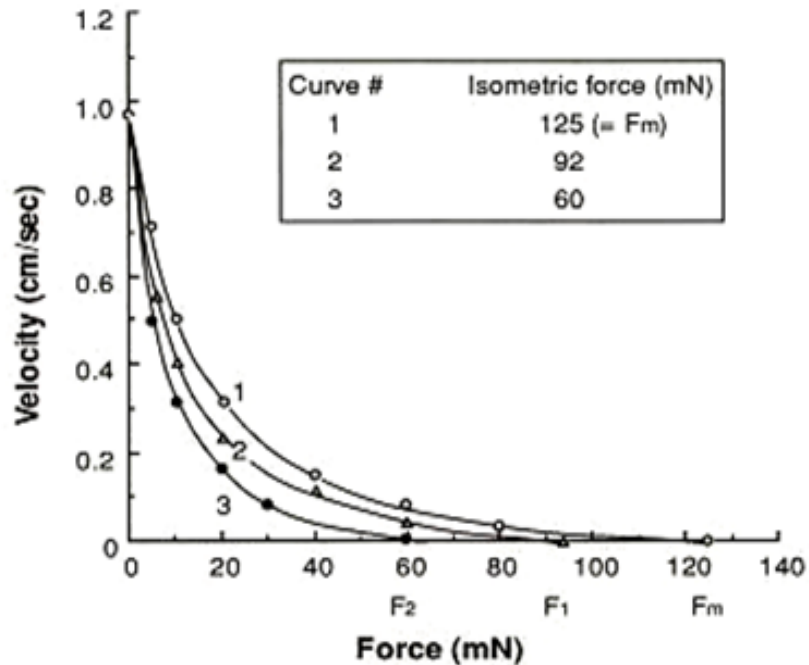
Comments
- The load–velocity curve obtained was hyperbolic, obeying Hill's equation:
  $$(P + a)(v + b) = b(F_m + a).$$
  P, load; v, shortening velocity; F_m, maximum isometric tension; a, heat constant; b, rate constant of energy liberation.
- The maximum velocity per unit muscle length was constant, irrespective of the initial muscle length.

Length–Tension Relation

| • Active tension | • Dog | • |
| • Passive tension | • Mesenteric artery | • |

Materials

- Dogs
- Superior mesenteric artery of approximately 1 mm inside diameter
- The artery stored in Krebs' solution at 4°C until used

Testing Methods and Experimental Conditions

- Specimen cut helically to obtain a strip 10–25 mm long, 0.8–1 mm wide, and approximately 0.2 mm thick
- Strip mounted in a bath of aerated Krebs' solution at 38°C
- Effect of stretch on the resting tension and contractility studied isometrically
- Electric current or epinephrine for stimulation

Data
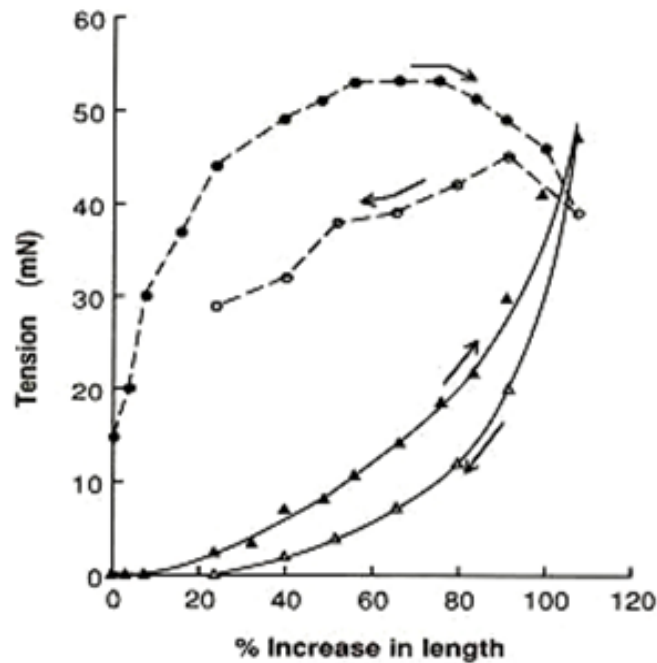
Comments

- Passive tension in response to stretch (▲) and release (△). Active tension developed in response to a standard stimulus in several increments of stretch (●) and decrements of release (○).
- After the strip has been stretched more than 50% of its initial length the tension rise is steep.
- With each increase in length there is a corresponding increase in magnitude of the response until an optimal length is reached.

141

Length–Tension Relation

• Stress–strain curve • Strain rate	• Dog, rabbit, etc. • Ureter	• Stress relaxation •

Materials

- Dogs, rabbits, guinea pigs, human fetuses
- Ureter
- Specimens obtained from dog and human fetuses kept in oxygenated Krebs' solution at 10°C until test

Testing Methods and Experimental Conditions

- Specimens immersed in bubbled, modified Krebs' solution at 37 ± 0.25°C
- Simple elongation and stress-relaxation tests in the longitudinal direction
- Preconditioned for all tests

Data

Curve	Animal	Lo (cm)	Strain rate (cm/min)
A	Rabbit	2.39	0.5
B	Dog	1.93	0.5
C	Guinea pig	2.04	0.5
D	Human fetus	1.47	1.0

DOG NO. 807 A, Lo=1.611 cm

Symbol	Initial stretch	To(kPa)
■	25% of Lo	0.75
○	37% of Lo	1.46
▲	50% of Lo	2.60
□	62% of Lo	8.94
△	68% of Lo	22.90
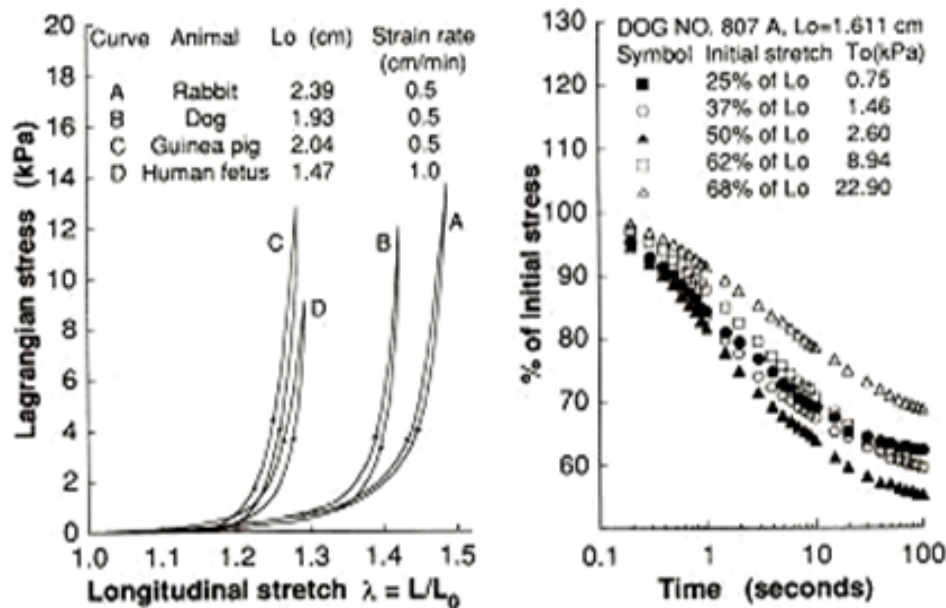
Comments

- Caption:
  L_0, preconditioned length or initial length; T_0, initial Lagrangian stress.
- These curves can be closely represented by exponential functions in the form
  $$T = (T^* + \beta)e^{\alpha(\lambda - \lambda^*)} - \beta.$$
  α, β, T^* and λ^*, constants; λ, stretch ratio.
- The time course of relaxation depends on amount of initial stretch.

Length–Tension Relation

• Stress–strain curve • Stress relaxation	• Guinea pig • *Taenia coli*	• Step–stretch • Spontaneous contraction

Materials
- Guinea pigs weighing 0.3–0.6 kg, Hartley strain
- Resting *Taenia coli*

Testing Methods and Experimental Conditions
- Specimen based in a bubbled physiological solution at 37°C at the in vivo length and equilibrated for 1 h before the experiments
- Epinephrine-treated solution to suppress spontaneous contraction
- Stress–relaxation characteristics before and after treatment with epinephrine
- Stress–strain relation in epinephrine at various strain rates
- Comparison with other kinds of muscle

Data

Entry	e_{ss}	σ_{ss} (kPa)
1	0.05	18.9
2	0.10	60.1
3	0.15	108.5
4	0.20	181.9
5*	0.10	88.3

Entry	Strain rate
1	0.02 Hz
2	0.20
3	2.00
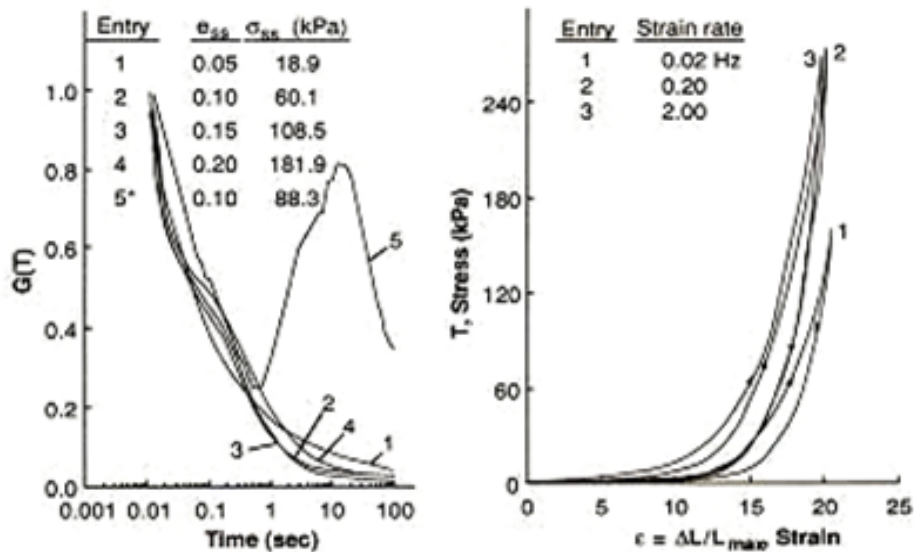
Comments
- Parameters:

  e_{ss}, strain at time (t_m) from beginning of step stretch to attain a constant length; σ_{ss}, stress at t_{ss}; $G(t)$, ratio σ/σ_{ss}; L_{max}, length at which the maximum isometric active tension is generated.
- Entry 5 with no epinephrine.
- σ_{ss} are lower after epinephrine injection, whereas the relaxation function $G(t)$ continues to monotonically decrease in a fashion similar to that in the latent period of the spontaneous specimen.
- The stress–strain relation is nonlinear and varies with strain rate but approaches a limit at high strain rates.
- The relation is similar to that of the aorta, but different from that of the papillary muscle, mesentery, and ureter.

Length–Tension Relation

|		
• Stress–strain curve • Time course of contraction	• Guinea pig • *Taenia coli*	• Isometric step stretch • Isotonic step loading

Materials
- Guinea pigs weighing 0.3–0.6 kg, Hartley strain
- *Taenia coli*

Testing Methods and Experimental Conditions
- Specimen mounted in the test chamber filled with bubbled physiological fluid at approximately the in vivo length L_{ph} and 37°C
- Isometric step stretch, isotonic step loading, length–tension, and stress–strain tests

Data
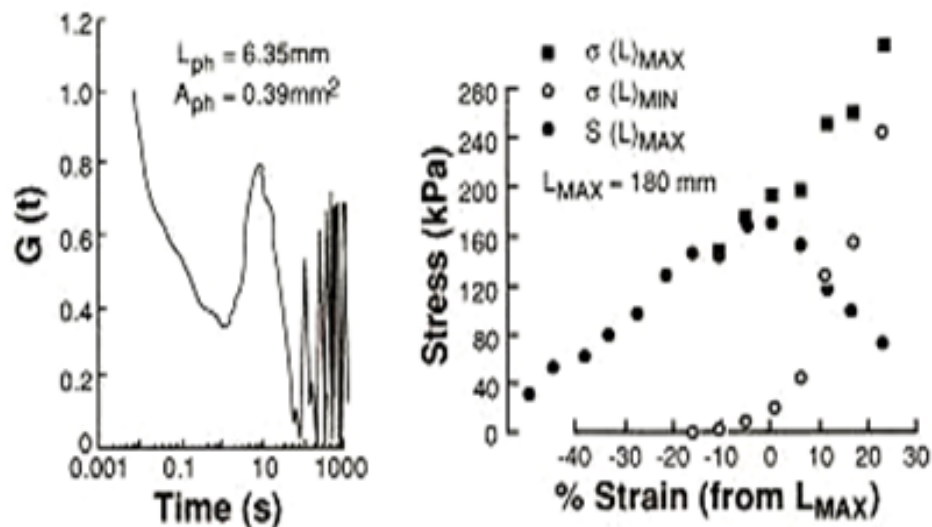
Comments
- Left diagram: Stress response to a 10% of L_{ph} step change in length. G(t), normalized stress response to an isometric step stretch; A_{ph}, the in vivo cross-sectional area.
- Right diagram: Functional dependence of $\sigma(L)_{max}$, $\sigma(L)_{min}$, and $S(L)_{max}$ on muscle length. $\sigma(L)_{max}$, maximum stress; $\sigma(L)_{min}$, minimum stress; $S(L)_{max}$, maximum active stress or $\sigma(L)_{max} - \sigma(L)_{min}$; L_{max}, optimum length.
- The response can be divided into two phases — the short time latent period for t < 1 s and the long time minute rhythm for t > 1 s.

Viscoelasticity

• Series elastic component • Quick release	• Dog • Common carotid artery	• Maxwell model • Voigt model

Materials
- Dogs
- Common carotid artery

Testing Methods and Experimental Conditions
- Cylindrical segment mounted in a tissue bath filled with Krebs–Ringer dextrose solution at 36°–37°C and restored to in situ length (about 4 cm)
- Pressure–diameter test
- Inflation pressure: 10–15 mmHg steps to 300 mmHg
- Norepinephrine for activation and potassium cyanide for inactivation
- Series elastic element studied using a quick-release procedure
- Estimation of series elastic element with both Maxwell and Voigt models

Data
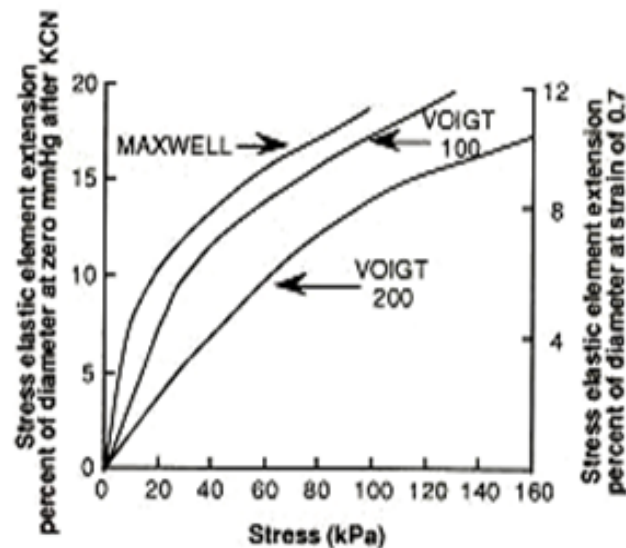
Comments
- Load–extension curves for the series elastic element of vessels excited isometrically at pressures between 50 and 150 mmHg.
- The computed series elastic element tension at an applied stress of 1.0×10^2 kPa was 18.9% for the Maxwell model and 14.7%–17.9% for the Voigt model.
- The values were reduced to 11.2% for the Maxwell model and 8.6%–10.5% for the Voigt model corresponding to the maximum active isometric tension.

145

Viscoelasticity

• Series elastic component • Stress–stiffness curve	• Dog • Common carotid artery	• Maxwell model • Voigt model

Materials
- Dogs
- Intact common carotid artery

Testing Methods and Experimental Conditions
- Cylindrical specimen of 10 cm in length mounted horizontally in a tissue bath filled with a Krebs–Ringer dextrose solution of $37 \pm 0.5°C$ at in situ length
- Pressure–diameter test to identify series elastic component (SEC)
- Static circumferential stress–strain curves and stress–stiffness curves to evaluate Maxwell and Voigt model elements at 33°, 36°, and 39°C
- Elastase or collagenase to digest the connective tissue component
- Activated with norepinephrine (NE), inactivated with potassium cyanide and sodium iodoacetate
- SEC stiffness computed for both models

Data
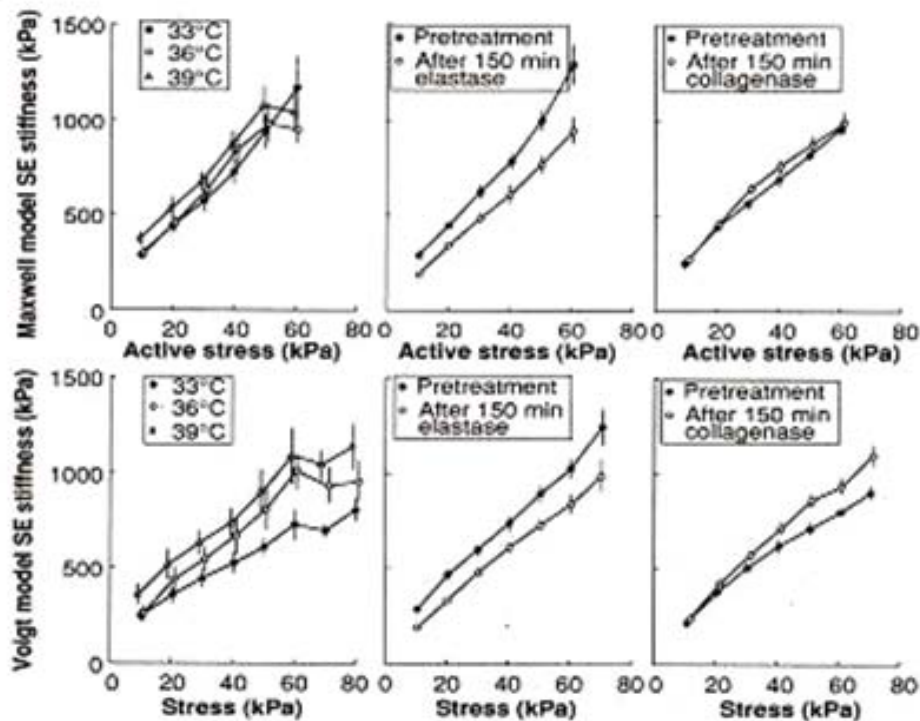
Comments
- Left diagrams, thermal variations; middle diagrams, elastase experiments; right diagrams, collagenase experiments. Values are mean ± SE.
- The Maxwell model is preferable to the Voigt model to describe the mechanical properties of the carotid artery wall.
- The SEC in intact carotid artery is primarily elastin.

A2.3 Mesentary Mechanical Properties

Force–Elongation Relation

• Extension • Elastic modulus	• Rabbit • Mesentery	• Constitutive equation •

Materials
- Rabbits
- Mesentery

Testing Methods and Experimental Conditions
- Tensile tests
- Stretch rate, 0.254 cm/min
- In a physiological solution at room temperature

Data
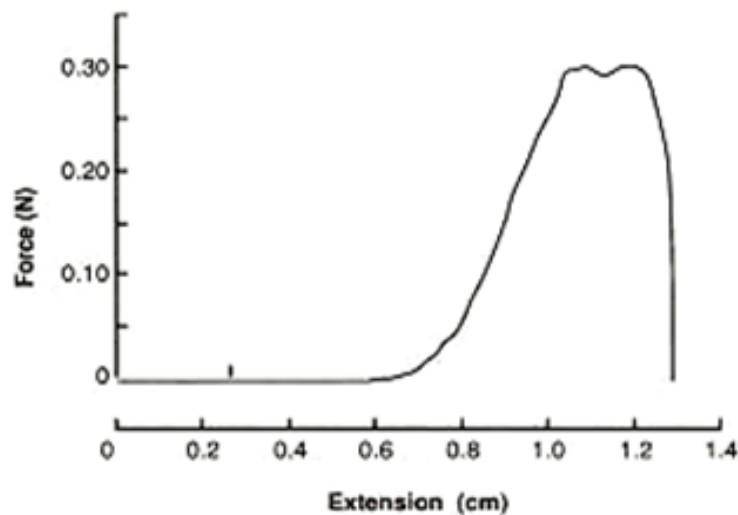
Comments
- The specimen failed by tearing at some unpredictable points.
- $dT/d\lambda = aT(1 - bT)$.

  T, tension; λ, extension ratio; a, b, constants.
- One typical example, $a = 12.4$, $b = -7.29 \times 10^{-3}$ Pa^{-1}.

A2.4 Skin Mechanical Properties

Force–Elongation Relation

• Extension ratio • Stiffness	• Rabbit • Skin	• Anisotropy •

Materials
- Albino male rabbits
- Rectangular specimen from an area exterior to the nipple line

Testing Methods and Experimental Conditions
- Biaxial stretch tests: first stretched in the x–direction then stretched in the y–direction, with the transverse stretch ratio kept at 1
- Uniaxial tension tests
- Stretch rate, 0.2 mm/s

Data
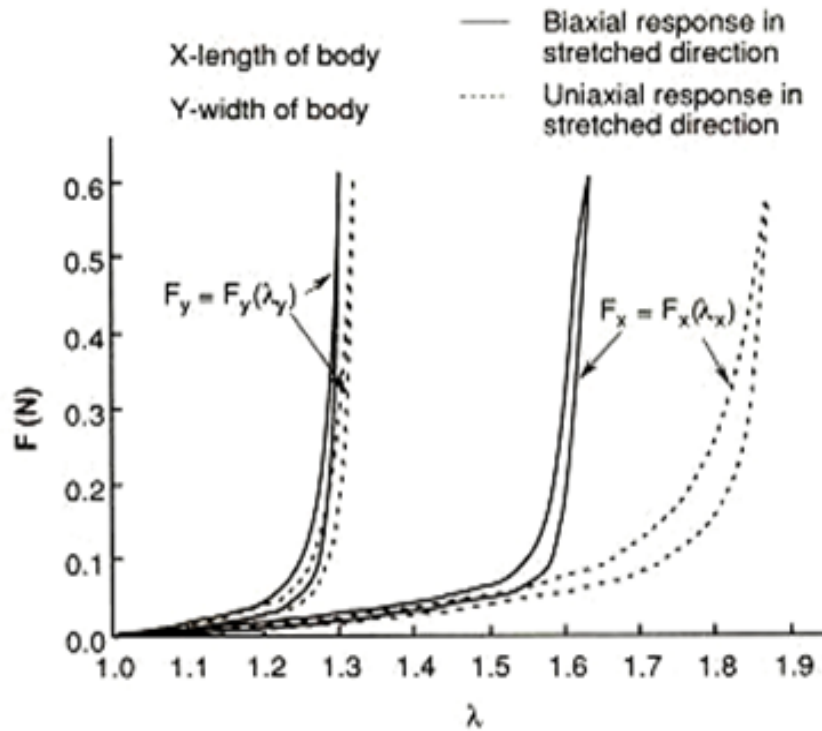
Stress–Strain Relation

• Tensile strength • Extensibility	• Rat • Skin	• Collagen • Gelation

Materials
- Rat dorsal skin
- Collagen film, which is obtained by gelation of collagen prepared from rat skin, followed by drying

Testing Methods and Experimental Conditions
- Strips of collagen films (2 mm wide) and strips of rat dorsal skin (2 mm wide) were immersed in Ringer's solution (pH 7.4, 22°C)
- Stress values for strip speciments were calculated as load values normalized to the measured cross sectional area
- Strain values were obtained by expressing deformation values in units of original specimen length

Data
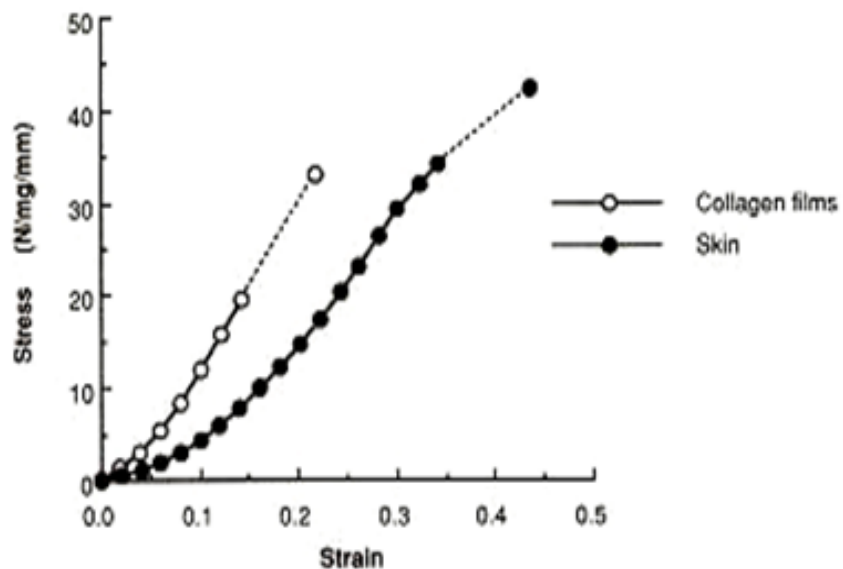
Comments
- The mechanical properties of the collagen films differed from those of the rat skin from which the film collagen was extracted, in being stiffer but with less strength and extensibility.

A2.5 Abdominal Wall Mechanical Properties

Force–Elongation Relation

• Tensile strength • Elastic stiffness	• Rabbit • Abdominal wall	• Position (Location) •

Materials
- Adult male albino rabbits
- Specimens excised from abdominal wall
- Specimen location: six from transverse plane, two from musculus rectus abdominis, and eight from linea alba

Testing Methods and Experimental Conditions
- Tensile tests
- Dumbbell-shaped and strip-shaped specimens
- Tests less than 4 hours after the animal was killed
- Temperature, 21°C ; relative humidity, 65%
- Crosshead speed, 20 mm/min

Data

Position	Breaking strength (N)	Energy absorption (N)	Maximum strain	Elastic stiffness (N)
I	2.90 ± 0.28	144.61 ± 22.85	0.80 ± 0.24	8.65 ± 4.75
II	3.32 ± 1.57	171.54 ± 49.82	0.69 ± 0.07	8.82 ± 4.18
III	2.95 ± 0.38	126.00 ± 44.24	0.70 ± 0.10	8.07 ± 1.58
IV	3.12 ± 0.78	145.72 ± 45.24	0.74 ± 0.10	7.83 ± 2.37
V	2.93 ± 0.71	150.55 ± 42.53	0.78 ± 0.13	7.90 ± 3.38
VI	2.82 ± 0.99	163.23 ± 69.77	0.76 ± 0.16	6.50 ± 2.31
Rectus	11.64 ± 2.77	7861.31 ± 372.07	1.50 ± 0.38	10.41 ± 5.21

All data are given as mean ± SD.
Positions I–VI correspond to the locations from lateral to central sides in the abdominal wall.

Position	Breaking strength (N)	Energy absorption (N)	Maximum strain	Elastic stiffness (N)
I	10.39 ± 1.66	431.74 ± 119.34	0.75 ± 0.16	21.77 ± 7.41
II	12.59 ± 3.89	533.84 ± 159.30	0.75 ± 0.17	26.22 ± 10.00
III	14.78 ± 5.55	557.61 ± 223.81	0.67 ± 0.14	32.27 ± 11.41
IV	16.95 ± 4.59	755.08 ± 367.07	0.72 ± 0.18	37.27 ± 11.41
V	17.13 ± 3.69	603.42 ± 224.17	0.56 ± 0.12	51.00 ± 17.83
VI	16.30 ± 4.55	476.85 ± 102.24	0.47 ± 0.08	55.95 ± 22.17
VII	17.32 ± 4.93	614.23 ± 269.09	0.58 ± 0.20	49.22 ± 15.66
VIII	19.95 ± 6.39	763.50 ± 411.50	0.59 ± 0.20	60.06 ± 24.41

All data are given as mean ± SD.
Position I–VIII correspond to the locations from cranial to caudal sides of the linea alba.

Comments
- Mechanical properties depended on the original locations and on the fiber direction.
- The results will be related to problems of wound healing.

A2.6 Nerve Mechanical Properties

Elastic Modulus

• Tensile strength • Stiffness	• Mice • Nerve	• Injured •

Materials
- Adult mice
- Sciatic nerves

Testing Methods and Experimental Conditions
- Tensile tests
- Stretch rate, 1.22 mm/s
- Nerve crush by the application for 20 s with mosquito forceps at a point midway between the sciatic notch and patella
- 2, 6, 12, and 24 days after crush
- Specimens divided into proximal, medial, and distal segments
- Specimens divided into ipsilateral and contralateral sides

Data

Treatment group	Biomechanical variables				
	Y (MPa)	σ_{pl} (MPa)	$(\Delta l/l_0)_{pl}$	μ (gm/cm)	A (cm^2)
Control	7.0	3.2	0.43	0.0031	0.0025
Experimental					
Day 2	4.6	2.6	0.63	0.0036	0.0028
Day 6	7.4	3.0	0.55	0.0036	0.0030
Day 12	9.4	4.2	0.51	0.0033	0.0025
Day 24	8.8	3.8	0.40	0.0033	0.0032
Proximal	5.9	3.0	0.58	0.0031	0.0027
Medial	8.7	3.4	0.45	0.0035	0.0028
Distal	8.0	3.2	0.54	0.0035	0.0031
Ipsilateral	7.4	3.2	0.51	0.0040	0.0031
Contralateral	7.6	3.5	0.53	0.0029	0.0026

Y, elastic moduli; σ_{pl}, stress at the proportional limit; $(\Delta l/l_0)_{pl}$, strain at the proportional limit; μ, mass per unit length; A, cross-sectional area

Comments
- Strength and stiffness increased, and elasticity decreased time dependently by injury.
- Changes in mechanical properties appeared to be related to the epineurium.

A2.7 Blood Vessels Mechanical Properties

Anisotropy

• Creep • Stress relaxation	• Dogs • Aorta, femoral, iliac	• Relaxation function • Regional variation

Materials
- Dogs of about 20 kg weight
- Thoracic and abdominal aortas, external iliac and femoral arteries

Testing Methods and Experimental Conditions
- Strips of 5 mm in width taken at 8 different regions between the aortic arch and femoral artery in either longitudinal or circumferential directions
- Medium: aerated Krebs–Ringer solution at 37°C
- Tensile test at constant strain rate
- Stress relaxation test
- Creep test

Data

Region	α	T^* (kPa) at $\lambda^* = 1.6$	E_0	$G(300)$	$G(t)$-slope
Circumferential segments					
Arch	0.88 ± 0.93	52.4 ± 5.4	89.2 ± 47.8	75.52 ± 5.53	-0.0326
Prox. thoracic	0.92 ± 0.68	57.3 ± 12.7	86.7 ± 31.3	79.17 ± 5.55	-0.0316
Mid-thoracic	1.24 ± 0.50	61.7 ± 8.3	88.4 ± 17.2	75.13 ± 6.75	-0.0345
Dist. thoracic	1.48 ± 0.04	66.2 ± 19.6	84.9 ± 8.4		-0.0369
Prox. abdom	3.24 ± 0.45	75.0 ± 14.7	34.2 ± 19.4	65.93 ± 10.06	-0.0432
Dist. abdom	3.88 ± 0.70	55.9 ± 11.3	15.7 ± 10.2	65.79 ± 5.93	-0.0452
Ext. iliac	4.70 ± 1.52	75.5 ± 19.6	6.6 ± 35.7	58.24 ± 9.39	-0.0423
Femoral	4.15 ± 0.83	70.6 ± 9.8	-1.4 ± 22.1	65.91 ± 12.15	-0.0426
Longitudinal segments					
Arch	1.50 ± 0.91	47.5 ± 6.9	55.4 ± 26.2	82.2 ± 2.02	-0.0256
Prox. thoracic	2.93 ± 0.83	61.2 ± 17.6	37.7 ± 27.5	86.3 ± 3.7	-0.0256
Mid-thoracic	2.41 ± 0.46	43.3 ± 2.9	49.8 ± 55.0	84.8 ± 5.73	-0.0195
Dist. thoracic	2.12 ± 0.38	45.1 ± 3.9	57.0 ± 44.2	85.4 ± 8.39	-0.0152
Prox. abdom	4.36 ± 0.39	69.8 ± 20.6	22.2 ± 7.9	88.1 ± 4.46	-0.0135
Dist. abdom	3.81 ± 0.51	56.6 ± 2.5	62.3 ± 19.7	75.0 ± 12.6	-0.0280
Ext. iliac	1.30 ± 0.28	67.8 ± 18.6	124.5 ± 6.1	48.3 ± 6.2	-0.0402
Femoral	1.06 ± 0.18	52.3 ± 12.7	83.5 ± 4.6	62.7 ± 8.4	-0.0400

All data are given as mean $\pm$ SD, $n = 7$.

Comments
- Stress–strain relationship:

  $dT/d\lambda = \alpha T + E_o$ (T, Lagrangian stress; λ, extension ratio; α and E_o, constants);

  α and E_o are given in the range 19.6 kPa $< T < T^*$, and average of values in strain rates between 4 and 40 mm/min.
- Normalized relaxation function:

  $G(t) = T(t, \lambda)/T(0, \lambda)$.
- The $G(t)$-slope, $dG/d \log_e t$ is evaluated at $t = 1$ s.

Anisotropy

• Distensibility • Stress–strain curve	• Dogs • Various veins	• Regional variation • Bilinear analysis

Materials

- Dog
- Superior vena cava, intrathoracic and abdominal portions of inferior vena cava, and jugular, axillary, common iliac, and femoral veins

Testing Methods and Experimental Conditions

- Longitudinal and circumferential strips, 5 mm in width
- Tensile test at crosshead speed of 5 mm/min
- Medium: aerated physiological salt solution at 30°C

Data
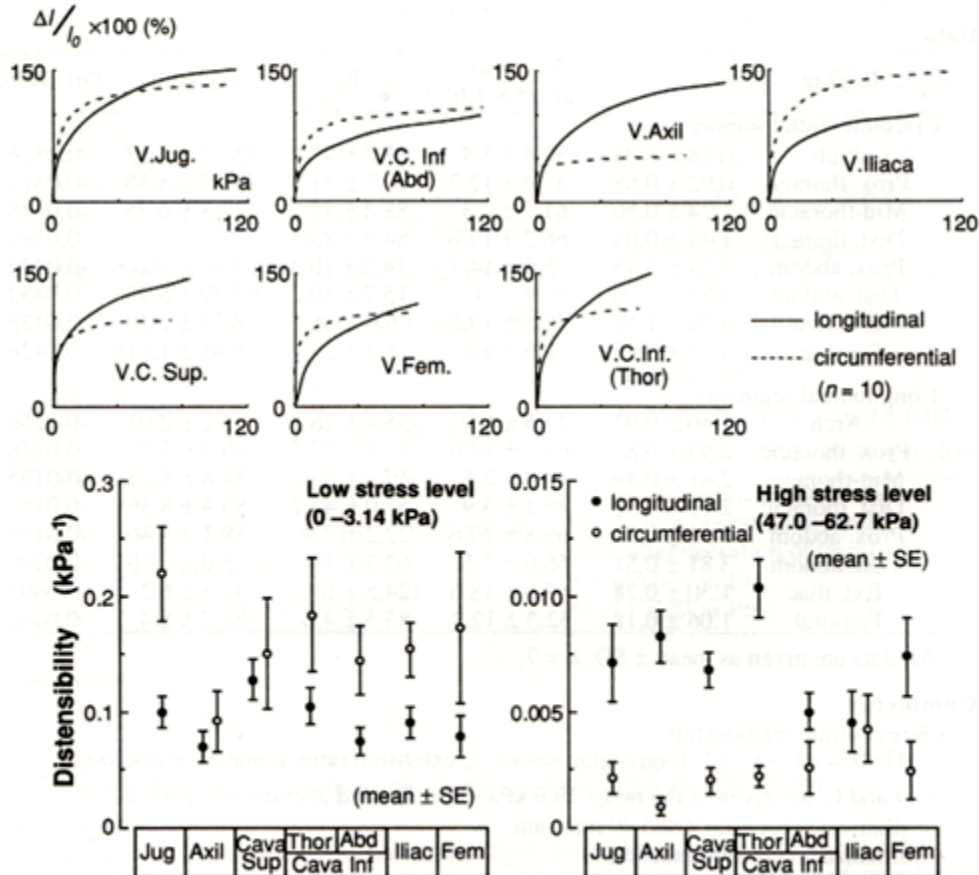
Compressibility

• Bulk modulus • Volumetric change	• Dogs • Aorta	• Incompressibility •

Materials

- Mongrel dogs; weight, 27.7–34.3 kg
- Descending thoracic aorta

Testing Methods and Experimental Conditions

- Tubular segment was stretched to a length of 3%–10% greater than the in vivo length and inflated with pressures greater than those in vivo (range 160–200 mmHg) for the measurement of pressure, outer diameter, and the longitudinal force
- Similar deformation in a closed chamber to measure volumetric change of the specimen
- Calculation of the bulk modulus

Data

Parameter	Value
Longitudinal strain $\Delta L/L_0$ (%)	40.0 ± 1.5
Circumferential strain $\Delta R/R_0$ (%)	70.0 ± 2.4
Intraluminal pressure P (kPa)	24.10 ± 0.36
Radial stress T_r (kPa)	-12.10 ± 0.19
Circumferential stress T_θ (kPa)	272.3 ± 9.3
Longitudinal stress T_z (kPa)	269.6 ± 33.5
Hydrostatic stress T_h (kPa)	176.3 ± 10.7
Volumetric strain $\Delta V/V_0$ (%)	0.0602 ± 0.0134
Bulk modulus k (MPa)	435 ± 90

All data are given as mean ± SE.

Comments

- Definition of parameters:

  Bulk modulus, $k = T_h/(\Delta V/V_o)$; hydrostatic stress, $T_h = (T_r+T_\theta+T_z)/3$; radial stress,

  $T_r = -P/2$; circumferential stress, $T_\theta = PR/H$; longitudinal stress, $T_z = (F+P\pi R^2)/2\pi RH$; F, longitudinal force; H, wall thickness; P, pressure; R, middle radius; ΔV, specimen volume change; V_o, original specimen volume.

154

Compressibility

• Radial compression • Stress–strain curve	• Rabbits • Thoracic aorta	• Incompressibility • Fluid extrusion

Materials
- Rabbits weighing approximately 2 kg
- Thoracic aorta, longitudinally cut

Testing Methods and Experimental Conditions
- Slab-like specimen sandwiched between transparent glass plates in air
- Radial compressive force-deformation relationship obtained after preconditioning
- Circumferential and longitudinal strains calculated from dimensional change of a mark made at the center of the adventitia surface of the specimen
- Amount of extruded fluid (Vf) under compression was measured to evaluate incompressibility under radial compression

Data

F (g)	T_r (kPa)	h (mm)	V_f/V_o
0	0	0.275 ± 0.008	0
100	5.71 ± 0.31	0.259 ± 0.007	0.0033 ± 0.0002
200	11.56 ± 0.74	0.252 ± 0.008	0.0083 ± 0.0006
300	17.13 ± 0.93	0.248 ± 0.008	0.0140 ± 0.0012
400	22.84 ± 1.24	0.245 ± 0.009	0.0185 ± 0.0012
500	28.55 ± 1.55	0.240 ± 0.009	0.0228 ± 0.0016
600	33.51 ± 2.16	0.236 ± 0.009	0.0255 ± 0.0015

All data are given as mean ± SE, $n = 4$.
V_f/V_o, relative amount of extruded fluid to specimen volume.
Specimen dimension: $l_{\theta o} = 12.141 \pm 0.595$ mm; $l_{zo} = 14.290 \pm 0.641$ mm.
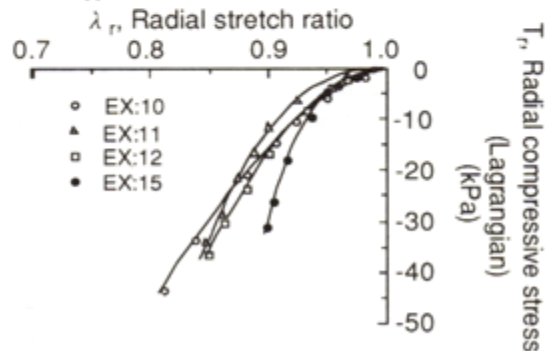
Comments
- The fluid extrusion was in the range of 0.50%–1.26% of the undeformed tissue volume per 10 kPa compressive stress, suggesting the tissue is only slightly compressible (or nearly incompressible).
- Figure shows loading paths from four radial compression experiments on rabbit thoracic arteries.

155

Creep

• Indentation property • Compliance	• Rabbits • Thoracic aorta	• Local property • Atherosclerosis

Materials

- Four to five-month-old New Zealand White rabbits weighing 2.6–3.5 kg
- Fed 1% cholesterol diet for 2–8 weeks
- Animals killed with an overdose of pentobarbitone
- Approx. 5.5 cm length of descending thoracic aorta

Testing Methods and Experimental Conditions

- Cylindrical segment was slit longitudinally in a line diametrically opposed to the intercostal ostia, opened out flat and stretched in a rack with its intimal surface uppermost to approximate to in vivo dimensions corresponding to a transmural pressure of 100 mmHg
- Local viscoelastic properties characterized with a microindentor consisting of a small spherical probe (25 μm in diameter) which is positioned gently on the intimal surface by preloading it with a force of 2 μN and then loading it with a force equivalent to 1 mg weight ($\sim$ 10 μN)
- Local compliance was calculated as the ratio of the resulting displacement of the probe measured 10 s after loading to the force applied to the probe

Data

156
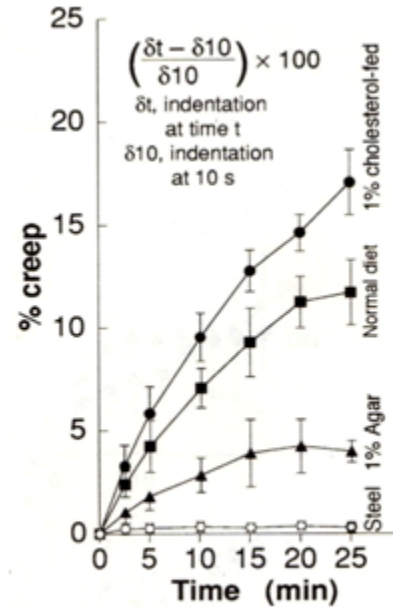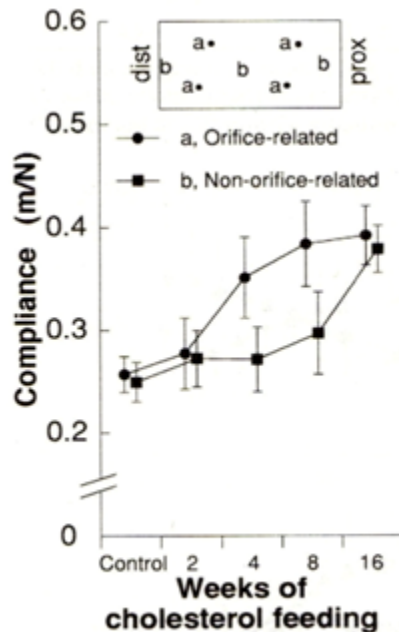
Elastic Modulus

• Incremental elastic modulus • Static P–D test	• Human • Aorta, carotid, iliac, femoral	• Age-related variation • Regional difference

Materials
- Human
- Thoracic and abdominal aortas, and carotid, iliac, and femoral arteries

Testing Methods and Experimental Conditions
- Stored frozen in physiological saline after excision at postmortem until use
- Grossly atheromatous vessels were discarded
- Static pressure–diameter measurement at in vivo length
- Pressure increased at each step of 10–20 mmHg in 2 min interval
- Medium: physiological saline at room temperature

Data

□ Upper thoracic
● Lower thoracic
■ Abdominal
◇ Iliac
▲ Femoral
○ Carotid

$\top\!\!\!\perp \pm 2$ SE
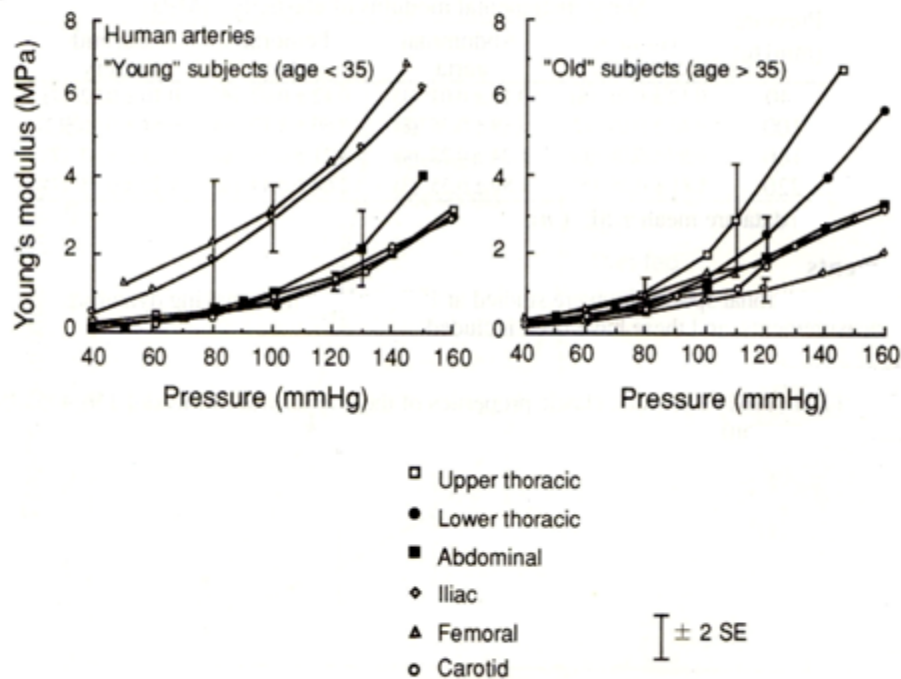
Comments
- Incremental elastic modulus, E_{inc}:

$$E_{inc} = 1.5R_i^2R_o/(R_o^2-R_i^2) \cdot \Delta P_i/\Delta R_o$$

  R_i, inner radius; R_o, outer radius; ΔR_o, radius increment over inner pressure increment of ΔP_i.

Elastic Modulus

• Pressure–strain elastic modulus • Diametrical change	• Human • Abdominal aorta	• Non-invasive measurement • Ultrasonic imaging

Materials
- Volunteers clinically free from hypertension, arteriosclerosis obliterans, cardiac disease, diabetes mellitus, and hyperlipidemia
- Abdominal aorta

Testing Methods and Experimental Conditions
- Each subject rested supine for 10 min before the measurement
- Pulsatile wall motion of the abdominal aorta observed at 3–5 cm distal to the branching site of the superior mesenteric artery
- Pulsatile diameter change measured with a new echo tracking device linked to real time ultrasonic B mode equipment
- Brachial artery pressure measured by the auscultatory method

Data

Group	1 (young adults)	2 (middle-aged subjects)	3 (elderly subjects)
n	20	21	20
Age (years)	24.6 ± 3.3	46.0 ± 7.0	75.5 ± 8.6
Med P (mmHg)	82.8 ± 10.4	95.6 ± 10.8	103.3 ± 13.6
ΔP (mmHg)	53.0 ± 13.9	49.5 ± 16.9	73.0 ± 19.8
D (mm)	16.7 ± 3.6*,#	17.0 ± 1.9#	15.3 ± 3.1
ΔD (mm)	1.22 ± 0.31**,##	0.80 ± 0.31##	0.45 ± 0.15
Strain (ΔD/D)	0.076 ± 0.024**,##	0.048 ± 0.024##	0.030 ± 0.010
E_p (kPa)	99 ± 34*,##	155 ± 68##	380 ± 205

All data are given as mean ± SD.
Med P, mediated blood pressure {(systolic + diastolic blood pressure)/2}; ΔP, pulse pressure; D, mean diameter of the abdominal aorta; ΔD, pulsatile diameter change in the abdominal aorta; E_p, pressure–strain elastic modulus.
*NS *vs* group 2; **$P < 0.001$ *vs* group 2; #NS *vs* group 3; ##$P < 0.001$ *vs* group 3.

Pressure–Diameter Relation

• Static P–D test •	• Human, rats • Finger, tail artery	• Smooth muscle activation • Inflation vs deflation

Materials
- Human finger arteries obtained at autopsy (age, 57–85 years)
- Ventral tail artery of Wistar rats; weight, 250–350 g

Testing Methods and Experimental Conditions
- Medium: aerated Tyrode's solution at 37°C
- Pressure–diameter relation of tubular specimen at in situ length obtained by changing pressure stepwise every 5 or 10 mmHg from −40 to 100 mmHg

Data

Rat tail artery

Human finger artery
(female, 83 years old)

p (mmHg)
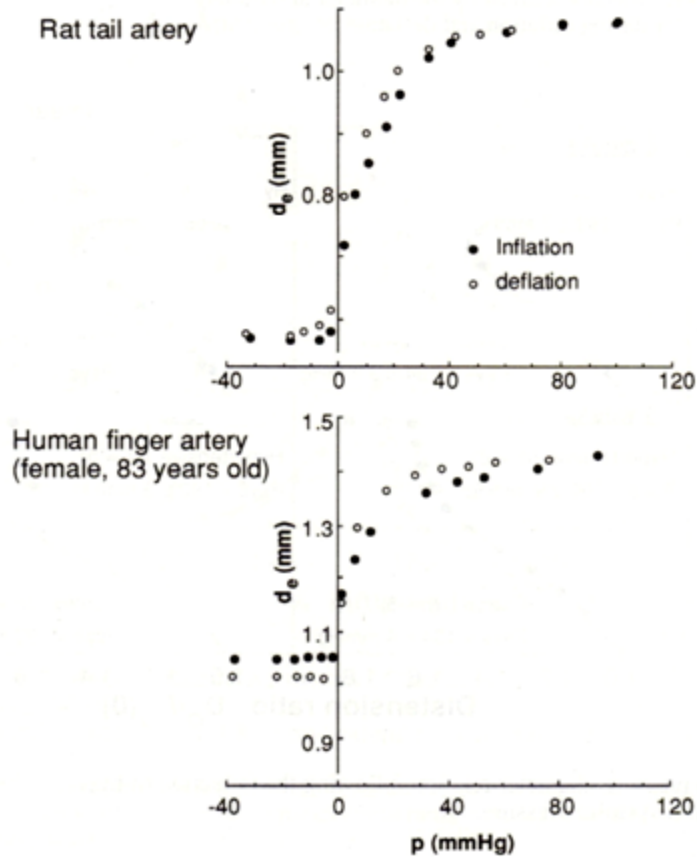
Comments
- Spontaneous rhythmic contractions observed in both specimens.
- Human finger arteries could contract to complete closure both spontaneously and after addition of noradrenaline, while rat tail arteries did not.

Pressure–Diameter Relation

• Stress–strain curve • Static P–D test	• Dogs • Iliac and carotid arteries	• Smooth muscle activation • Characteristic impedance

Materials
- Fifteen young, healthy, adult mongrel dogs
- Carotid and iliac arteries

Testing Methods and Experimental Conditions
- Tubular specimen (in vivo length) in an aerated physiological salt solution at 37°C
- Quasi-static pressure–diameter relation at inflation rate of 1 mmHg/s between 0 and 250 mmHg (Passive)
- Norepinephrine (5 µg/ml) added to medium to activate smooth muscle
- One-time inflation at a rate of 0.2 mmHg/s from 0 to 250 mmHg (Active)

Data
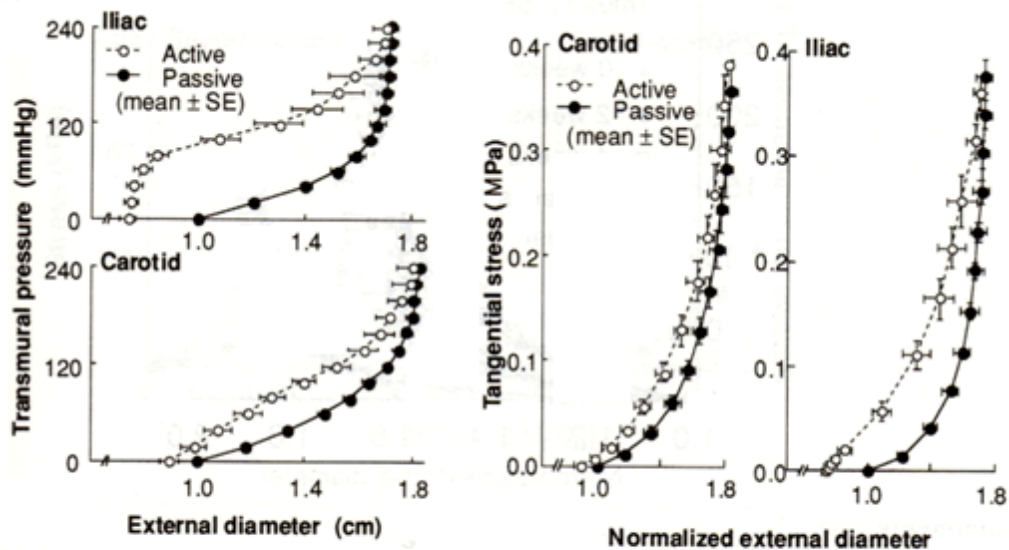
Comments
- Also presented:
  Incremental elastic modulus *vs* strain;
  Characteristic impedance *vs* transmural pressure.
- Values of external diameter were normalized for each segment by dividing by the value at zero pressure for passive conditions before averaging.

Pressure–Diameter Relation

• Stress–strain curve • Static P–D test	• Puppies • Mesenteric artery	• Developmental change • Biochemical analysis

Materials
- A litter of puppies and their mother (to ensure homogeneity of animal group)
- Mesenteric artery

Testing Methods and Experimental Conditions
- Tubular specimen in aerated physiological salt solution at 37°C
- Pressure–diameter relation obtained at inflation rate of 1 mmHg/s
- Diameter measured with a cantilever transducer

Data
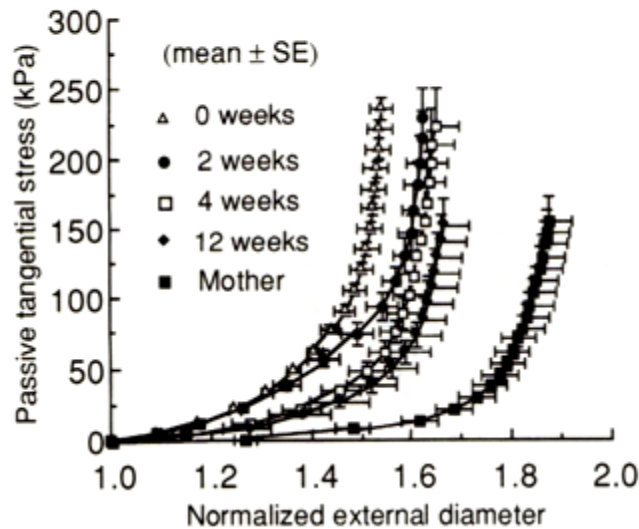
Comments
- Also presented:
  Response to smooth muscle contraction;
  Changes in connective tissue and electrolyte contents during growth.
- Relation between passive tangential wall stress and external diameter for superior mesenteric artery at various ages.
- Diameter is normalized by dividing by value at zero pressure and in vivo length.
- Values of wall stress and normalized diameter were averaged at specific values of transmural pressure for all animals in each age group.

Pressure–Diameter Relation

• Tension–length curve • Static pressure–volume test	• Human • Iliac artery	• Effect of digestion • Effect of preservation

Materials

- Human
- External iliac artery obtained at autopsy
- Stored in the refrigerator in 1/10000 saline solution of methiolate

Testing Methods and Experimental Conditions

- Static pressure–volume test on fresh specimen at room temperature
- No restraint on the longitudinal direction
- Fresh specimen digested by formic acid to remove collagen or by trypsin to remove elastin
- Study effects of collagen and elastin digestions

Data

Tension-length diagram
Human external iliac artery
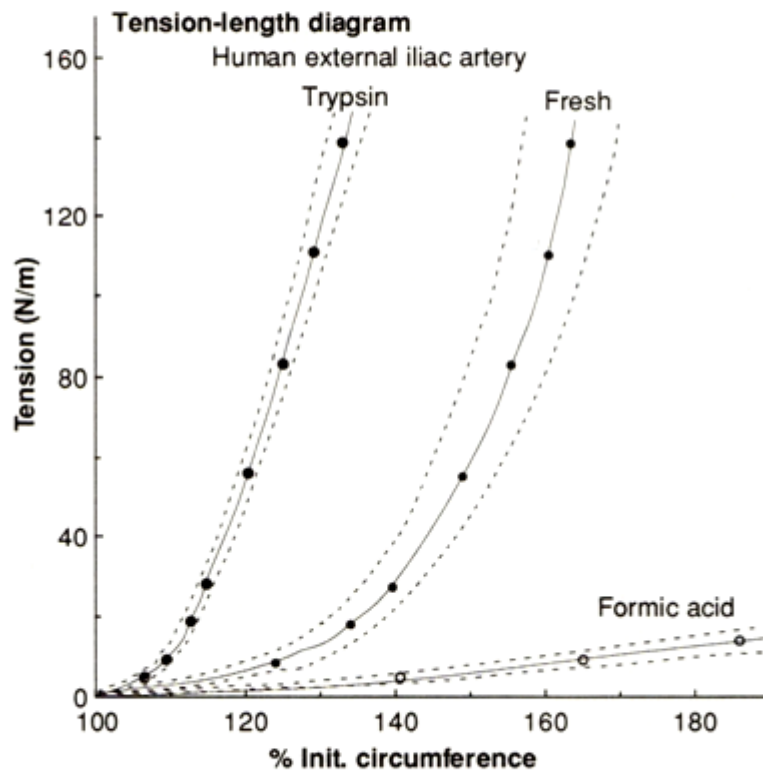
Comments

- The figure shows the elastic diagram of an iliac artery representing the mean of the results on nine vessels of the young to middle age group (20–50 years). The broken lines indicate the standard error.
- No change in the distensibility curves was detectable during periods up to 10 days.

Shear Property

• Multi-axial test • Torsion test	• Dogs • Aorta, carotid artery	• Test system •

Materials
• A common carotid artery and a descending thoracic aorta

Testing Methods and Experimental Conditions
• Cylindrical specimen
• Medium: oxygenated calcium-free Krebs solution with 2 mM EGTA at 37°C
• Quasi-static inflation test under constant axial length
• Quasi-static axial extension test under constant diameter
• Quasi-static torsion test under constant axial length
• Quasi-static torsion test under constant diameter

Data
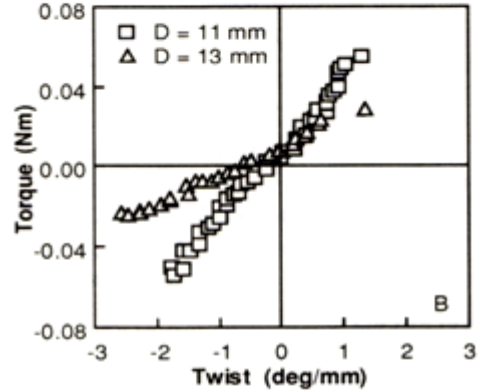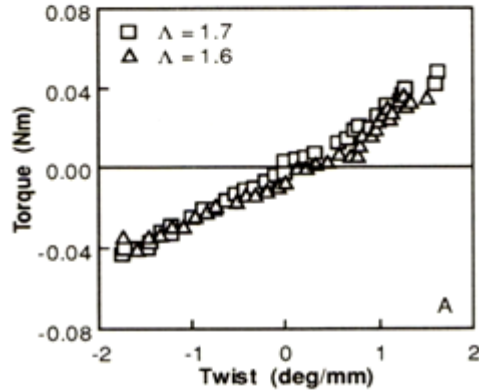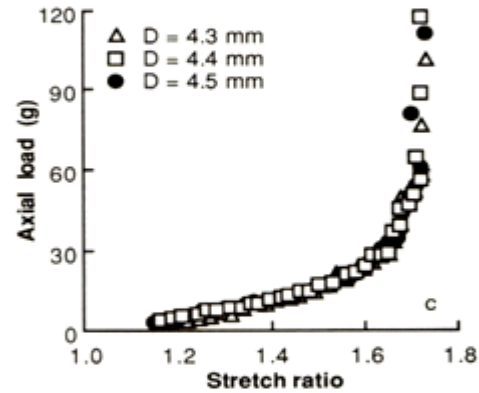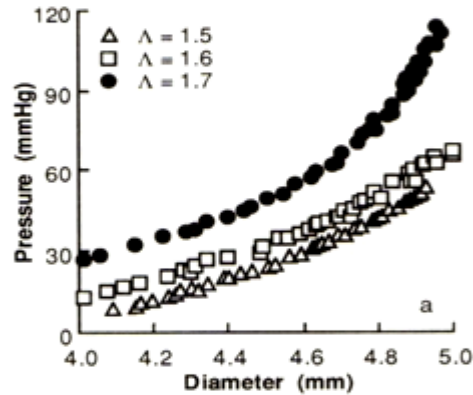
Tensile Property

• Axial property • Force–length relation	• Dogs • Carotid and femoral	• Axial tethering •

Materials
- Mongrel dogs
- Carotid and femoral arteries

Testing Methods and Experimental Conditions
- Medium: Ringer–Tyrode solution at 37°C with 100 mg/l of KCN to deactivate smooth muscle
- Axial force–length relation measured on tubular segments at different constant pressures (0, 20, 40, 80, 120, 160, and 200 mmHg)

Data

Legend: ● 0 mmHg   + 20 mmHg   ■ 40 mmHg   × 80 mmHg
○ 120 mmHg   ◆ 160 mmHg   △ 200 mmHg

Upper graph (Force (μN) vs Length (mm), 0–300 μN, 30–45 mm):
$\alpha = 0.81 \pm 0.06$
$\beta = 1.49 \pm 0.02$ (x 10^{-2} mmHg^{-1})
$L_0 = 28.2 \pm 0.2$ (mm)
$L_v = 45.1 \pm 0.1$ (mm)
$L_m = 43.6 \pm 0.1$ (mm)
$F_v = 245 \pm 2$ (μN)
(L_v, F_v)

Lower graph (Force (μN) vs Length (mm), 0–400 μN, 20–30 mm):
$\alpha = 0.56 \pm 0.03$
$\beta = 1.27 \pm 0.02$ (x 10^{-2} mmHg^{-1})
$L_0 = 19.2 \pm 0.1$ (mm)
$L_v = 29.2 \pm 0.1$ (mm)
$L_m = 26.8 \pm 0.1$ (mm)
$F_v = 382 \pm 3$ (μN)
(L_v, F_v)
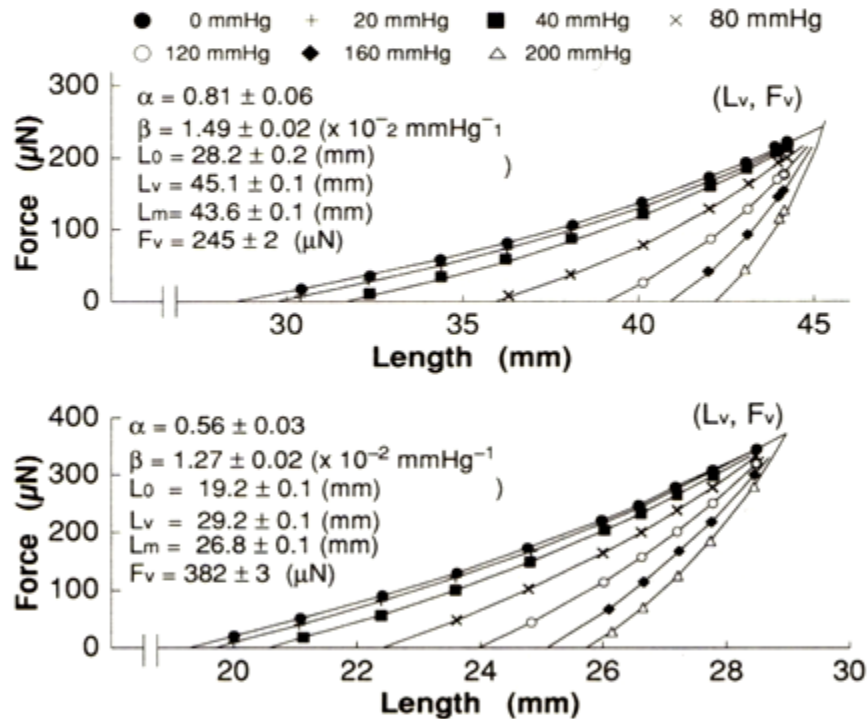
Comments
- Formula used to fit length-force data:

$$F = F_v(L - L_s)/\{L_v - L_s + \alpha(L_v - L)\}$$

$L_s = L_o + (L_m - L_o)(1 - e^{-\beta P})^2$;   ($L_o$, L_v, L_m, F_v, α, and β are constants).
- The length–force curves for the different pressures tend to have a common point of intersection, which corresponds to the length of the artery in vitro.
- Similar results were obtained for canine aorta, human carotid and iliac arteries.

164

Viscoelasticity

• Dynamic elastic modulus • Pulse wave velocity	• Dogs • Aorta, iliac, femoral	• In vivo measurement • Hemodynamics

Materials

- Mongrel dogs and greyhounds (age, approximately 2–4 years), weight 12.5–31 kg (mean 22 kg)
- Upper descending, midthoracic, lower thoracic, and midabdominal aortas, and iliac, femoral, and saphenous arteries

Testing Methods and Experimental Conditions

- Anesthetized with pentobarbital sodium, 20–35 mg/kg i.v.
- Mechanical ventilation
- Simultaneous measurement of pressure and diameter
- Fourier analysis up to 10 harmonics

Data

Weight (kg)	D_o (mm)	γ	BP (mmHg)	Frequency (Hz)	E_{dyn} (kPa)	$\eta\omega$ (kPa)	c (m/s)
Upper descending thoracic aorta							
25 ± 2	19.0 ± 0.8	0.12 ± 0.02	110 ± 7	1.86 ± 0.37	290 ± 50	33 ± 15	4.5 ± 0.2
Midthoracic aorta							
23 ± 1	14.3 ± 0.9	0.14 ± 0.01	105 ± 4	2.09 ± 0.16	300 ± 30	26 ± 7	4.9 ± 0.2
Lower thoracic aorta							
26 ± 1	13.8 ± 0.6	0.11 ± 0.02	112 ± 9	1.77 ± 0.04	570 ± 100	58 ± 17	5.9 ± 0.3
Midabdominal aorta							
23 ± 1	10.6 ± 0.7	0.12 ± 0.01	115 ± 6	2.03 ± 0.20	980 ± 130	123 ± 23	8.5 ± 0.4
Iliac artery							
21 ± 2	4.6 ± 0.3	0.16 ± 0.01	105 ± 7	1.93 ± 0.26	1100 ± 240	226 ± 69	10.2 ± 0.7
Femoral artery							
22 ± 1	4.4 ± 0.1	0.13 ± 0.01	118 ± 4	1.83 ± 0.16	1460 ± 260	224 ± 70	10.4 ± 0.5
Saphenous artery							
26	1.5	0.12	100	1.08	6060	300	22.0

Values are mean ± SE.

Comments

- Pressure–strain elastic modulus: $E_p = (\Delta P)/(\Delta D/D_o)$, where ΔP and ΔD are pressure and diameter changes, respectively, and D_o mean outer diameter.
- Dynamic incremental elastic modulus: $E_{inc} = 1.5E_p(1-\gamma)^2/\{1-(1-\gamma)^2\}$, where $\gamma = h/R_o$; h, wall thickness; R_o, outer radius.
- Complex elastic modulus: $E_{dyn} = E_{inc} \cdot \cos\phi$, where ϕ is the phase of the complex elastic modulus.
- Viscous modulus: $\eta\omega = E_{inc} \cdot \sin\phi$, where $\eta\omega$ is the viscous modulus, and ω is the angular frequency.
- Pulse wave velocity: $c = (1.5E_{dyn} \cdot \gamma/\rho)^{1/2}$, where r is the density of blood.

Viscoelasticity

• Dynamic elastic modulus • Viscous retarding force	• Human • Aorta, carotid, iliac, femoral	• Age-related variation • Frequency dependency

Materials
- Human
- Thoracic and abdominal aortas, and carotid, iliac, and femoral arteries

Testing Methods and Experimental Conditions
- Stored frozen in physiological saline after excision at post mortem until use
- Grossly atheromatous vessels were discarded
- Medium, physiological saline at room temperature
- Dynamic pressure–diameter measurement
  (mean pressure, 100 mmHg; amplitude, ±5–15 mmHg; frequency, 1–10 Hz)

Data
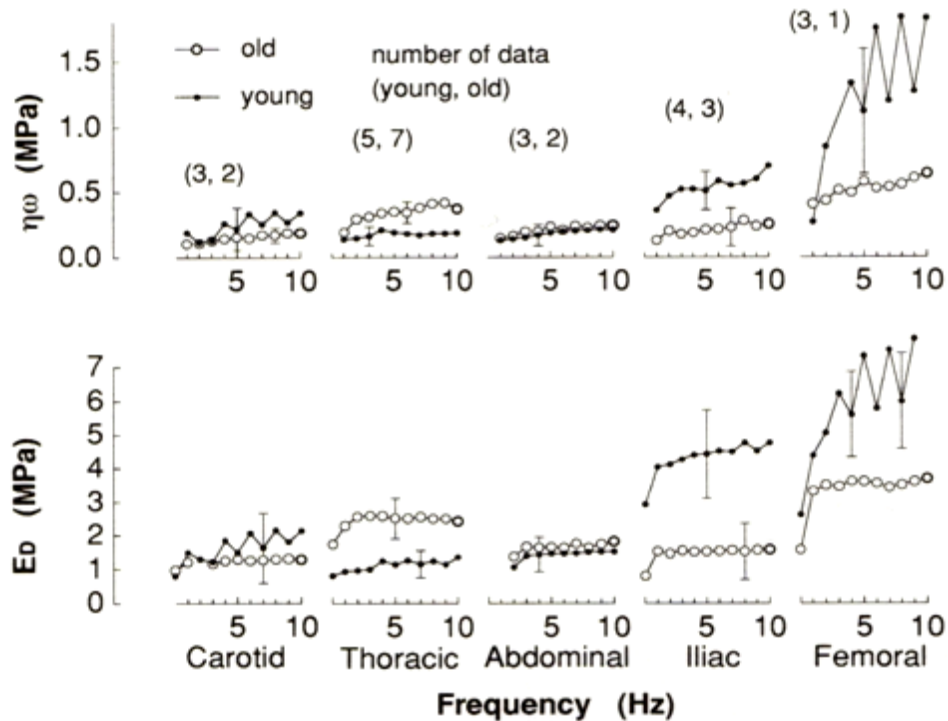
Comments
- Dynamic modulus:

  $E_D = E_C \cos \phi$, dynamic elastic component;

  $\eta \omega = E_C \sin \phi$, viscous retarding force.

  E_C, the amplitude of complex elastic modulus; ϕ, phase difference.

Viscoelasticity

• Pressure–strain elastic modulus • Vessel dimension	• Human, dogs • Coronary artery	• In vivo measurement •

Materials
- Coronary arteries without gross atheromatous deposits from 5 subjects; age, 14–40 years
- Left circumflex coronary arteries (LCCA) of greyhounds (weight, 20–27 kg)

Testing Methods and Experimental Conditions
- Human coronary artery within 24–96 h postmortem
- In vivo length not known (stretched until no buckling occurred during pressurization)
- Static pressure–diameter test in normal saline at room temperature (20–150 mmHg)
- Dynamic measurement at amplitudes of 15 mmHg at frequencies of 0.5–10 Hz
- Dog LCCA exposed through thoracotomy under pentobarbital anesthesia and ventilation
- Pressure–diameter relation on the beating heart measured with an electrical caliper and a pressure transducer connected to an anterior ventricular branch via a catheter

Data

Artery	Age (years)	D_o (cm)	γ	E_p (stat) (MPa)	E_{stat} (MPa)	E_p (dyn) (MPa) (2Hz)	E_{dyn} (MPa) (2Hz)	E_{dyn}/E_{stat} (2Hz)
LAD 1	30	0.57	0.13	0.701	3.20	1.78	8.38	2.62
LAD 2	40	0.52	0.25	0.619	1.22	1.15	2.64	2.16
LAD 3	20	0.39	0.10	0.551	3.50	1.21	7.72	2.20
LCCA 1	40	0.56	0.23	0.472	1.01	0.66	1.40	1.39
LCCA 2	36	0.44	0.12	0.663	1.45	0.93	2.11	1.45
RCA 1	14	0.44	0.10	0.663	3.50	0.72	4.50	1.15
Mean	30	0.49	0.17	0.602	2.31	1.07	4.46	1.83
SE	4	0.03	0.03	0.032	0.49	0.17	1.21	0.24

D_o, mean outside diameter; γ, wall thickness + outside radius; E_p (stat), static pressure/strain elastic modulus; E_{stat}, static elastic modulus; E_p (dyn), dynamic pressure/strain elastic modulus; E_{dyn}, dynamic elastic modulus.
LAD, left anterior descending artery; LCCA, left circumflex coronory artery; RCA, right coronary artery. LAD 2 and LCCA 1 from same subject.

Dog	Wt. (kg)	Frequency (Hz)	BP (mmHg)	Δp (mmHg)	D_o (cm)	E_p (MPa)	γ	E_{dyn} (MPa)
1	25.4	2.78	101	32.0	0.32	0.201		
2	28.1	2.50	105	18.0	0.37	0.262	0.174	0.82
3	21.8	2.40	102	18.7	0.36	0.164	0.093	1.48
4	24.5	1.56	126	25.1	0.32	0.274	0.126	1.33
5	22.7	1.66	98	10.9	0.39	0.195	0.083	1.53
6	26.3	2.66	124	18.1	0.37	0.249	0.128	1.18
7	25.0	2.60	102	23.1	0.33	0.149	0.081	1.21
8	25.4	2.24	102	19.0	0.35	0.168	0.142	0.70
9	28.2	2.70	119	25.8	0.36	0.364	0.095	2.47

Δp, pulse pressure; E_p, pressure–strain elastic modulus.

Comments
- Elastic parameters:

  Pressure–strain elastic modulus, $E_p = (\Delta P/\Delta D_o)D_o$

  Elastic modulus, $E = 1.5E_p[D_i^2/(D_o^2 - D_i^2)]$

    D_o and D_i, outer and inner diameters; ΔD_o, diametrical change caused by pressure change ΔP.

References

[01]   Laparoscopic abdominal access and prevention of injury – Ronald Kolata, DVM. Ethicon Endo-Surgery, Inc. Cincinnati, Ohio.

[02]   http://www.youtube.com/watch?v=W-ZPa1NzcgM&feature=related

[03]   Fast finite element modeling for surgical simulation – Berkeley J. et al, Medicine Meets Virtual Reality.

[04]   Real-time deformable models of non-linear tissues by model reduction techniques – Niroomandi S. et al, Elsevier, Comp. Methods and Prog. in Bio. 2008.

[05]   Truth cube: Establishing physical standards for soft tissue simulation – Kerdok A. et al, Elsevier, Medical Image Analysis.

[06]   Towards realistic soft-tissue modeling in medical simulation – Delingette H., Proceeding of IEEE. 1998.

[07]   Comparing algorithms for soft tissue deformation: Accuracy metrics and benchmarks – Alterovitz R, et al, Technical Report.

[08]   Finite element modeling in surgery simulation – Bro-Neilsen M, Proceedings of the IEEE. 1998.

[09]   Anatomy-based facial tissue modeling using the finite element method – Keeve E. et al, IEEE transactions.1996.

[10]   Finite element model of the breast for predicting mechanical deformations during biopsy procedures – Azar F. et al, Proceedings of the IEEE workshop on Mathematical Methods in Biomedical Image Analysis.

[11]   Real-time finite element modeling for surgery simulation: An application to virtual suturing. Mimic Technologies Inc.

[12]   A computational technique for interactive needle insertions in 3D nonlinear material – Nienhuys H. et al, Proceedings of the IEEE, Intl. Con. on Robotics and Automation, 2004.

[13]   An efficient and scalable haptic modeling frame work for needle insertion simulation in percutaneous therapies training system – Qin, J. et al.

[14]   Needle insertion into soft tissue: A survey – Abolhassani N., Medical Engineering and Physics, 2007.

[15]   Force modeling for needle insertion into soft tissue – Okamura A. M. et al, IEEE Trans. Bio. Eng., 2004.

[16]   A velocity-dependent model for needle insertion in soft tissue – Crouch J. R. et al, Springer-Verlag Berlin Heidelberg, 2005.

[17]   Interactive simulation of needle insertion models – DiMaio S. P. et al, IEEE Trans. on Bio. Eng., 2005.

[18]   Needle steering and motion planning in soft tissues – DiMaio S.P. et al, IEEE Trans. on Bio. Eng., 2005.

[19]   Needle steering and model-based trajectory planning – DiMaio S.P. et al, Springer-Verlag Berlin Heidelberg, R.E Ellis and T.M. Peters(Eds), 2003.

[20]   Needle insertion modelling for the interactive simulation of percutaneous procedures – DiMaio S.P. et al, Springer-Verlag Berlin Heidelberg, T. Dohi and R. Kikinis (Eds), 2002.

[21]   Modeling of needle insertion forces for robot-assisted percutaneous therapy – Simone C. et al, Proceeding of the IEEE, International Conference on Robotics and Automation, 2002.

[22]   Needle Insertion Modeling and Simulation – DiMaio S. P. et al, Proceedings of the IEEE, Intl. Con. on Robotics and Automation, 2002.

[23]   Mechanical properties of human abdominal wall measured in vivo during for laparoscopic surgery – C. Song et al. 2006.

[24]   Real laparascopic surgery video edited in windows movie maker.

[25]   Biomechanics: Mechanical properties of living tissues – Fung Y.C, Springer-Verlag, New York, 1993.

[26]   http://en.wikipedia.org/wiki/Von_Mises_yield_criterion

[27]   http://www.sensable.com/documents/documents/Premium_1.5_6DOF.pdf

[28]   http://www.fda.gov/MedicalDevices/Safety/AlertsandNotices/

ucm197339.htm

[29]   Strength of biological materials - Hiroshi Yamada, M.D, The Williams and Wilkins Company, Baltimore, 1970.

[30]   Atlas of the visible human male – Victor M. Spitzer and David G. Whitlock, Jones & Bartlett Publishers, Sudbury, Massachusetts, 1998.

[31]   http://www.uchsc.edu/sm/chs

[32]   www.nlm.nih.gov/research/visible/visible_human.html

[33]   http://www.instantanatomy.net/abdomen.html

[34]   http://anatomy.uams.edu/anatomyhtml/antabdominalwall.html

[35]   http://education.yahoo.com/reference/gray/subjects/subject/118

[36]   http://home.comcast.net/~wnor/abdomen1.htm

[37]   http://home.comcast.net/~wnor/skel&wallsabd.htm

[38]   http://emedicine.medscape.com/article/1297226-overview

[39]   http://science.nationalgeographic.com/science/health-and-human-body/human-body/skin-article.html

[40]   http://www.boddunan.com/education/20-Medicine%20/2778-understanding-the-anatomy-of-abdominal-muscles.html?Surgery=

[41]   Influence of age and sex on abdominal muscle and subcutaneous fat thickness - Hiroaki Kanehisa et al. 2004.

[42]   http://www.nhlbisupport.com/bmi/

[43]   Regional differences in ultrasonic assessment of subcutaneous fat thickness in the abdomen: effects on the TRAM flap – Yano K et al. 2002.

[44]   A rehabilitative ultrasound imaging investigation of lateral abdominal muscle thickness in healthy aging adults – Stetts DM et al.

[45]   Abdominal muscle size and symmetry in normal subjects – Gabrielle Rankin et al. 2006.

[46]   Data book on mechanical properties of living cells, tissues and organs –
         H.Abe, K.Hayashi, M.Sato (Eds), Springer, New York, 1996.

[47]   LS – Dyna Keyword Manual, May 2007, Version 971.

[48]   Skin density in hairless rat: Evidence of regional differences –
         Rins M. et al.

[49]   http://en.wikipedia.org/wiki/muscle

[50]   http://en.wikipedia.org/wiki/Finite_strain_theory

[51]   http://en.wikipedia.org/wiki/Neo-Hookean_solid